Target tracking and source seeking using unmanned aerial vehicles with input constraints

Zhu, Senqiang

2014

Zhu, S. (2014). Target tracking and source seeking using unmanned aerial vehicles with input constraints. Doctoral thesis, Nanyang Technological University, Singapore.

https://hdl.handle.net/10356/59961

https://doi.org/10.32657/10356/59961

TARGET TRACKING AND SOURCE SEEKING USING UNMANNED AERIAL VEHICLES WITH INPUT CONSTRAINTS

ZHU SENQIANG

School of Electrical & Electronic Engineering

A thesis submitted to the Nanyang Technological University
in fulfillment of the requirements for the degree of
Doctor of Philosophy

2014

Statement of Originality

I hereby certify that the work embodied in this thesis is the result of original research and has not been submitted for a higher degree to any other University or Institution.

Date	ZHU SENQIANG

Acknowledgement

My first debt of gratitude must go to my supervisor, Professor Danwei Wang. He continuously provided me the insightful vision, positive encouragement, patient discussions and scientific advice throughout my doctoral program. Without Prof. Wang's constantly strong support, I would not have completed my dissertation.

I am also very grateful to my co-supervisor, Dr. Chang Boon Low, for his valuable guidance and kindly help during the last two years of my PhD study. His expertised comments and suggestions have been greatly helpful for my academic work.

I also would like to thank my friends at Intelligent Robotics Lab. Their friendship and assistance has meant more to me than I could ever express. Special thanks go to Dr. Baolin Wu, Mr. Qiang Shen, and Mr. Guoyi Chi for their valuable advice and friendly help. My gratitude also goes to the technical staffs in the lab for their invaluable friendly assistance through the whole process.

I wish to thank my loved parents, brother and grandparents whose unreserved love, care, and understanding provided me inspiration and courage in dealing with the stress of graduate school. I also want to thank my parents-in-law for their unconditional support. Finally, I would like to dedicate this work to my beloved wife and son, whose love and support are a great driving force.

Contents

Abstract

The potential applications of unmanned aerial vehicles (UAVs) in both military and civilian fields have spurred the research on UAV control. Although great progresses in this area have been made by researchers worldwide, practical and theoretical challenges are still abundant. This thesis focuses on the problems of target tracking and source seeking using UAVs subject to input constraints.

Ground target tracking is an important application of UAVs. Due to UAV inherent motion constraints, the fixed-wing UAV generally can not stay on top of the ground target. Standoff tracking is one possible solution to target tracking. In the first part of the thesis, a single UAV is used to achieve moving ground target tracking. A guidance law is introduced to generate a desired relative course for the UAV. Based on the desired relative course, a saturated heading rate controller is proposed to achieve standoff target tracking. A rigorous global stability proof of the system with the proposed controller is provided. As the ground target velocity may be unknown, a bounded adaptive observer is designed to estimate the unknown constant target velocity and background wind.

Ground target could be friendly or adversarial. For adversarial target tracking or hazardous target tracking, safety and tracking performance are two critical issues for the UAV. In order to achieve adversarial target tracking, the initial condition of the UAV is analyzed, and two types of tracking scenarios are defined: exposure avoidance and minimum exposure time. A bang-bang controller is proposed to

achieve target tracking in both scenarios.

Advances in sensing, communication and control systems make it possible for multiple UAVs to carry out missions cooperatively. A circular formation strategy for target tracking is proposed in this thesis. Firstly, a guidance law based heading rate controller is designed for circular tracking. A notion called temporal phase is introduced for multi-UAV cooperation. Based on the temporal separation, a bounded variable airspeed controller is developed to achieve equal temporal separation.

Source seeking is a potential application of multi-UAV cooperation. In the past decades, single vehicle is successfully used for source seeking. However, the time cost and extreme movement are two challenging issues to be addressed. Cooperation of multiple UAVs makes it possible to attain better source seeking performance. This thesis proposes a leader-follower formation strategy for source seeking. Based on the measurement of all UAVs, the scalar field gradient at the leader location is estimated using least-squares method. After that, an adaptive observer is designed to estimate the source velocity. By using the estimated gradient and source velocity, a heading rate controller for the leader is developed to achieve level tracking. Then, heading rate controller for follower UAVs is also proposed to achieve circular formation around the leader.

Finally, conclusions and some recommendations are presented.

List of Figures

List of Tables

Symbols and Acronyms

(x, y)	UAV position
(x_r, y_r)	UAV relative position
(W_x, W_y)	Background wind
(T_x, T_y)	Moving target velocity
T_v	Moving target velocity magnitude
(x_t, y_t)	Target position
(x_s, y_s)	Source position
ψ	Heading angle
θ	Clock angle
χ	Relative course angle
v	UAV airspeed
u	UAV heading rate
τ	Temporal phase
$\Lambda(\cdot)$	Eigen value function
$\vec{G} = col(G_x, G_y)$	Estimated gradient

H	Hessian matrix
$\vec{v}_s$	Source velocity
f_i	Scalar field value
∇	Gradient operator
$\|\| \cdot \|\|$	2-norm
$\|\| \cdot \|\|_\infty$	Infinity-norm
Subscript i	The ith UAV

Chapter 1

Introduction

1.1 Background and Motivation

During the past decades, technological advances in electronic, power and payload systems have led to the development of Unmanned Aerial Vehicles (UAVs). As compared to human piloted aircrafts, UAVs are generally smaller, cheaper and potentially more cost effective. Meanwhile, using UAVs in dangerous missions can effectively avoid the threats to the pilots. Hence, UAVs have been gradually applied to both military and civilian fields for various purposes, such as surveillance [1–3], border patrol [4], search and rescue [5], convoy protection [6], etc. The first UAV "Aerial Target" was developed in 1916, which was remotely piloted. Since then, with the development and maturing of applicable technologies, various types of UAVs have been developed such as "Predator" [7] and "Global Hawk" [8]. Historically, most UAVs including "Aerial Target" and "Predator" were remotely piloted. However, remote piloting may not be suitable for the missions that are long in duration, have unreliable communication links or involve large numbers of vehicles [9]. Therefore, UAV autonomy defined as the ability to make decisions without human intervention, is increasingly pursued by researchers since it is essential for many

applications. The research towards UAV autonomy includes numerous significant aspects, such as path planning, tracking control, and autonomous cooperation for multiple UAVs.

There are mainly two types of UAVs: fixed-wing UAVs and rotary-wing UAVs. This thesis will focus on the control problems of fixed-wing UAVs. A fixed-wing UAV must maintain a forward airspeed so that the force generated by the wings can lift the vehicle (without entering into stall condition). Due to the physical limits of the jet engine, there exists a maximum bound on the engine thrust [10,11]. In addition, there is also a constraint on the roll angle of the fixed-wing UAV (limited roll motion), which has a direct influence on the heading rate. These constraints and limitations have imposed a significant challenge on the fixed-wing UAV control design. Position control plays a key role in carrying out the specified UAV missions. In terms of various applications, position control algorithms for UAVs can be generally categorized into the following types: target tracking, trajectory tracking, path following, waypoint following, and area sampling [9]. Target tracking problem refers to controlling the UAV to track a target (stationary or moving) with a desired position offset. Trajectory tracking problem is to control the UAV to reach and follow a geometric path with associated time law from a given initial configuration. Path following is to force the UAV to follow a specified geometric path which is independent of time. Waypoint following requires the UAV to fly over some specified point in sequence. In area sampling, the UAV must be controlled to fly in the vicinity of a particular location. It can be observed that there are different constraints imposed on these five types of control algorithms. For example, as compared to path following, trajectory tracking requires to satisfy the time constraints.

Recently, substantial developments in network and communication technologies make it possible to achieve cooperation of multiple UAVs. Cooperation implies that the autonomous control of one vehicle is dependent on the autonomous control of

another vehicle, and vice versa. Generally, cooperative control problems for multiple UAVs can be categorized into two classes [12]. One class is non-formation control problem such as cooperative timing problem and cooperative fire monitoring. The other is formation control problem such as cooperative target localization and formation flight. As compared to a single UAV, cooperation of multiple UAVs has many obvious advantages including improved sensitivity, high accuracy, enhanced robustness, as well as high cost and energy efficiency. For example, using multiple sensors mounted on multiple different UAVs to localize or track a ground target can get better accuracy. UAVs flying in a V-shape formation can maximize the energy efficiency. And in some missions, cooperation of multiple UAVs is even necessary where single UAV can not achieve the desired objectives.

As compared to the conventional mobile robot control, the flight control is more challenging due to the inherent properties of UAVs. Many existing control approaches for mobile robots are not directly applicable to UAVs. Target tracking is a significant task which is utilized in many UAV applications, such as battlefield surveillance and convoy protection. If ground target has a lower movement speed or is even stationary, UAVs may not be able to stay on top of the target due to the stall condition. To solve this problem, several trajectories such as circular orbit and periodic pass-by trajectories are proposed in the literature. However, control input constraints of UAVs must be taken into account during control design. For different applications, the requirements of target tracking are different. If the target is friendly, UAVs may need to fly as close as possible to the target. In contrast, if the target is hostile or hazardous, UAVs must be maintained to keep a standoff distance to the target. Moreover, if the distance between the UAV and the hostile target is too close, the UAV should be driven to fly out of the threatened area as soon as possible. How the control design can guarantee tracking performance while minimizing the threats to the UAV is still an open question. Although UAVs now

can access more and more information about themselves and targets thanks to the technological advances, lack of crucial information may still exist in some cases. For example, the velocity of the target may not be available for the UAVs. When only the target position is known, how to design a constrained controller to achieve moving target tracking is worth of study.

In order to enhance the performance of target tracking, multiple UAVs can be used to cooperatively carry out missions. Although there exist a lot of cooperative control algorithms proposed for multi-agent systems in the literature, most of them are hindered from UAV application due to the inherent properties of the fixed-wing UAV. Therefore, it motivates the development of cooperation strategies and control methodologies suitable for UAVs. Since UAVs fly in the sky which could be obstacle-free, the UAVs can be applied to explore the complicated environment, especially hazardous or polluted area. In such applications, UAVs can be used to find the sources which could be polluted source, acoustic source or thermal source due to forest fire. For the source seeking problem, the generic property is that only part information of the source is known to the UAV such as the field value while the source position or movement is totally unknown. Most of the previous works in source seeking consider to use single robot. Cooperation of multiple agents introduces a new direction to solve this kind of problem. However, the research on cooperative source seeking is still far from maturity. This thesis mainly focuses on the following issues: target tracking and source seeking.

1.2 Literature Review

The research on UAV flight control has been widely explored in control community and other related communities. Numerous different results have been provided in the literature. This section is to review various control strategies and approaches

on target tracking, source seeking and multi-agent cooperation.

1.2.1 Target Tracking

Tracking control is a fundamental task for UAVs and generally includes trajectory tracking control and target tracking control. Since trajectory tracking is equivalent to target tracking in some cases where target trajectory is designated as the desired target for UAV to track, it is necessary to briefly review the works on trajectory tracking as well. The kinematic model of a fixed-wing UAV which is equipped with a low level fight control system (i.e. low level attitude hold, velocity hold and heading rate hold autopilots) is similar to the kinematic model of a nonholonomic mobile robot. There have been numerous studies on tracking control of mobile robots. Therefore this section will review not only the literature on UAV tracking control, but also the literature on mobile robot tracking control.

The classical approach for trajectory tracking of mobile robot is to utilize linearization techniques which include local linearization [13], linearization [14] and output feedback linearization [15]. In [16], backstepping technique is applied to achieve global tracking result for both kinematic and dynamic models. In [17], a saturated controller is proposed to solve the regulation and tracking problems of a nonholonomic mobile robot simultaneously, where the path may consist of a straight line, a circle, or a path approaching the origin. Reference [18] proposed a model-based control design strategy based on passivity and normalization, where the controller satisfies the input constraints. For the fixed-wing UAV, the input constraints are different from those imposed on the mobile robots, i.e. the UAV must maintain a positive forward airspeed. Existing trajectory tracking controllers for mobile robot are not directly applicable for trajectory tracking of the UAVs. Recently, a saturated trajectory tracking controller for the UAVs based on control Lyapunov function (CLF) approach is proposed in [10]. Firstly, the CLF is used to obtain a feasible

control set for the constrained input case. Based on the feasible control set, a number of feasible control strategies are generated to achieve accurate tracking. In [11], as the continuation and extension of [10], a saturated controller for a more accurate kinematic model is proposed by using backstepping technique.

In area surveillance and convoy protection, the UAVs are usually required to perform target tracking, and several control strategies have been developed in the literature, such as vector field approach [9,19], good helmsman approach [20], M-PC based approach [21,22], etc. Target tracking can mainly be classified into two categories: standoff target tracking and non-standoff target tracking [23]. Standoff tracking requires the UAV to fly around a target with a desired distance (standoff distance), but non-standoff tracking does not have such a constraint. In [24], a non-standoff trajectory is designed to guide the UAV to periodically fly over the target for convoy protection. As compared to non-standoff tracking, standoff tracking has more advantages in the practical applications. In target tracking missions, especially ground target tracking, the targets could be adversarial, friendly, or unidentified. For adversarial target tracking, the UAV must avoid to be too close to the target so as to reduce its exposure to the target. For friendly target tracking such as convoy protection, the UAV is also required to keep a distance to search the surrounding environment. In addition, the speed of ground target is generally slower than the UAV, so the UAV has to orbit around the target due to its inherent properties.

In [25], by using backstepping method, a globally asymptotically stable controller is proposed for mobile robot to achieve target tracking, where the mobile robot is forced to keep a desired distance to the target. However, in this approach, the velocity input of mobile robot is allowed to be negative. In [26] and [27], S. Park et al. proposed a nonlinear guidance logic to achieve path following for curved trajectory. In this approach, one point on the desired path is designated as the reference point, and a lateral acceleration command is generated to drive the vehicle to the reference

point. However, this nonlinear guidance method can not be directly applied to the mission where the UAV is used to track the ground target, because the velocity of ground vehicle is usually slower than the airspeed of the UAV. A path following approach called "good helmsman" is introduced to follow a standoff path in [20]. In this "good helmsman" path following approach, the vehicle kinematics is described by Serret-Frenet formulas in terms of path parameters, and then the controller is designed to simultaneously regulate both the course error and cross track error to zero so that the UAV converges to the desired path. In addition, a linear observer for wind is constructed to reorient the desired path. Rafi et al. [28] proposed an autonomous navigation algorithm to guide the UAV with physical constraints to follow a moving target.

Recently, a Lyapunov guidance vector field approach which stems from potential field work is introduced to guide the UAVs to achieve target tracking [23,29–32]. In [19], one Lyapunov vector field approach is proposed to generate desired course and a sliding mode based controller is designed to drive the UAV to follow the desired course so that the UAV achieves standoff tracking. This approach is robust to the unknown wind, but it may lead to high gain on the course rate controller to resist the unknown wind and this approach also does not consider the target motion. A similar vector field approach is also described in [29], and this approach uses heading rate control input exclusively to obtain the desired circular orbit while holding a constant airspeed. But this approach falls short of giving a proof of global stability. Another different Lyapunov guidance vector field approach is introduced in [23] to guide the UAVs to track a target. This Lyapunov vector field is firstly designed to achieve stationary target tracking without background wind, and further this vector field is modified to achieve moving target tracking in the presence of background wind. The performance of this approach for the case with unknown constant velocities of target motion and wind is also analyzed to demonstrate the robustness of the

approach. In [9], general techniques for constructing vector fields for UAVs are provided. By using the vector field as motion primitive, it enables decisions to be moved to higher level in the control hierarchy and simplifies the construction of more complex behavior. Based on the work in [23], Summers et al. [31] provided a formal proof for heading and standoff radius convergence with heading error located in the second and third quadrants. In [33], a dynamic path planning algorithm is proposed for UAV tracking, and tangent vector field is used to generate a minimum-time path for UAVs. As an extension of the work in [33], a modified dynamic path-planning algorithm in [34] and [35] is proposed for routing UAVs to track ground targets based on a combination of tangent vector field guidance and Lyapunov vector field guidance.

In practice, background wind is usually inevitable, and is commonly 20%-60% of the desired airspeed of the UAVs [19]. Meanwhile, the target motion also has to be considered, especially for the adversarial target tracking. In [31], Summers et al. proposed an adaptive estimation approach to estimate the unknown target motion and background wind using a variable airspeed controller under the assumption that the initial heading error is zero. Another adaptive control approach is also proposed in [36] to achieve standoff target tracking in the presence of unknown background wind and target motion. In this approach, a variable heading rate controller is utilized while the airspeed is held constant. However, the heading rate input constraint is not taken into account.

All the above target tracking approaches drive the UAV to achieve a desired circular orbit. However, none of these approaches explicitly considers exposure avoidance of the UAV to the adversarial target. The adversarial target can be treated as an obstacle or a threat zone. Obstacle avoidance has been a topic of great interest for many years, and several approaches have been proposed for this problem, such as potential field approaches [37,38], barrier Lyapunov function [39], optimal

approaches,etc. During target tracking, whether the UAV can avoid exposure to the target depends on its initial state. When the UAV can avoid exposure to the target, the target can be treated as an obstacle. However, when the UAV can not avoid exposure to the target, the area around the target can be treated as a threat zone. Thus, the aim of the controller design is to minimize the exposure time of the UAV to the adversarial target. In [40], the target is located at the radar detection zone, and an optimal approach based on Mixed Integer Linear Programming (MILP) is proposed to optimize the trajectory for UAVs. In [41], the UAV needs to fly over a threat zone to reach the target within a specified time. Then, bicriteria optimization is used to explore the tradeoff between flying time and risk. For the UAV with constant airspeed, minimizing the exposure time is equivalent to minimizing the path length in the threat zone. In [42], the problem of finding the minimum arc-length path between two points for Dubins vehicle is formulated and studied by Dubins. This problem has been extensively studied using optimal control theory in [43] [44]. The above researches focus on minimizing the path between two points. However, how to find the minimum path in the threat zone for the UAV is still an open question. Recently, an optimal approach to finding the maximum path in the circle for UAVs is proposed in [45] to provide convoy protection to ground vehicles.

1.2.2 Source Seeking

The purpose of source seeking is to find the source in the unknown environment based on the source field measurement. The field generated by the unknown source could be vector field or scalar field, and in this thesis, scalar field source seeking is the research issue of interest.

Many different approaches have been proposed to address the problem of source seeking in the literature. These works can mainly be classified into two categories: single-agent source seeking, and multi-agent source seeking. For single-agent source

seeking, if the gradient of the scalar field can be directly measured, then source localization or seeking can be achieved by adopting a simple gradient climbing strategy. However, most agents can only measure the scalar field value instead of the gradient. In order to estimate the scalar field gradient, one commonly used method is to maneuver the robot with sinusoidal inputs [46,47]. An angular velocity controller for a nonholonomic agent without position information is proposed to achieve source seeking in [46], while the forward speed is constant. In contrast, in [47], the forward speed is tuned to achieve source seeking with constant angular velocity. In [48], as an extension of [46], a 3-D source seeking approach is proposed. Two control schemes are designed for the underactuated 3-D vehicles to converge to the source.

Recently, a sliding mode based method is introduced to seek the source in [49], where the field value and its change rate at the current location of the mobile robot are required to be known. The proposed sliding mode based turning rate controller can drive the robot to the desired vicinity of the field maximizer in a finite time and afterwards the robot remains in this region. A target following result is presented in [50], where a sliding mode controller similar to that in [49] is designed to guide the robot to asymptotically converge to the desired distance to the target. However, since the change rate of the field value is required in both [49] and [50], the measurement noise may result in a significant error in the computation. In [51], a stochastic source seeking approach is proposed for the nonholonomic mobile robot to converge to the unknown source. Firstly, a stochastic trajectory is generated by extending simultaneous perturbation stochastic approximation technique, and then a simple source seeking controller is designed to follow this trajectory so that switching source seeking is achieved.

Another way to achieve source seeking is to use multiple robots. Multi-robot cooperation for source seeking has several advantages over single robot, such as higher

precision, faster convergence and more robust performance. There also has been a large body of research works in this area in the literature. In [52], a stable cooperative control strategy for mobile sensor networks is proposed to achieve gradient climbing in a sensed and distributed environment. Formation stabilization and gradient climbing are decoupled in the proposed control strategy so that these two tasks can be dealt with separately. Moreover, an approach to estimate the gradient at the center of virtual body is also developed. In [53], a provably convergent cooperative Kalman filter is designed to estimate the gradient at the center of the formation. A geometric approach is adopted to design formation controllers, where the formation shape and orientation dynamics can be decoupled from the dynamics of the formation center based on the Jacobi transformation. However, the proposed control strategies in the above two papers are based on double integrator dynamics and therefore can not be directly applied to UAV control due to the physical constraints of the fixed-wing UAV, such as nonholonomic property. A nonlinear filter is proposed in [54] for target tracking with range measurement only. Based on the measured range, the proposed nonlinear filter is used to estimate the position, velocity and acceleration of the target. However, this approach is not applicable to the problem of unknown scalar field source seeking since the structure of the field distribution is unknown.

In [55], a gradient climbing problem to steer a group of vehicles to the extremum of an unknown scalar field distribution is studied. In this paper, the leader is first used to estimate the gradient by dithering its position, and after that the leader is controlled to achieve gradient climbing. The followers are controlled to follow the leader by using passivity based coordination rules. It is worth noting that the gradient is estimated by the leader only in this paper. In [56], the problem of multiagent deployment over a source is explored. Based on the heat partial differential equation and extremum seeking, a source seeking control algorithm is designed to

deploy the group of agents around the source. In [57–59], vision-based geolocation using multiple UAVs is studied, where information filters are used to estimate the target position. Recently, communication constraints are taken into account for source seeking by several researchers. In [60], distributed source seeking is studied subject to all-to all and limited communication. Based on the gradient estimated by the group of robots, a cooperative controller is proposed to achieve source seeking, and furthermore, the theoretical upper bound on the tracking error is provided as well. In [61], collaborative estimation of gradient by a formation of AUVs under communication constraints is discussed. Under the assumption that the formation is fixed, the proposed consensus approach can achieve exact gradient estimation. In [62], a circular formation of UAVs are used to achieve source seeking. In order to approximate the gradient direction, the UAVs are required to be evenly separated on the circle. Variable airspeed and heading rate controllers are designed to attain such formation. However, the requirement of equal space separation constrains the motion of formation center so that the convergence rate may be slow. Most of the above works assume that the sources or targets are stationary. In practice, there also exist many moving scalar field sources, such as acoustic signal on a moving vehicle.

1.2.3 Formation Control

Advances in sensing, communication and control systems have made it possible for multiple agents to cooperatively complete missions. Among all cooperation scenarios, formation control becomes an active research topic in the past decade due to its broad applications. Numerous studies in formation control have been made on many issues such as formation stability [63–65], controllability of different formation topologies [66–70], formation safety and uncertainty [71]. In general, there are two kinds of formation control problems: formation regulation and formation track-

ing [72]. Various control approaches have been proposed to solve the problems of formation control in terms of different applications. Roughly, these approaches can be classified into three categories: leader-follower, behavior-based, virtual structure.

In leader-follower approach, some agents are designated as leaders which move along a predefined trajectory, while the other agents are designated as followers which maintain a desired distance and orientation to the leader. In [73], a navigation strategy based on nearest neighbor tracking is proposed for a fleet of mobile robots to move in a desired formation pattern. In [74], under the assumption that only local sensor information is available for each robot, two types of feedback controller are proposed to maintain formations of multiple robots. The leader-follower structure is also used in coordinated target tracking control [31]. In this paper, the target is considered as the leader, one of the engaging UAVs is designated as the first follower which is forced to orbit around the target with a desired distance, and then the other UAVs as the second followers are responsible to orbit around the target and maintain the desired angular spacing with the neighboring UAV ahead of them. In addition, a vector field approach is introduced to guide the behavior of the single UAV, and rigid graph theory is adopted to study the information architecture in the formation. Recently, a leader-follower formation control strategy which accounts for input constraints is proposed in [75]. In this paper, by restricting the set of leader possible paths and admissible positions of follower with respect to the leader, the control input of the follower satisfies the input constraints. Meanwhile, the follower position with respect to the leader is not fixed, and varies in proper circle arcs centered at the leader. Although the leader-follower approach is intuitive and easy to implement, there exist some disadvantages. For instance, mission success depends heavily on the leader, i.e., the failure of leader will lead to the mission failure.

The behavior-based approach is a decentralized implementation and generally several behaviors are prescribed for each agent. In behavioral approach, the final control

action is a weighted average of the control for each behavior quantified by potential function. In [76], formation behaviors are combined with other navigational behaviors so that navigational goals, hazard avoidance and formation keeping are simultaneously achieved . In [15], a behavior-based approach is proposed to carry out formation maneuvers for groups of mobile robots. In this approach, instead of the inertial position, the hand position of mobile robot is controlled, and the nonholonomic system is transformed to double integrator system by using output feedback linearization. Two error functions are defined for the competing behaviors which are to move the robot to the desired destination as specified in the formation pattern and to maintain formation during transition. Three behavioral strategies which include saturated control are presented to achieve formation maneuvers. However, utilization of hand position results in that the heading of mobile robot is uncontrolled. Meanwhile, the saturated control for mobile robot is also not applicable for the fixed-wing UAV due to the allowance of negative velocity in mobile robot control. In addition, the behavioral approach is difficult to guarantee precise formation keeping during maneuvers.

The third approach of formation control is virtual structure approach. The concept of virtual structure is first introduced in [77] to achieve high precision formation control of mobile robots. In [78], a general centralized coordination architecture based on the virtual structure approach is proposed to achieve the spacecraft formation control. It is easy to prescribe formation maneuvers using virtual structure approach, but there is no feedback from spacecraft to the virtual structure. Based on the work in [78], [79] presented a decentralized control architecture for spacecraft formation flying. In addition, the formation feedback is included from spacecraft to the virtual structure via the virtual structure instantiation. In [70], formation error is defined by a Lyapunov formation function based on virtual structure, and formation feedback is incorporated to the virtual leaders through parameterized trajectories.

Following the idea in [70], in [80], a group of satisficing control laws for formation control of mobile robots are derived by combining Lyapunov formation function approach with the satisficing control paradigm. In [81], virtual structure and artificial potential field based strategies are integrated to realize formation tracking control for a team of unicycles with collision avoidance property. In [82], an approach to 3D formation tracking control for the UAVs based on virtual structure is proposed. With a suitable structure's speed and small feedback gains, the control inputs satisfy the input constraints of the UAVs. However, there is no formation feedback from the UAVs to the virtual structure and only local stability has been provided as well. A constructive method to design output feedback cooperative controllers is presented in [83] to force a group of mobile robots to perform desired formation tracking with limited sensing range. In this approach, an interlaced observer is designed to estimate the unmeasured robot velocities and a novel potential function is designed to avoid collision between robots.

As each of the above three control strategies has its advantages and disadvantages, there are many approaches combining two or more of these strategies, see, for example, [81,83]. There are also many other approaches used for formation control. The rigid graph theory is used to study the characteristics of 2D and 3D formations in [84–87]. In [88], passivity is used as a design tool to achieve group coordination. In [89], model predictive control (MPC) approach is used to achieve leader-follower based formation flight. In this approach, a cost function for the formation flight control is obtained and the input and output constraints are also considered. Collective motion of multiple Newtonian particles in time invariant flowfield is studied in [90], where heading rate controller is designed for each agent to achieve circular formation. Later, following the paper [90], collective motion of multiple Newtonian particles in time varying flowfield is studied in [91,92].

1.3 Contributions

This thesis focuses on the control problems of target tracking and source seeking using UAVs. Input constraints of the UAV due to its inherent properties are taken into account through the whole thesis. The major contributions of the thesis are as follows:

1. Ground target tracking using a single UAV with control input constraints is achieved. As compared with the existing works, control input saturation is explicitly taken into account based on a guidance law. A rigorous theoretical proof for global convergence by using the proposed saturated controller is provided. This proof shows that the UAV with an arbitrary initial state can asymptotically converge to a desired circular orbit around the target. A bounded adaptive observer is developed to estimate unknown constant background wind and target motion. The boundedness of the estimate allows the integration of the observer and the saturated controller.

2. The problem of adversarial ground target tracking using a single UAV with input constraints is solved. By considering the initial conditions and the inherent properties of the UAV, two task scenarios are analyzed and defined: avoiding exposure to the target and minimizing the exposure time. Most works in the literature focus on one of these two scenarios. In this thesis, a unified bang-bang controller for both scenarios is designed to achieve adversarial ground target tracking. The proposed controller can guarantee the UAV to achieve the desired circular tracking around the target while avoiding exposure to the target or minimizing the exposure time.

3. Cooperative control for multiple UAVs is developed to achieve target tracking. Based on the guidance law, the heading rate controller and airspeed controller of UAVs can be decoupled and designed separately. While there

exist background wind and target movement, it may not be able to distribute UAVs around the target with a specific spacial separation due to the UAV input constraints. Thus, a new notion called temporal phase is introduced to represent the temporal separation. Then, a cooperative control strategy is proposed to achieve the desired temporal separation and the stability proof is also provided.

4. The problem of unknown moving scalar field source seeking using multiple UAVs is investigated. A leader-follower control strategy is proposed to achieve circular formation flight, where heading rate controller for each follower UAV is developed. The cooperation of multiple UAVs in the circular formation allows the leader UAV to estimate the gradient of the scalar field and the source velocity. Based on the estimated gradient and source velocity, a level tracking guidance law is designed for the leader UAV. In order for the leader to follow the guidance law, a sliding mode based heading rate controller is designed. As compared with the gradient climbing approach proposed in the literature, level tracking in a circular formation has the following two advantages: the fixed-wing UAV constraints can be taken into account so that feasible UAV commands can be obtained; UAVs can avoid to be too close to the hazardous source. The gradient estimation error and its influence on moving source velocity estimation and level tracking accuracy are also explored.

1.4 Organization of The Thesis

The remainder of this thesis is organized as follows:

Chapter 2: UAV dynamics model is introduced. Mathematical preliminary is briefly provided.

Chapter 3: A guidance law is introduced and analyzed. Based on the guidance

law, a saturated heading rate controller is proposed, and the complete proof for the convergence of the UAV to the desired circular orbit is provided. An adaptive observer for unknown wind and target motion is developed. Simulation results are provided to illustrate the proposed approach.

Chapter 4: A bang-bang heading rate controller is proposed to achieve the desired circular tracking around the target while avoiding exposure of the UAV to the target or minimizing the exposure time.

Chapter 5: A new notion called temporal phase is proposed to represent the temporal separation. Based on this notion, a cooperative control strategy is proposed to achieve temporal separation of UAVs while tracking a moving target. In addition, the stability proof of target tracking with multiple UAVs is provided.

Chapter 6: Moving source seeking problem is solved in this chapter. Leader-follower formation strategy is adopted for multi-UAV cooperation. The scalar field gradient and the source velocity are estimated. Heading rate controllers for all UAVs are proposed to achieve source seeking. The gradient estimation error is analyzed and its influence on moving source velocity estimation and level tracking accuracy is explored as well.

Chapter 7: Conclusions are given and future works are recommended.

Chapter 2

System Modeling and Preliminaries

In this chapter, UAV kinematics and relative motions with respect to target are provided and analyzed. Several basic control theorems used in this thesis are also briefly introduced.

2.1 UAV Kinematics

This thesis considers the control problems of fixed-wing UAVs. It is assumed that UAVs are equipped with low level flight control systems including attitude hold, velocity hold and heading rate hold autopilots. In addition, the altitude of the UAV is held constant. Then, the kinematics of the UAV is simplified into 2-D form [93,94] as follows:

$$\begin{aligned} \dot{x} &= v\cos\psi \\ \dot{y} &= v\sin\psi \\ \dot{\psi} &= u \end{aligned} \tag{2.1}$$

where, as illustrated in Fig. 2.1, $(x, y) \in \mathbf{R}^2$ is the two-dimensional position of the fixed-wing UAV in the inertial frame, $\psi \in [-\pi, \pi)$ is the UAV heading which is the

angle between the UAV direction and the x axis of the inertial frame, and v, u are the two control input signals which are airspeed and heading rate respectively.

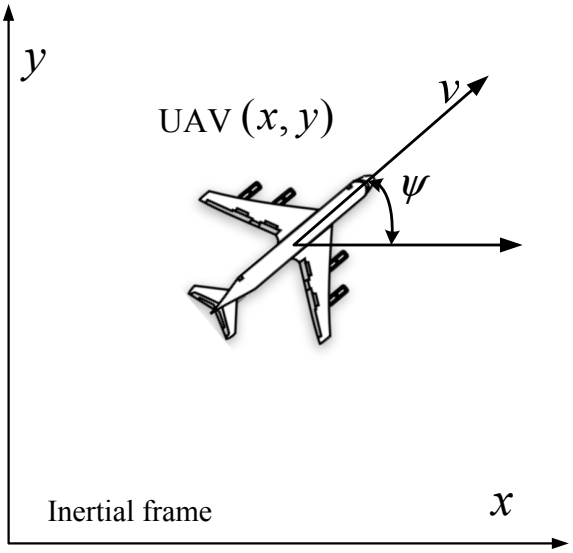

Figure 2.1: UAV kinematics

Remark 2.1: In reality, the response of the low level autopilot to the airspeed command may not be instantaneous [10]. However, when the airspeed command is constant or slowly varying in time, the transient response of the airspeed autopilot is quick enough with respect to the high level dynamics. Therefore, it is reasonable to assume that when the airspeed command is constant or slowly varying in time, it can be held. By decoupling the altitude dynamics, altitude autopilot can be designed to hold the UAV altitude independently. Since the UAV altitude can be controlled independently, a suitable altitude can be chosen for ground target tracking. UAV heading rate is actually determined by the roll angle and the airspeed, and roll motion system needs to take some time to response to the command. Thus, heading rate command can not be implemented instantaneously. However, on the one hand, the nonlinear relationship between UAV heading rate and roll angle makes system analysis and controller design very complicated; on the other hand, the UAV model with heading rate as the control input captures the essential kinematics of the UAV motion [29]. Hence, 2-D UAV model (2.1) is used in this thesis. Although roll

motion is not taken into account in the analysis, it is involved in the simulation to verify the developed approaches.

Due to the stall condition and thrust limitation [10,11], the airspeed of the UAV could be neither too slow nor too fast. It is also well known that the heading rate depends on the roll angle of the UAV. While the airspeed is constant, large roll angle results in a fast heading rate. However, too large roll angle may lead to UAV flipping. Therefore, the following input constraints should be enforced on the UAV

$$0 < v_{min} \leq v \leq v_{max}; |u| \leq \omega_{max}. \tag{2.2}$$

Remark 2.2: it can be noted that the airspeed should not be zero or negative, so that many control approaches for mobile robots cannot be directly applied to UAVs. It is well known that the heading rate also depends on the airspeed, however, to simplify the problem, constant heading rate constraint is used in this thesis. If the airspeed is constant, there also exists a minimum turning radius.

2.2 Relative Motion

In the previous section, the UAV kinematic model is introduced. In order to design controllers for target tracking and source seeking, relative motion of the UAV with respect to the target or source needs to be provided as well. The relative motion without background wind is expressed as follows:

$$\begin{aligned} \dot{x}_r &= v\cos\psi - \dot{x}_t \\ \dot{y}_r &= v\sin\psi - \dot{y}_t \\ \dot{\psi} &= u \end{aligned} \tag{2.3}$$

where, $(x_r, y_r) \in \mathbf{R}^2$ is the relative position of the fixed-wing UAV with respect to the target, $(\dot{x}_t, \dot{y}_t) \in \mathbf{R}^2$ is the target velocity.

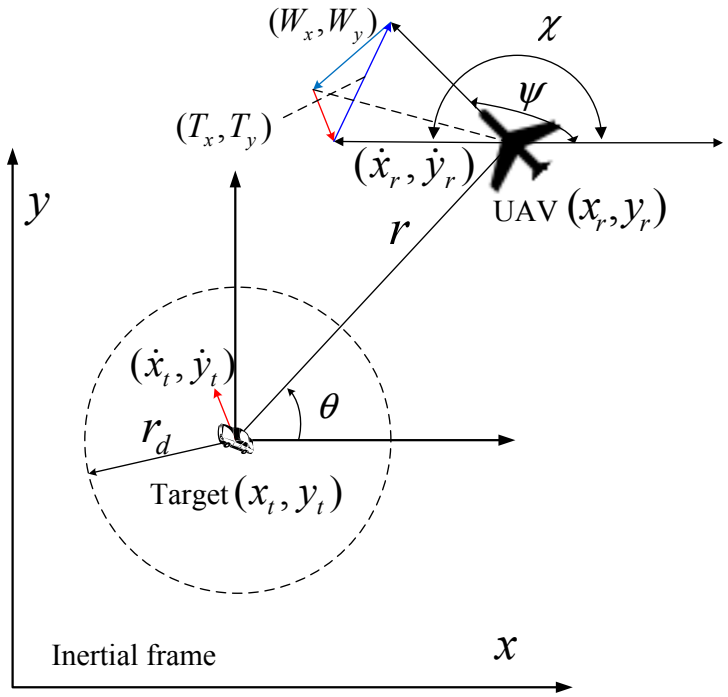

Figure 2.2: Geometry of ground target tracking in wind.

In practice, background wind is usually inevitable, and strong wind may significantly affect the target tracking mission. Therefore, it is necessary to take into account background wind during the controller design. The relative motion in the presence of background wind is given by the following equations:

$$\begin{aligned} \dot{x}_r &= v\cos\psi + W_x - \dot{x}_t \\ \dot{y}_r &= v\sin\psi + W_y - \dot{y}_t \\ \dot{\psi} &= u \end{aligned} \tag{2.4}$$

where, $(W_x, W_y) \in \mathbf{R}^2$ is the background wind velocity.

Note that from the relative motion (2.4), target velocity and background wind velocity affect the UAV relative motion in the same way. For the sake of simplicity, these two velocities can be combined to a single velocity term $(T_x, T_y) = (\dot{x}_t - W_x, \dot{y}_t - W_y)$ (see Fig. 2.2) which is called moving target velocity [23] in this thesis.

The relative motion of the UAV can be rewritten as

$$\dot{x}_r = v\cos\psi - T_x, \dot{y}_r = v\sin\psi - T_y, \dot{\psi} = u. \tag{2.5}$$

If the airspeed is held constant, i.e. $v = v_0$, as well as the moving target velocity is constant and slower than the airspeed, i.e. $T_x^2 + T_y^2 < v_0^2$. By combining the moving target velocity with the airspeed, the following relative motion model is obtained:

$$\dot{x}_r = v_r\cos\chi, \dot{y}_r = v_r\sin\chi, \dot{\chi} = \lambda_u(\psi)u \tag{2.6}$$

where, as illustrated in Fig. 2.2, χ denotes the relative course angle, v_r denotes the relative speed, and

$$\begin{aligned} v_r &= (v_0^2 + T_x^2 + T_y^2 - 2v_0(T_x\cos\psi + T_y\sin\psi))^{\frac{1}{2}}, \\ \chi &= \arctan 2(v_0\sin\psi - T_y, v_0\cos\psi - T_x), \\ \lambda_u(\psi) &= \frac{v_0^2 - v_0(T_x\cos\psi + T_y\sin\psi)}{v_r^2} \geq \frac{1}{2}. \end{aligned}$$

The relative motion model (2.6) can also be expressed in polar coordinates as

$$\begin{bmatrix} \dot{r} \\ r\dot{\theta} \end{bmatrix} = \begin{bmatrix} \dot{x}_r\cos\theta + \dot{y}_r\sin\theta \\ -\dot{x}_r\sin\theta + \dot{y}_r\cos\theta \end{bmatrix} = \begin{bmatrix} v_r\cos(\chi - \theta) \\ v_r\sin(\chi - \theta) \end{bmatrix} \tag{2.7}$$

where $r = (x_r^2 + y_r^2)^{\frac{1}{2}}$ is the horizontal distance between the UAV and the target, and θ is the clock angle (see Fig. 2.2).

2.3 Preliminaries

In this section, several definitions and theorems are introduced, which will be used in this thesis.

LaSalle's Invariance Principle

First, consider the following system:

$$\dot{x} = F(x), x(t_0) = x_0, \tag{2.8}$$

where $F : D \to \mathbf{R}^n$ is a locally Lipschitz function defined over a domain $D \subset \mathbf{R}^n$.

Definition 2.1 [95] (Invariant Set) A set $\mathbb{C} \in \mathbf{R}^n$ is an invariant set for a dynamic system (2.8), if every trajectory of the system (2.8) starting in $\mathbb{C}$ remains in $\mathbb{C}$ for all future and past time, i.e.,

$$x(0) \in \mathbb{C} \Rightarrow x(t) \in \mathbb{C}, \forall t \in \mathbf{R}. \tag{2.9}$$

Definition 2.2 [95] (Positively Invariant Set) A set $\mathbb{C} \in \mathbf{R}^n$ is a positively invariant set for a dynamic system (2.8), if every trajectory of the system (2.8) starting in $\mathbb{C}$ remains in $\mathbb{C}$ for all future time, i.e.,

$$x(0) \in \mathbb{C} \Rightarrow x(t) \in \mathbb{C}, \forall t \geq 0. \tag{2.10}$$

Theorem 2.1 [95] (LaSalle's Invariance Principle) Let $\Omega \subset \mathbb{C}$ be a compact set that is positively invariant with respect to the dynamics (2.8). Let $V(x)$ be a continuously differentiable function on $\mathbb{C}$ such that $\dot{V}(x) \leq 0$ in Ω. Let E be the set of all points in Ω where $\dot{V}(x) = 0$ and let M be the largest invariant set contained in E. Then every solution starting in Ω converges to M as $t \to \infty$. If $V(x) > 0$ and $M = 0$, then the origin 0 is asymptotically stable.

Barbalat's Lemma

Lemma 2.1 [96] (Barbalat's Lemma) Suppose $g(t) \in C^1(a, \infty)$ and $\lim_{t\to\infty} g(t) = \alpha$ where $\alpha < \infty$. If $\dot{g}(t)$ is uniformly continuous, then $\lim_{t\to\infty} \dot{g}(t) = 0$.

Corollary 2.1 [96] Suppose $g(t) \in C^1(a, \infty)$ and $\lim_{t\to\infty} g(t) = \alpha$ where $\alpha < \infty$.

If $\ddot{g}(t)$ exists and is bounded, then $\lim_{t\to\infty} \dot{g}(t) = 0$.

Pontryagin's Minimum Principle

In realistic systems, state and control input constraints commonly occur. In such situations, Pontryagin's minimum principle can be used to find the possible optimal control for a dynamical system. According to Pontryagin's minimum principle, the Hamiltonian must be minimized by the optimal control. However, this principle is a necessary condition for optimality, that is, controls that satisfy this principle may not be optimal [97]. Next, the detailed principle will be described.

Consider the following system:

$$\dot{x}(t) = F(x(t), u(t), t), x(0) = x_0, u(t) \in U \subset \mathbf{R}^m \tag{2.11}$$

where $F : \mathbf{R}^n \times \mathbf{R}^m \times \mathbf{R} \to \mathbf{R}^n$ is a function of (x, u, t), $x \in \mathbf{R}^n$ is the system state, u is the control input, U is the admissible control set, and $t \in \mathbf{R}$ is the time. A cost function J is defined as follows:

$$J = Q(x(T_f)) + \int_0^{T_f} g(x(t), u(t), t)dt. \tag{2.12}$$

where $Q(x(T_f)$ is the terminal condition, and T_f is the system terminal time. The Hamiltonian of the optimal control problem is given as:

$$\mathcal{H} = g(x(t), u(t), t) + \lambda^T[F(x(t), u(t), t), x(t_0)]. \tag{2.13}$$

where λ is the costate.

Theorem 2.2 [97] Consider the system (2.11). If the control $u^* \in U$ that causes the system (2.11) to follow an admissible trajectory minimizes the cost function (2.12), in terms of the Hamiltonian (2.13), the necessary conditions for u^* to be an

optimal control are as follows:

$$\dot{x}^* = \frac{\partial \mathcal{H}(x^*(t), u^*(t), \lambda^*(t), t)}{\partial \lambda} = F(x^*(t), u^*(t), t), \tag{2.14}$$

$$\dot{\lambda}^* = -\frac{\partial \mathcal{H}(x^*(t), u^*(t), \lambda^*(t), t)}{\partial x}, \tag{2.15}$$

$$\mathcal{H}(x^*(t), u^*(t), \lambda^*(t), t) \leq \mathcal{H}(x^*(t), u(t), \lambda^*(t), t), \tag{2.16}$$

for all time $t \in [0, T_f]$ and all admissible control $u \in U$,

$$\lambda^*(T_f) = \frac{\partial Q(x^*(T_f)}{\partial x}, \tag{2.17}$$

$$\frac{\partial Q(x^*(T_f))}{\partial t} + \mathcal{H}(x^*(T_f), u^*(T_f), \lambda^*(T_f), T_f) = 0. \tag{2.18}$$

If the Hamiltonian does not depend explicitly on time and the terminal time is free, then the condition (2.18) can be converted to

$$\mathcal{H}(x^*(T_f), u^*(T_f), \lambda^*(T_f)) = 0. \tag{2.19}$$

Asymptotic Stability of Cascade-Connected Systems [98]

Consider the following cascade connected nonlinear systems:

$$\begin{aligned} \dot{x} &= P(x, z) \\ \dot{z} &= Q(z), \end{aligned} \tag{2.20}$$

where $x \in \mathbf{R}^n, z \in \mathbf{R}^m$, $P(0,0) = 0, Q(0) = 0$, P is locally Lipschitz on $\mathbf{R}^n \times \mathbf{R}^m$, and Q is locally Lipschitz on $\mathbf{R}^m$.

Theorem 2.3 [98] (Locally Asymptotic Stability) Consider the system (2.20). Consider the system (2.20). Suppose the equilibrium $x = 0$ of the subsystem $\dot{x} = P(x, 0)$ is locally asymptotically stable and the equilibrium $z = 0$ of the subsystem $\dot{z} = Q(z)$ is locally asymptotically stable. Then, the equilibrium $(x, z) = (0, 0)$ of the system (2.20) is locally asymptotically stable.

Theorem 2.4 [98] (Globally Asymptotic Stability) Consider the system (2.20).

Consider the system (2.20). Suppose the equilibrium $x = 0$ of the subsystem $\dot{x} = P(x, 0)$ is globally asymptotically stable and the equilibrium $z = 0$ of the subsystem $\dot{z} = Q(z)$ is globally asymptotically stable. If the integral curves of the composite system are defined for all $t \geq 0$ and bounded, then the equilibrium $(x, z) = (0, 0)$ of the system (2.20) is globally asymptotically stable.

Chapter 3

Ground Target Tracking with Input Constraints

Ground target tracking is an important application of UAVs, and many control strategies have been developed in the literature. In this chapter, the problem of ground target tracking using a single fixed-wing UAV with control input constraints is studied. Background wind and target motion are also considered during controller design. In the case of unknown constant background wind and target motion, an adaptive observer is developed to guarantee bounded estimate.

3.1 Problem Formulation

In general, the speed of ground target is slower than the fixed-wing UAV or even stationary, so the UAV may not be able to stay on top of the target due to the stall condition. To solve this problem, there are mainly two types of control strategies: non-standoff target tracking and standoff target tracking. In many applications, standoff distance between the UAV and target is required to guarantee sensing and communication, such as convoying a friendly vehicle and monitoring an adversarial target. Lyapunov vector field approaches are proposed in [19,23,31] to generate a

guidance law for target tracking. However, when input constraints and an arbitrary heading error are taken into account, the formal proof for global stability is not provided. In addition, the presence of background wind and target motion significantly affects the target tracking performance if they are not well dealt with during controller design. Although an adaptive estimation approach in [31] is proposed to estimate the velocities of unknown background wind and target motion, the variable airspeed controller and the assumption that the initial heading error is zero limit its applicability.

Motivated by the studies in [19,23,31], this chapter aims to develop a control algorithm to achieve standoff target tracking in the presence of background wind and target motion. Firstly, a guidance law is introduced to generate the desired relative course angle. Based on this guidance law, a saturated heading rate controller, accounting for the physical constraints of the UAV, is proposed to regulate the actual relative course angle to the desired one while the airspeed is held constant. This proposed approach guarantees that the UAV with an arbitrary initial state can asymptotically converge to a desired circular orbit around the target. A rigorous proof for the global stability of target tracking is also provided. In order to estimate unknown constant background wind and target motion, an adaptive observer is developed to guarantee bounded estimate.

3.2 Standoff Target Tracking

Based on the relative motion models described in (2.6) and (2.7), this section is to develop a control strategy to achieve standoff target tracking with a desired distance r_d. The following assumptions are required during control strategy design.

Assumption 3.1*:* The moving target velocity (T_x, T_y) is constant and known.

Assumption 3.2*:* The airspeed of the UAV v is held constant and $v = v_0$.

Remark 3.1: In general, background wind speed and ground target movement are time varying. However, UAV motion is usually much faster so that moving target velocity can be considered as a constant velocity. Thanks to the low level pilot, constant airspeed can be automatically maintained with a quick enough transient response.

3.2.1 Guidance Law

In [23], guidance vector field is utilized to generate a desired velocity for the UAV to track. Since the airspeed is constant, the desired velocity is determined by its direction (UAV heading). If the UAV can always track the desired heading, it will eventually converge to the circular orbit around the designated ground target with a desired distance r_d. Therefore, the desired heading acts as the guidance law. In this section, a guidance law for the relative course is introduced as follows:

$$\chi_d = \theta + \phi \tag{3.1}$$

where $\theta = \begin{cases} \arctan2(y_r, x_r) & \text{if } r > 0 \\ \chi & \text{if } r = 0 \end{cases}$ and $\phi = 2\arctan(\frac{r}{r_d})$.

It can be observed from (3.1)that, when $r \to 0$, the desired relative course approaches the direction away from the target, and when $r \to \infty$, the desired relative course directly points to the target. In addition, the desired relative course is discontinuous at the point $r = 0$, which is exactly on top of the target. It will be shown that if the UAV follows this guidance law, then it will converge to the desired circular orbit asymptotically. Consider the following Lyapunov function candidate

$$V(r) = (r - r_d)^2. \tag{3.2}$$

Differentiating this Lyapunov function leads to the following equation

$$\dot{V} = 2(r - r_d)\dot{r} = -\frac{2v_r(r - r_d)^2(r + r_d)}{r^2 + r_d^2} \leq 0. \tag{3.3}$$

By LaSalle's invariance principle, r asymptotically converges to the desired distance r_d. It is worth noting that the above result is derived under the assumption that the relative course is aligned with the desired relative course generated by the guidance law. However, in general, there exists an angle error between the actual relative course and the desired relative course initially. The relative course error can be defined by

$$\chi_e = \chi - \chi_d \in [-\pi, \pi). \tag{3.4}$$

When $r > 0$, the desired relative course rate can be obtained by taking the derivative of (3.1) as

$$\begin{aligned}\dot{\chi}_d = \dot{\theta} + \dot{\phi} &= \frac{v_r}{r}\sin(\chi - \theta) + \frac{\partial \phi}{\partial r}\dot{r} \\ &= \frac{v_r}{r}[\sin(\chi_e + \phi) + \sin(\phi)\cos(\chi_e + \phi)].\end{aligned} \tag{3.5}$$

It is observed from (3.5) that when $r \to 0$, $\dot{\chi}_d$ may approach infinity while there exists a relative course error. When $r = 0$, the desired relative course rate can not be derived from (3.1). Thus, it needs to define the desired relative course rate at the point $r = 0$ as follows:

$$\dot{\chi}_d = \frac{4v_r}{r_d}. \tag{3.6}$$

In order to guarantee that the desired relative course rate without a relative course error is feasible to track, it is assumed that the maximum heading rate satisfies the following condition:

$$w_{max} \geq \frac{4(v_0 + (T_x^2 + T_y^2)^{\frac{1}{2}})^2}{v_0 r_d}. \tag{3.7}$$

Remark 3.2: Since the maximum heading rate is determined by the physical properties of the UAV such as maximum allowable roll angle, one can choose the desired distance so that the inequality (3.7) is satisfied.

3.2.2 Saturated Controller Design

This section focuses on designing the heading rate controller to achieve ground target tracking. A saturated heading rate controller is proposed and the global convergence of target tracking is rigorously proved.

The proposed guidance law (3.1) provides a desired relative course. In order to make the actual course to follow the desired one, one may design a relative course rate controller such as a PD controller. Then, according to the relative motion model (2.6), the relative course rate can be converted to the corresponding heading rate. Unfortunately, due to the physical constraints of the fixed-wing UAV, the heading rate may reach saturation. Thus, the actual heading rate may not be able to implement the designed relative course rate controller. In this section, instead of designing the relative course rate controller, a new saturated heading rate controller is directly proposed as follows:

$$u = \begin{cases} w & \text{if } |w| \leq w_{max} \\ sgn(w)w_{max} & \text{if } |w| > w_{max} \end{cases} \tag{3.8}$$

where $w = -k\chi_e + \frac{\dot{\chi}_d}{\lambda_u(\psi)}$ and $k > 0$.

It is observed from formula (3.8) that, the proposed controller includes a feedback term and a feedforward term when it is not saturated. It is clear that this controller satisfies the kinematic constraints of the fixed-wing UAV.

3.2.3 Stability Analysis

In this section, it proceeds to prove that the proposed heading rate controller can drive the UAV to follow the guidance law. The airspeed of the UAV is assumed to be constant in this chapter. However, the relative speed v_r varies as the UAV heading changes. Moreover, the variation of the relative speed has a significant influence on the relative course rate. Therefore, the relation between the relative speed and the heading has to be explored. The following lemma is introduced to indicate this relation.

Lemma 3.1: If the moving target velocity is slower than the airspeed, i.e., $v_0^2 \geq T_x^2 + T_y^2$, then $\frac{v_r}{\lambda_u(\psi)} \leq \frac{(v_0+(T_x^2+T_y^2)^{\frac{1}{2}})^2}{v_0}$.

Proof: By assumptions 3.1 and 3.2, the moving target velocity and the airspeed of the UAV are constant. Thus, ψ is the only variable in v_r and $\lambda_u(\psi)$. Let

$$\begin{aligned} F(\psi) &= \frac{v_r}{\lambda_u(\psi)} \\ &= \frac{(v_0^2 + T_x^2 + T_y^2 - 2v_0(T_x\cos\psi + T_y\sin\psi))^{\frac{3}{2}}}{v_0^2 - v_0(T_x\cos\psi + T_y\sin\psi)} \end{aligned}$$

For the sake of simplicity, the following notations are introduced: $T_v = (T_x^2 + T_y^2)^{\frac{1}{2}}$, $\eta = \arctan2(T_x, T_y)$ and $\xi = \sin(\psi + \eta)$. Then $F(\psi)$ can be rewritten as

$$F(\psi) = \frac{(v_0^2 + T_v^2 - 2v_0T_v\xi)^{\frac{3}{2}}}{v_0^2 - v_0T_v\xi} \tag{3.9}$$

By differentiating the function $F(\psi)$ with respect to ξ, it is obtained that

$$F_\xi(\psi) = \frac{v_0T_v(v_0^2 + T_v^2 - 2v_0T_v\xi)^{\frac{1}{2}}(T_v^2 + v_0T_v\xi - 2v_0^2)}{(v_0^2 - v_0T_v\xi)^2}$$

Because $\xi \in [-1, 1]$, it can be observed that $F_\xi(\psi) < 0$. When $\xi = -1$, the function $F(\psi)$ reaches the maximum. Therefore, $F(\psi) \leq \frac{(v_0+T_v)^2}{v_0}$, which completes

the proof of Lemma 3.1.

Remark 3.3: Lemma 3.1 will be used to provide a bound for the relative course rate while the heading rate input constraint is provided.

Next, the performance of the UAV under the proposed controller will be explored.

Firstly, the condition that the UAV locates at the position $r = 0$ at $t = t_0$ needs to be discussed. According to the definition of the guidance law, the relative course error $\chi_e = 0$ when $r = 0$. Moreover, it can be obtained that

$$\begin{aligned}\lim_{t\to t_0^+} \chi_d(t) &= \lim_{t\to t_0^+} \theta + \lim_{r\to 0} \phi = \lim_{t\to t_0^+} \arctan2(y_r, x_r) \\ &= \lim_{t\to t_0^+} \arctan2(\dot{y}_r, \dot{x}_r) = \chi(t_0) = \chi_d(t_0). \end{aligned} \tag{3.10}$$

and when $\chi_e = 0$, the desired relative course rate at $t \geq t_0$:

$$\dot{\chi}_d = \frac{4v_r r_d^3}{(r^2 + r_d^2)^2}. \tag{3.11}$$

Equation (3.10) implies that the desired relative course χ_d is right continuous at $r = 0$ with respect to t. Thus if the relative course rate is chosen as $\dot{\chi} = \dot{\chi}_d$, the UAV will always follow the guidance law, i.e. $\chi = \chi_d$ for $t \geq t_0$. According to Lemma 3.1, the following can be derived

$$u = \frac{\dot{\chi}_d}{\lambda_u(\psi)} = \frac{4v_r r_d^3}{(r^2 + r_d^2)^2 \lambda_u(\psi)} \leq \frac{4(v_0 + T_v)^2}{v_0 r_d}. \tag{3.12}$$

It can be observed from (3.12) that the proposed heading rate controller (3.8) is able to provide the desired relative course rate. Therefore, if the UAV locates at the position $r = 0$ at t_0, the proposed heading rate controller will guarantee the UAV to follow the guidance law for $t > t_0$, which in turn implies that the UAV will converge to the desired circular orbit.

Now, it is ready to consider the condition that the UAV locates at the position

$r > 0$. Since $\dot{\chi}_d$ is the feedforward term of the heading rate controller, it is necessary to analyze its property. It is noted from (3.5) that, the desired relative course rate is related to the relative course error. The following lemma will study this relation and provide bounds for the desired relative course rate.

Lemma 3.2: For the system given by (2.6) and the guidance law given by (3.1), there exists a positive constant $k_1 > 0$ such that,

$$\dot{\chi}_d \leq \lambda_u(\psi) w_{max} + k_1 \sin\chi_e, \quad \chi_e \in [-\pi, 0) \tag{3.13}$$

$$\text{and } \dot{\chi}_d \geq -\lambda_u(\psi) w_{max} + k_1 \sin\chi_e, \quad \chi_e \in [0, \pi) \tag{3.14}$$

Proof: According to Lemma 3.1 and the maximum heading rate (3.7), the following inequality can be obtained.

$$\lambda_u(\psi) w_{max} \geq \frac{4(v_0 + T_v)^2 \lambda_u(\psi)}{v_0 r_d} \geq \frac{4v_r}{r_d}$$

The proof will be discussed in two cases in terms of the relative course error.

Case 1: $\chi_e \in [0, \pi)$

When $\chi_e = 0$, $\dot{\chi}_d = \frac{4v_0 r_d^3}{(r^2+r_d^2)^2} \geq -\lambda_u(\psi) w_{max} + k_1 \sin\chi_e$, which implies that k_1 can be any positive constant.

When $\chi_e \in (0, \pi)$, $F(\chi_e, r)$ is defined as follows:

$$\begin{aligned} F(\chi_e, r) &= \frac{1}{\sin\chi_e}\left(\dot{\chi}_d + \frac{4v_r}{r_d}\right) \\ &= \frac{1}{\sin\chi_e}\left\{\frac{v_r}{r}[\sin(\phi+\chi_e) + \sin\phi\cos(\phi+\chi_e)] + \frac{4v_r}{r_d}\right\}. \end{aligned}$$

If $F(\chi_e, r)$ has a positive lower bound, it implies that there exists a positive constant k_1 which makes the inequality (3.14) hold. Next, $F(\chi_e, r)$ is shown to have a positive lower bound. By partially differentiating the function $F(\chi_e, r)$ with respect

to χ_e, it yields that

$$\frac{\partial F(\chi_e, r)}{\partial \chi_e} = \frac{-4v_r r_d^3}{(r^2 + r_d^2)^2 \sin^2 \chi_e} + \frac{-4v_r \cot \chi_e}{r_d \sin \chi_e} \tag{3.15}$$

It is noted from (3.15) that, when $\cos \chi_e = \frac{-r_d^4}{(r^2+r_d^2)^2}$, $F(\chi_e, r)$ reaches its minimum value with respect to χ_e. Then the following inequality can be obtained.

$$\begin{aligned} F(\chi_e, r) &\geq F(\chi_e, r)|_{\cos \chi_e = \frac{-r_d^4}{(r^2+r_d^2)^2}} \\ &\geq \frac{v_r}{r}\left[\frac{r_d^4 - r^4 - 4r^2 r_d^2}{(r^2 + r_d^2)^2}\right] + \frac{4v_r}{r_d}\left[1 - \frac{r_d^8}{(r^2 + r_d^2)^4}\right]^{\frac{1}{2}} \\ &\geq \frac{v_r}{r_d}\left[\frac{r_d^5 - r^4 r_d - 4r^2 r_d^3}{r(r^2 + r_d^2)^2} + \frac{4(r^4 + 2r_d^2 r^2)}{(r^2 + r_d^2)^2}\right] \\ &= \frac{v_r}{r_d}\left[1 + \frac{r_d^5 - r_d^4 r - 4r_d^3 r^2 + 6r_d^2 r^3 - r_d r^4 + 3r^5}{r(r^2 + r_d^2)^2}\right] \end{aligned}$$

For the sake of simplicity, let $x = \frac{r}{r_d} > 0$, and it yields that

$$\begin{aligned} F(\chi_e, r) &\geq F(x) \\ &= \frac{v_r}{r_d}\left[1 + \frac{1 - x - 4x^2 + 6x^3 - x^4 + 3x^5}{x(x^2 + 1)^2}\right] \\ &> \frac{v_r}{r_d} > 0 \end{aligned}$$

Thus, there exists a positive constant $0 < k_1 \leq min\left\{\frac{v_r}{r_d}\right\}$ such that the inequality (3.14) holds.

Case 2: $\chi_e \in [-\pi, 0)$

The proof for this case is similar to the former case. In order to simplify the proof procedure, the following function is defined:

$$g(\chi_e) = \begin{cases} \dot{\chi}_d - \lambda_u(\psi) w_{max} - k_1 \sin \chi_e, \ \chi_e \in [-\pi, 0) \\ \dot{\chi}_d + \lambda_u(\psi) w_{max} - k_1 \sin \chi_e, \ \chi_e \in [0, \pi) \end{cases} \tag{3.16}$$

It is noted from (3.16) that $g(\chi_e) = -g(\chi_e + \pi)$ when $\chi_e \in [-\pi, 0)$. Moreover, according to the result of the case 1, it can be derived that

$$g(\chi_e) = \dot{\chi}_d + \lambda_u(\psi) w_{max} - k_1 \sin \chi_e \geq 0, \;\; \chi_e \in [0, \pi).$$

If $\chi_e \in [-\pi, 0)$, then $\chi_e + \pi \in [0, \pi)$. With the function (3.16), it yields that

$$g(\chi_e) = \dot{\chi}_d - \lambda_u(\psi) w_{max} - k_1 \sin \chi_e = -g(\chi_e + \pi) \leq 0,$$

which implies that the inequality (3.13) holds. Thus, the proof for this lemma is completed.

Remark 3.4: Lemma 3.2 analyzes the property of the desired relative course rate. Based on this analysis, the convergence of the relative course angle to the desired relative course under the proposed heading rate controller will be investigated in the sequel.

Lemma 3.3: If the control law (3.8) is applied to the system (2.6), there exists a positive constant $k_2 > 0$ with $k_2 \leq \frac{k}{2}$ and $k_2 \leq k_1$ such that

$$\dot{\chi}_e \geq -k_2 \sin \chi_e, \chi_e \in [-\pi, 0); \dot{\chi}_e \leq -k_2 \sin \chi_e, \chi_e \in [0, \pi).$$

Proof: According to the definition of χ_e, the derivative of the relative course error can be obtained by

$$\dot{\chi}_e = \dot{\chi} - \dot{\chi}_d. \tag{3.17}$$

The heading rate controller (3.8) is transformed to the constrained relative course

rate controller.

$$\begin{aligned}\dot{\chi} &= \lambda_u(\psi)\dot{\psi} \\ &= \begin{cases} \Omega & \text{if } |\Omega| \le \lambda_u(\psi)w_{max} \\ sgn(\Omega)\lambda_u(\psi)w_{max} & \text{if } |\Omega| > \lambda_u(\psi)w_{max} \end{cases}\end{aligned} \tag{3.18}$$

where $\Omega = -k\lambda_u(\psi)\chi_e + \dot{\chi}_d$. By combining the result of Lemma 3.2 and the constrained relative course rate controller (3.18), the proof of Lemma 3.3 is given as follows:

Case 1: $\chi_e \in [-\pi, 0)$

If $-k\lambda_u(\psi)\chi_e + \dot{\chi}_d > \lambda_u(\psi)w_{max}$,

$\dot{\chi}_e = \lambda_u(\psi)w_{max} - \dot{\chi}_d \ge -k_1 \sin\chi_e \ge -k_2 \sin\chi_e$;

else if $-k\lambda_u(\psi)\chi_e + \dot{\chi}_d < -\lambda_u(\psi)w_{max}$,

$\dot{\chi}_e = -\lambda_u(\psi)w_{max} - \dot{\chi}_d \ge -k\lambda_u(\psi)\chi_e \ge -k_2 \sin\chi_e$;

else $|-k\lambda_u(\psi)\chi_e + \dot{\chi}_d| \le \lambda_u(\psi)w_{max}$,

$\dot{\chi}_e = -k\lambda_u(\psi)\chi_e \ge -k_2 \sin\chi_e$.

Case 2: $\chi_e \in [0, \pi)$

If $-k\lambda_u(\psi)\chi_e + \dot{\chi}_d > \lambda_u(\psi)w_{max}$,

$\dot{\chi}_e = \lambda_u(\psi)w_{max} - \dot{\chi}_d < -k\lambda_u(\psi)\chi_e \le -k_2 \sin\chi_e$;

else if $-k\lambda_u(\psi)\chi_e + \dot{\chi}_d < -\lambda_u(\psi)w_{max}$,

$\dot{\chi}_e = -\lambda_u(\psi)w_{max} - \dot{\chi}_d \le -k_1 \sin\chi_e \le -k_2 \sin\chi_e$;

else $|-k\lambda_u(\psi)\chi_e + \dot{\chi}_d| \le \lambda_u(\psi)w_{max}$,

$\dot{\chi}_e = -k\lambda_u(\psi)\chi_e \le -k_2 \sin\chi_e$.

Remark 3.5: Lemma 3.3 provides a slowest convergence rate bound for the relative course error. In practice, the convergence rate may be much faster than this given rate. For example, when $\chi_e = -\pi$, it can be computed from (3.5) that $\dot{\chi}_d = -\frac{4v_r r_d^3}{(r^2+r_d^2)^2}$ and $\dot{\chi}_e = min\left\{k\lambda_u(\psi)\pi, \lambda_u(\psi)w_{max} + \frac{4v_r r_d^3}{(r^2+r_d^2)^2}\right\} > 0$ according to

the proof of Lemma 3.3.

Lemma 3.3 shows that the relative course error will asymptotically converge to zero. However, the time when the relative course error converges to zero has not been determined. In addition, the problem that whether the distance between the UAV and the target will approach infinity while the relative course error converges to zero needs to be discussed. Therefore, the following lemma is introduced to determine the bound of the distance r.

Lemma 3.4: Given an initial relative course error $\chi_{e0} \in (-\pi, \pi)$, if the control law (3.8) is applied to the system (2.6), the distance r in (2.7) has an upper bound r_{sup}, where

$$r_{sup} = r_0 + \frac{v_0 + T_v}{k_2} \ln \left| \frac{\tan(\frac{\chi_{e0}}{2})}{\tan(\frac{\phi_0}{2} - \frac{\pi}{4})} \right|.$$

Proof: It is noted from Lemma 3.3 that, for $\chi_{e0} \in (-\pi, \pi)$, the relative course error χ_e varies according to the following inequality:

$$\left| \tan\left(\frac{\chi_e}{2}\right) \right| \leq \left| \tan\left(\frac{\chi_{e0}}{2}\right) \right| e^{-k_2 t}. \tag{3.19}$$

Case 1: $|\chi_{e0}| \in [0, \frac{\pi}{2}]$

It is assumed that the initial distance $r_0 > r_d$. If $r > r_d$ and $\chi_{e0} \in [0, \frac{\pi}{2}]$, $\cos(\phi + \chi_e) < 0$. Then it is observed from (2.7) that $r < r_0$. If $\chi_{e0} \in [-\frac{\pi}{2}, 0]$, it can be derived from (3.19) that r has an upper bound as follows:

$$r \leq (v_0 + T_v)t_1 + r_0. \tag{3.20}$$

where $t_1 = \frac{1}{k_2} \ln \left| \frac{\tan(\frac{\chi_{e0}}{2})}{\tan(\frac{\phi_0}{2} - \frac{\pi}{4})} \right|$ and $\phi_0 = \arctan(\frac{r_0}{r_d})$.

Case 2: $|\chi_{e0}| \in (\frac{\pi}{2}, \pi)$

For this case, the time t_2 when the relative course error $|\chi_{e0}|$ decreases to $\frac{\pi}{2}$ is

analyzed. It can be obtained from (3.19) that

$$t_2 = \frac{1}{k_2} \ln \left| \tan(\frac{\chi_{e0}}{2}) \right|. \tag{3.21}$$

Combining these two cases, the upper bound of the distance r can be computed via the following calculation.

$$\begin{aligned} r \leq r_{sup} &= r_0 + (v_0 + T_v)(t_1 + t_2) \\ &= r_0 + \frac{v_0 + T_v}{k_2} \ln \left| \frac{\tan(\frac{\chi_{e0}}{2})}{\tan(\frac{\phi_0}{2} - \frac{\pi}{4})} \right|. \end{aligned} \tag{3.22}$$

Remark 3.6: In this lemma, the condition that $\chi_e = -\pi$ is not considered. In fact, when $\chi_e = -\pi$, $\dot{\chi}_e > 0$, which implies that after a short time t_3, the relative course error $\chi_e \in (-\pi, \pi)$. It also implies that $r \leq r_{sup} + (v_0 + T_v)t_3$ when the initial relative course error $\chi_{e0} = -\pi$.

Now, it is ready to prove the stability of the proposed guidance approach with control input constraints in the presence of moving target velocity.

Theorem 3.1: Given an initial relative course error $\chi_{e0} \in (-\pi, \pi)$, the system given by (2.6) and (2.2) with u given by (3.8) and χ_d given by (3.1) asymptotically converges to the desired trajectory, i.e. $r \to r_d$ and $\chi \to \chi_d$.

Proof: Consider the Lyapunov function candidate:

$$V = \frac{1}{2}(r - r_d)^2 + \frac{\mu}{2}\chi_e^2. \tag{3.23}$$

The proof will be provided in two cases in terms of the relative course error χ_e.
Case 1: $|\chi_e| \in (\frac{\pi}{2}, \pi)$

Differentiating the function V with respect to time, it yields that

$$\begin{aligned}\dot{V} &= (r-r_d)\dot{r} + \mu\chi_e\dot{\chi}_e \\ &\leq (r-r_d)v_r\cos(\phi+\chi_e) - \mu k_2\chi_e\sin\chi_e \\ &< (r_{sup}+r_d)(v_0+T_v) - \mu k_2\frac{\pi}{2}\sin\chi_{e0}.\end{aligned}$$

Let $\mu \geq \frac{2(r_{sup}+r_d)(v_0+T_v)}{k_2\pi\sin\chi_{e0}}$, then $\dot{V} < 0$.

Case 2: $|\chi_e| \in [0, \frac{\pi}{2}]$

$$\begin{aligned}\dot{V} &= (r-r_d)\dot{r} + \mu\chi_e\dot{\chi}_e \\ &\leq -\mu k_2\chi_e\sin\chi_e - \frac{(r-r_d)^2(r+r_d)v_r\cos(\chi_e)}{r^2+r_d^2} - \frac{2(r-r_d)rr_dv_r\sin(\chi_e)}{r^2+r_d^2} \\ &\leq -\mu k_2\chi_e\sin\chi_e - \frac{(r-r_d)^2(r+r_d)v_r}{r^2+r_d^2} - 2v_r(r-r_d)\sin\frac{\chi_e}{2}\sin(\frac{\chi_e}{2}+\phi) \\ &\leq -\frac{(r-r_d)^2(r+r_d)v_r}{r^2+r_d^2} + 2v_r|r-r_d||\sin\frac{\chi_e}{2}| - 2\mu k_2\sin^2(\frac{\chi_e}{2})\end{aligned}$$

Let $\mu \geq \frac{(r_{sup}^2+r_d^2)(v_0+T_v)}{k_2(r_{sup}+r_d)}$, then

$$\begin{aligned}\dot{V} &\leq -\mu k_2\sin^2(\frac{\chi_e}{2}) - \left\{\left[\frac{(r+r_d)v_r}{r^2+r_d^2}\right]^{\frac{1}{2}}|r-r_d| - \left[\frac{(r^2+r_d^2)v_r}{r+r_d}\right]^{\frac{1}{2}}\left|\sin(\frac{\chi_e}{2})\right|\right\}^2 \\ &\leq 0. \qquad (3.24)\end{aligned}$$

It can be observed from the cases 1 and 2 that, when $\mu \geq \max\left\{\frac{2(r_{sup}+r_d)(v_0+T_v)}{k_2\pi\sin\chi_{e0}}, \frac{(r_{sup}^2+r_d^2)(v_0+T_v)}{k_2(r_{sup}+r_d)}\right\}$, the corresponding time derivative of the Lyapunov function V is always nonpositive, i.e. $\dot{V} \leq 0$. It is also noted from (3.24) that, $\dot{V} = 0$ implies that $r = r_d$ and $\chi_e = 0$. By LaSalle's Invariance principle, it can be obtained that $r \to r_d$ and $\chi \to \chi_d$ asymptotically.

Remark 3.7: During the proof of Theorem 3.1, the choice of the parameter μ determines the sign of the time derivative of the Lyapunov function. In fact, μ

is only used in the stability proof and does not affect the controller and system performance. Thus, the value of μ can be freely chosen. However, the existence of μ that leads to non-positive time derivative of the Lyapunov function depends on the upper bound of the distance r_{sup}. In Lemma 3.4, it is proved that r_{sup} is bounded. Hence, There exists a suitable μ which makes the time derivative of the Lyapunov function non-positive.

Remark 3.8: Theorem 3.1 does not consider the condition that $\chi_e = -\pi$. However, when $\chi_e = -\pi$, $\dot{\chi}_e > 0$, which implies that $\chi_e = -\pi$ is not an equilibrium point and can asymptotically converge to 0. Moreover, the condition that $r = 0$ also has been discussed in this section. Therefore, the proposed heading rate controller can guarantee the global convergence of the UAV to the desired circular orbit.

3.3 Adaptive Estimate for Moving Target Velocity

In the previous section, the ground target tracking in the presence of known constant moving target velocity is discussed. In this section, an adaptive observer will be developed to estimate unknown moving target velocity. Generally, the UAV airspeed is faster than the moving target velocity and the proposed control approach also requires that the moving target velocity is slower than the nominal airspeed v_0. Therefore, during the estimation, the estimate of the moving target velocity should be bounded.

The relative motion model (2.4) is used in this section with an unknown moving target velocity (T_x, T_y). Here, T_x and T_y are constant and it is assumed that there exists an upper bound T^* such that $|T_x| \leq T^*$ and $|T_y| \leq T^*$. $(\widehat{T}_x, \widehat{T}_y)$ is introduced to denote the estimate of (T_x, T_y), and then the actual moving target velocity and

its estimate are defined as follows [31]:

$$T_x = T^* \tanh \varphi_x, \quad T_y = T^* \tanh \varphi_y \tag{3.25}$$

$$\widehat{T}_x = T^* \tanh \widehat{\varphi}_x, \quad \widehat{T}_y = T^* \tanh \widehat{\varphi}_y \tag{3.26}$$

where φ_x and φ_y are unknown constants, as well as $\widehat{\varphi}_x$ and $\widehat{\varphi}_y$ are the corresponding estimates. Here, hyperbolic function $\tanh(x)$ is introduced to bound the estimates.

The adaptive observer can be formulated by the following equations:

$$\begin{cases} \dot{\widehat{x}}_r &= v\cos\psi - \widehat{T}_x + k_3\widetilde{x}_r \\ \dot{\widehat{y}}_r &= v\sin\psi - \widehat{T}_y + k_4\widetilde{y}_r \end{cases} \tag{3.27}$$

where $\widetilde{x}_r = x_r - \widehat{x}_r$ and $\widetilde{y}_r = y_r - \widehat{y}_r$.

By combining the relative motion model(2.4) and the proposed adaptive observer (3.27) with the adaptive update laws $\dot{\widehat{\varphi}}_x$ and $\dot{\widehat{\varphi}}_y$, the corresponding error dynamics is derived as follows:

$$\begin{aligned} &\dot{\widetilde{x}}_r = -\widetilde{T}_x - k_3\widetilde{x}_r, \quad \dot{\widetilde{y}}_r = -\widetilde{T}_y - k_4\widetilde{y}_r; \\ &\dot{\widehat{\varphi}}_x = -\gamma\widetilde{x}_r, \qquad\qquad \dot{\widehat{\varphi}}_y = -\gamma\widetilde{y}_r. \end{aligned} \tag{3.28}$$

where $\widetilde{T}_x = T_x - \widehat{T}_x$ and $\widetilde{T}_y = T_y - \widehat{T}_y$. Now, it is ready to verify the stability of the adaptive observer. Consider the following function

$$\begin{aligned} V = &\frac{1}{2}\widetilde{x}_r^2 + \frac{1}{2}\widetilde{y}_r^2 + \frac{1}{\gamma}T^*(\log\cosh\widehat{\varphi}_x - \widehat{\varphi}_x\tanh\varphi_x) \\ &+ \frac{1}{\gamma}T^*(\log\cosh\widehat{\varphi}_y - \widehat{\varphi}_y\tanh\varphi_y). \end{aligned} \tag{3.29}$$

By differentiating this function V with respect to time t, it is obtained that

$$\begin{aligned}\dot{V} &= \widetilde{x}_r\dot{\widetilde{x}}_r + \widetilde{y}_r\dot{\widetilde{y}}_r + \frac{1}{\gamma}T^*(\dot{\widehat{\varphi}}_x \tanh\widehat{\varphi}_x - \dot{\widehat{\varphi}}_x \tanh\varphi_x) \\ &\quad + \frac{1}{\gamma}T^*(\dot{\widehat{\varphi}}_y \tanh\widehat{\varphi}_y - \dot{\widehat{\varphi}}_y \tanh\varphi_y) \\ &= \widetilde{x}_r(-\widetilde{T}_x - k_3\widetilde{x}_r) + \widetilde{y}_r(-\widetilde{T}_y - k_4\widetilde{y}_r) - \frac{1}{\gamma}\widetilde{T}_x\dot{\widehat{\varphi}}_x - \frac{1}{\gamma}\widetilde{T}_y\dot{\widehat{\varphi}}_y \\ &= -k_3\widetilde{x}_r^2 - k_4\widetilde{y}_r^2 \leq 0.\end{aligned}$$

Next, it will be shown that the function V is lower bounded. Firstly, the following function $F(x) = \log\cosh x - x\tanh x_0$ is defined. Differentiating the function $F(x)$ with respect to x yields that

$$F_x(x) = \frac{dF(x)}{dx} = \tanh x - \tanh x_0. \tag{3.30}$$

It is observed from (3.30) that, when $x = x_0$, $F(x)$ reaches the minimum. Thus, the third and the fourth terms in the function (3.29) have minimum values when $\widehat{\varphi}_x = \varphi_x$ and $\widehat{\varphi}_y = \varphi_y$. Hence,

$$\begin{aligned}V &\geq \frac{T^*}{\gamma}(\log\cosh\varphi_x - \varphi_x\tanh\varphi_x + \log\cosh\varphi_y - \varphi_y\tanh\varphi_y) \\ &\geq \frac{-2T^*}{\gamma}\log 2.\end{aligned} \tag{3.31}$$

Therefore, the function V is lower bounded. Moreover, $\ddot{V} = 2k_3\widetilde{x}_r(\widetilde{T}_x + k_3\widetilde{x}_r) + 2k_4\widetilde{y}_r(\widetilde{T}_y + k_4\widetilde{y}_r)$ is bounded. Thus, by Barbalat's lemma [96], it can be shown that $\dot{V} \to 0$ as $t \to \infty$, which also implies that $\widetilde{x}_r \to 0$ and $\widetilde{y}_r \to 0$.

In addition, $\ddot{\widetilde{x}}_r = -\dot{\widetilde{T}}_x - k_3\dot{\widetilde{x}}_r = k_3(\widetilde{T}_x + k_3\widetilde{x}_r) - \frac{4T^*\gamma\widetilde{x}_r}{(e^{\widehat{\varphi}_x} + e^{-\widehat{\varphi}_x})^2}$, which implies that $\ddot{\widetilde{x}}_r$ is bounded. By Barbalat's lemma, it can be obtained that, $\dot{\widetilde{x}}_r = -\widetilde{T}_x - k_3\widetilde{x}_r \to 0$, which in turn implies that $\widetilde{T}_x \to 0$. Similarly, it can also be shown that $\widetilde{T}_y \to 0$.

Based on this proposed adaptive observer, the corresponding controller for ground

target tracking is designed as (3.8). The overall control architecture is illustrated in Fig. 3.1.

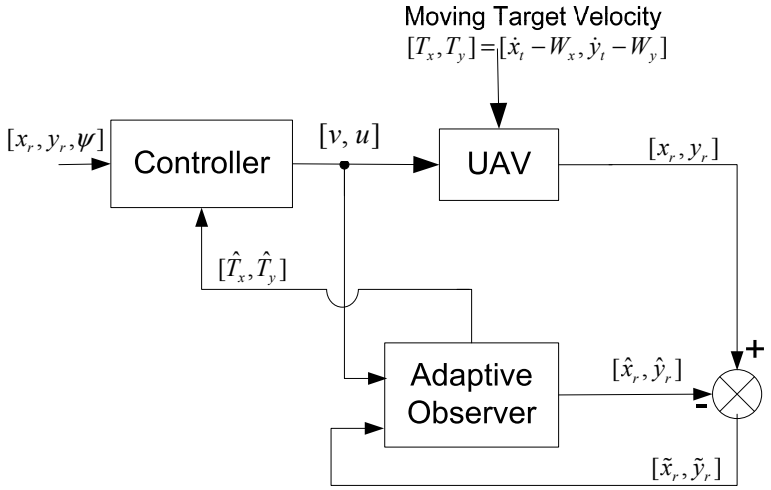

Figure 3.1: Target tracking control architecture based on an adaptive observer

3.4 Simulation Results

In this section, simulation results are presented to demonstrate the effectiveness of the proposed approach. The simulation includes four scenarios: scenario one and scenario two describe ground target tracking with known constant moving target velocity; scenario three and scenario four carry out ground target tracking with unknown moving target velocity. In scenario two and scenario four, the measurement noise of the relative position and the uncertainty of the moving target velocity are taken into account to verify the robustness of the proposed approach. Table 3.1 shows the specifications of the UAV and control law parameters.

3.4.1 Scenario One

In this scenario, the UAV starts the mission of ground target tracking at the relative position $(x_r, y_r) = (10, 0)$m with initial heading angle $\psi_0 = \frac{\pi}{2}$. As illustrated

Table 3.1: UAV specifications and control law parameters

Parameter	Value
Nominal airspeed v_0	20 m/s
Maximum heading rate w_{max}	0.5 rad/s
Desired distance r_d	400 m
Heading rate feedback gain k	0.2
Target velocity	$(2, 3)$ m/s
Background wind	$(-5, -2)$ m/s
Upper bound T^*	10 m/s

in Fig. 3.2, the heading rate controller reaches saturation at the beginning of the tracking mission and finally heading rate converges to the desired heading rate. Fig. 3.3 shows the trajectory of the UAV with respect to the inertial coordinate frame, while Fig. 3.4 shows the trajectory of the UAV with respect to the moving target in the presence of background wind. From Fig. 3.4 and Fig. 3.5, it can be observed that the distance between the UAV and the target finally converges to the desired one. In addition, as depicted in Fig. 3.6 that the relative course error asymptotically converges to zero even in the presence of large initial relative course error. It is also worth noting that, a sinusoidal function is used to bound the convergence rate in the section 3.2, but usually the actual convergence rate is much faster than this bound.

3.4.2 Scenario Two

In scenario one, the relative position of the UAV with respect to the target and the moving target velocity are assumed to be known accurately. However, the measurement noise and system uncertainty always exist in practice. Therefore, the measurement noise of the relative position (x_r, y_r) and the uncertainty of the moving target velocity (T_x, T_y) have to be considered. In this scenario, bounded

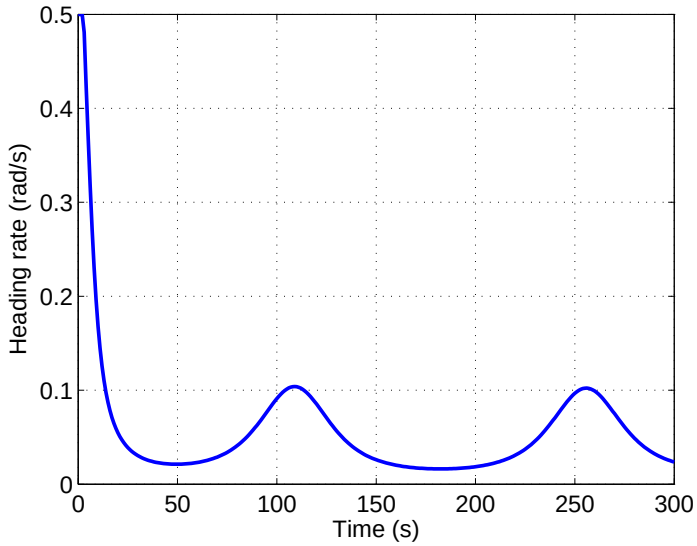

Figure 3.2: Heading rate control input (Scenario one)

random uncertainties $\delta T_x, \delta T_y \in (-2, 2)$m/s are added to the moving target velocity and zero mean random measurement errors with a variance $\Delta = 4$ are introduced as the noise in the relative position measurement. Moreover, it is well known that the heading rate of the UAV is dependant on the roll angle. Thus, in this scenario, $\ddot{\psi} = k_5(\dot{\psi}_c - \dot{\psi})$ will be used to approximate the dynamics of the heading rate, where $\dot{\psi}_c$ is the commanded heading rate from Eq. (3.8) and $k_5 = 1$.

Fig. 3.7 shows the actual moving target velocity, where it can be observed that the actual velocity is time-varying around its nominal value. The heading rate control input is depicted in Fig. 3.8, where heading rate reaches saturation at the beginning of the mission. When the control gain k_5 is small enough, the heading rate will not reach saturation. However, it will take much longer time for the UAV to converge to the desired orbit. The distance between the UAV and the target as well as the relative course error are described in Fig. 3.9 and Fig. 3.10, respectively. It is noted that the distance can converge to the neighborhood of the desired distance r_d in the presence of measurement noise and uncertainty.

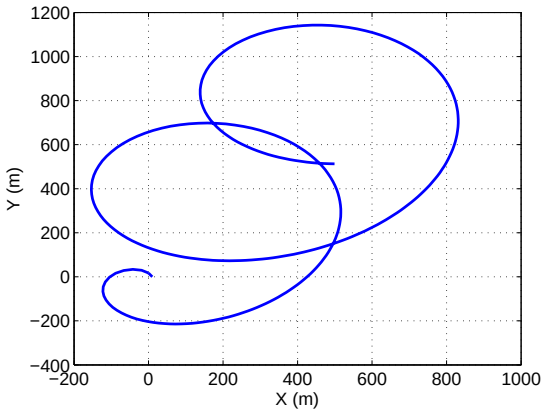

Figure 3.3: Trajectory w.r.t inertial frame (Scenario one)

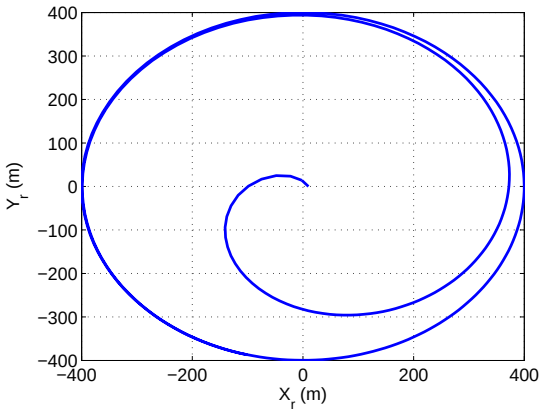

Figure 3.4: Trajectory w.r.t target (Scenario one)

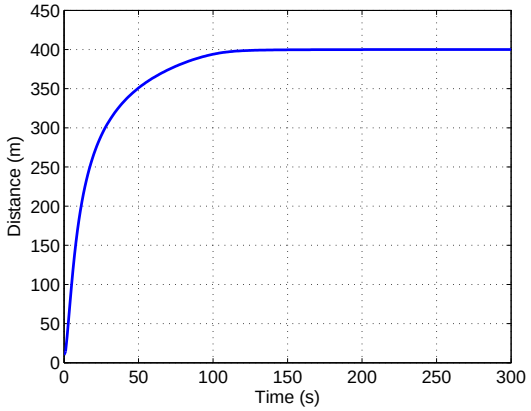

Figure 3.5: Distance between UAV and target (Scenario one)

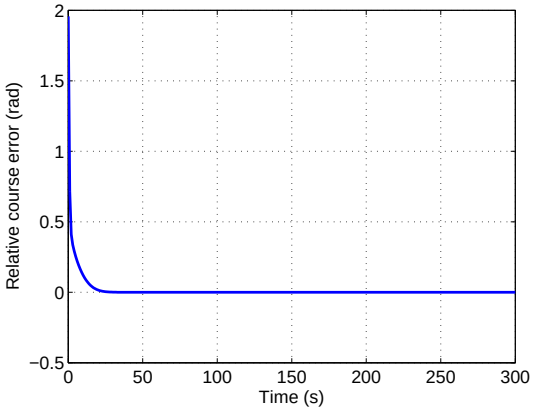

Figure 3.6: Relative course error (Scenario one)

3.4.3 Scenario Three

In this scenario, the nominal moving target velocity are unknown. Firstly, for the purpose of comparison, ground target tracking without moving target velocity estimation is presented, where the moving target velocity is considered to be zero during controller design. Then, ground target tracking with moving target velocity estimation is presented, where an adaptive observer is designed to estimate the unknown moving target velocity. In this scenario, measurement noise and uncertainty are not taken into account. The initial state of the UAV is the same as that in

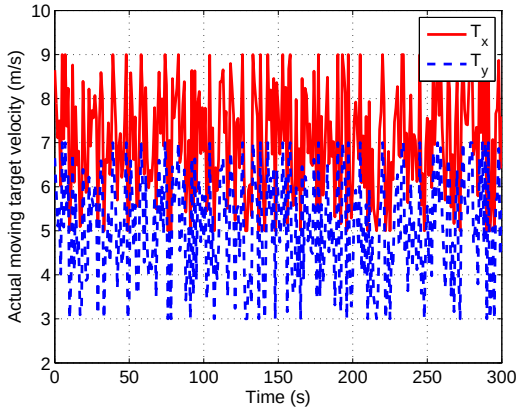

Figure 3.7: Actual moving target velocity (Scenario two)

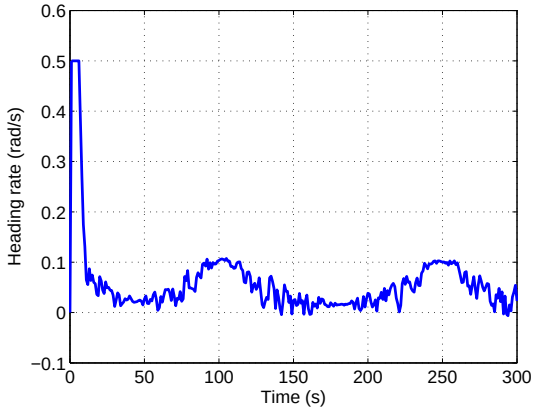

Figure 3.8: Heading rate control input (Scenario two)

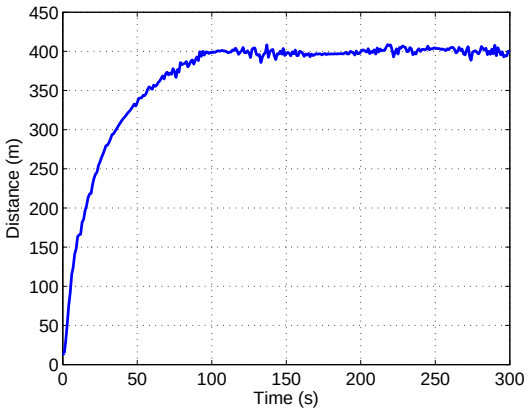

Figure 3.9: Distance between UAV and target (Scenario two)

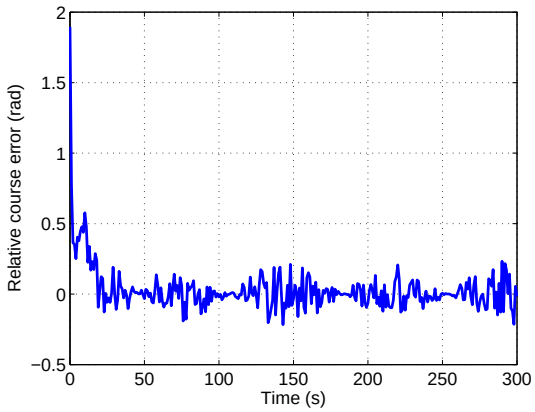

Figure 3.10: Relative course error (Scenario two)

scenario one.

Figs. 3.11 and 3.12 show the ground target tracking results (the distance and the relative course error) without moving target velocity estimation. It can be observed that the distance between UAV and target varies significantly, which may lead to task failure, such as loss of communication. In comparison, Figs. 3.13-3.16 show the target tracking results with an adaptive observer. As depicted in Fig. 3.13 that, the estimate of the moving target velocity eventually converges to the actual one. Thus, based on the saturated heading rate controller (Fig. 3.14), it can be noted that from Figs. 3.15 and 3.16, the distance and the relative course finally converge

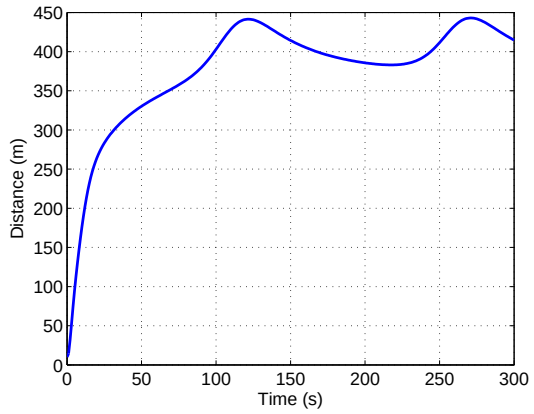

Figure 3.11: Distance between UAV and target(Scenario three)

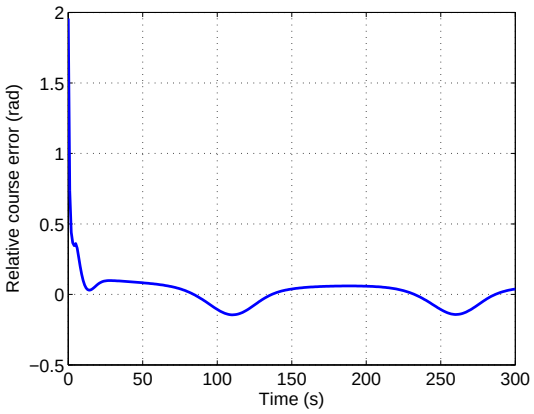

Figure 3.12: Relative course error (Scenario three)

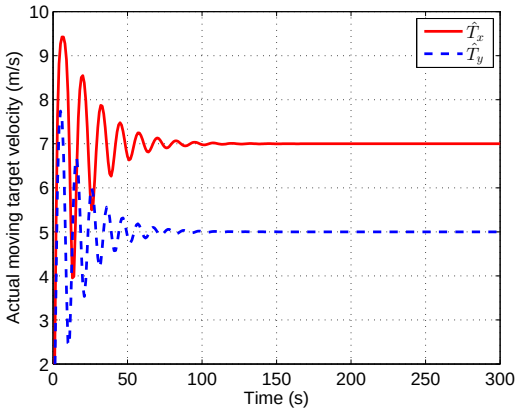

Figure 3.13: Adaptive estimate of moving target velocity (Scenario three)

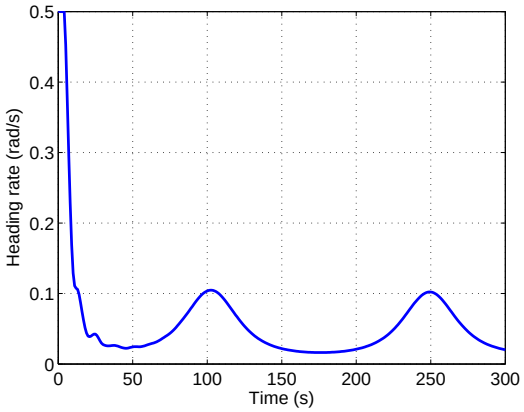

Figure 3.14: Heading rate control input (Scenario three)

to the desired values.

3.4.4 Scenario Four

As compared with scenario three, this scenario takes measurement noise and uncertainty into account. The actual moving target velocity is $(7 + \delta T_x, 5 + \delta T_y)$m/s, where the definition of $(\delta T_x, \delta T_y)$ is the same as that in scenario two and the relative position measurement noise is also the same as that in scenario two. Fig. 3.17 shows that, the adaptive estimate for the moving target velocity does not converge

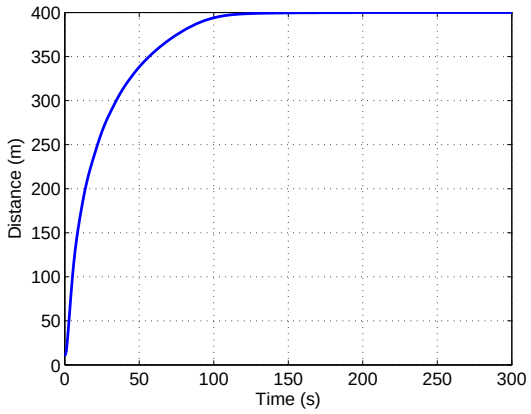

Figure 3.15: Distance between UAV and target (Scenario three)

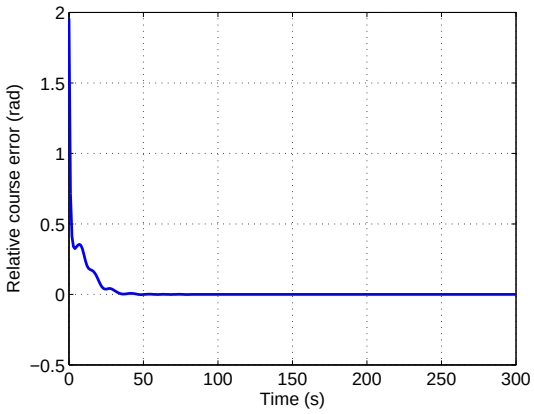

Figure 3.16: Relative course error (Scenario three)

to the nominal velocity as the moving target velocity is not constant. However, the adaptive estimate varies around the nominal velocity $(7, 5)$m/s. Due to the boundedness of the adaptive estimate, the heading rate control input can be generated by the proposed controller (3.8) as shown in Fig. 3.18. Fig. 3.19 shows that, since there exists an error in the adaptive estimate of moving target velocity, the relative course can not converge to the desired one. However, It can be observed from Fig. 3.20 that the UAV still can converge to the neighborhood of the desired orbit with a small distance error.

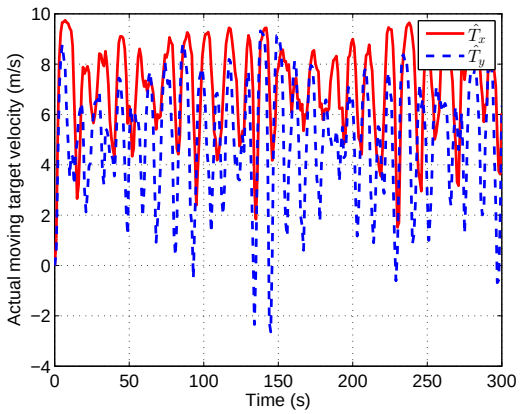

Figure 3.17: Adaptive estimate of moving target velocity (Scenario four)

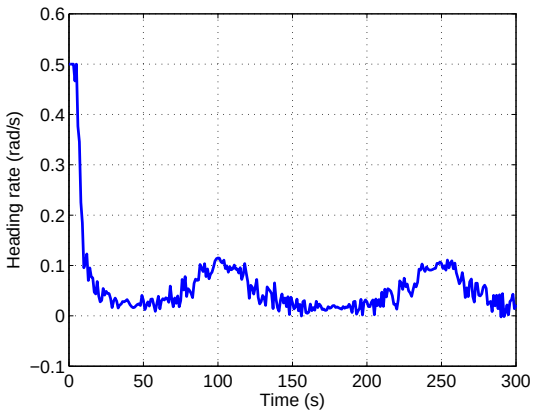

Figure 3.18: Heading rate control input (Scenario four)

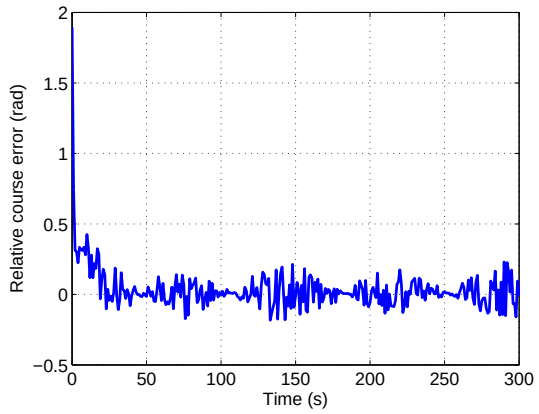

Figure 3.19: Relative course error (Scenario four)

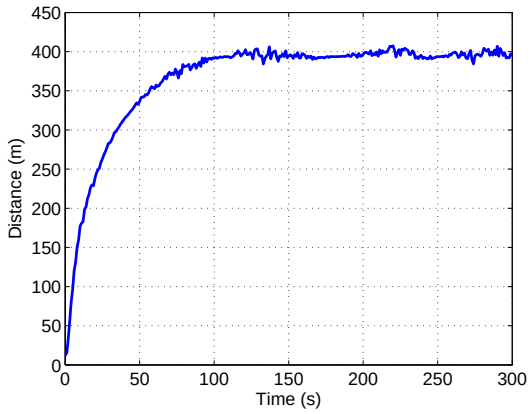

Figure 3.20: Distance between UAV and target (Scenario four)

3.5 Conclusions

This chapter shows that a saturated heading rate controller based on a guidance law is able to achieve stable ground target tracking in the presence of background wind and target motion. The global asymptotical convergence of the system with any initial position and heading angle is guaranteed by the proposed saturated heading rate controller. In addition, a constrained adaptive observer is constructed to estimate unknown moving target velocity. The constrained adaptive estimate makes the proposed saturated heading rate controller feasible. Simulation results show that the proposed approach is robust to the uncertainty of the system and suitable for performing standoff target tracking.

Chapter 4

Adversarial Target Tracking

4.1 Introduction

In Chapter 3, ground target tracking using a single UAV is discussed, where the distance between the UAV and target can eventually converge to the desired standoff distance. In practical applications, the target could be friendly or adversarial. For adversarial target tracking, tracking performance and UAV safety are two important considerations during tracking controller design. If the UAV is too close to the target, the UAV may be detected or even attacked by the adversarial target. If the UAV is too far away from the target, tracking performance may be degraded. Therefore, It is necessary to study adversarial target tracking control algorithms while avoiding exposure of the UAV to the target or minimizing the exposure time.

The adversarial target can be treated as an obstacle or a threat zone. Obstacle avoidance has been a topic of great interest for many years, and several approaches have been proposed for this problem, such as potential field approaches [37], barrier Lyapunov function [39], optimal approaches [41], etc. Due to the inherent properties of the fixed-wing UAV, in some cases, the UAV is inevitable to fly into the threat zone around the target. In these cases, the UAV should fly out of the threat region

as soon as possible so that the exposure time is minimized. For the UAV with constant airspeed, minimizing the exposure time is equivalent to minimizing the path length in the threat zone. Many optimal approaches have been proposed to solve the problem on minimizing the path between two points [40,43–45]. However, how to find the minimum path in the threat zone for the UAV is still an open question.

This chapter aims to solve the problem of adversarial ground target tracking using UAVs with input constraints. In order to guarantee tracking performance and UAV safety, a bang-bang heading rate controller is proposed. Firstly, the case that the UAV can avoid exposure to the target is analyzed. The proposed controller guarantees that the UAV can achieve the desired circular orbit while avoiding exposure if the initial state of the UAV is well located. Then, the case that the UAV can not avoid exposure to the target is also analyzed. The proposed controller ensures that the UAV can escape from the threat zone in minimum time, i.e., minimum exposure time.

4.2 Problem Statement

This section firstly presents the kinematic model of the fixed-wing UAV with input constraints. Then, the guidance law for target tracking is provided. Finally, the problem studied in this chapter is described.

4.2.1 UAV Model

The kinematic model (2.1) with input constraints (2.2) is used in this chapter. The following two assumptions are required:

Assumption 4.1*:* The adversarial target is stationary and located at the origin.

Assumption 4.2*:* The airspeed of the UAV v is held constant and $v = v_0$.

Remark 4.1: There are many stationary adversarial targets such as Radar station and stationary battle tank. Since the target is hostile, it is impossible for the UAV to communicate with the ground target to access the velocity. Thus, if the UAV is much faster than the ground target, it is reasonable to assume that the target is stationary.

The UAV model can also be expressed in polar coordinates as

$$\begin{bmatrix} \dot{r} \\ r\dot{\theta} \end{bmatrix} = \begin{bmatrix} \dot{x}\cos\theta + \dot{y}\sin\theta \\ -\dot{x}\sin\theta + \dot{y}\cos\theta \end{bmatrix} = \begin{bmatrix} v_0\cos(\psi-\theta) \\ v_0\sin(\psi-\theta) \end{bmatrix} \tag{4.1}$$

where $r = (x^2+y^2)^{\frac{1}{2}}$ is the horizontal distance between the UAV and the origin, and $\theta = \text{arctan2}(y,x) \in [-\pi,\pi)$ is the clock angle (see Fig. 2.2).

4.2.2 Target Tracking Guidance

According to the assumption 4.1, the relative motion model is equivalent to the UAV kinematic model. The guidance law with the desired standoff distance r_d is introduced as follows:

$$\psi_d = < \theta + \phi > \tag{4.2}$$

where ψ_d is the desired heading angle, and $\phi = 2\text{arctan}(\frac{r}{r_d})$. $<>$ is used to represent the wrapped angle, i.e., $< \theta+\phi > \in [-\pi,\pi)$. The properties of this guidance law are the same as that of the guidance law (3.1)

4.2.3 Problem Formulation

In order to describe the problem clearly, several definitions are provided first. Here, it is assumed that when the distance between the UAV and the adversarial target is smaller than a specified distance r_t, the UAV can be detected by the target, i.e., the UAV is exposed to target.

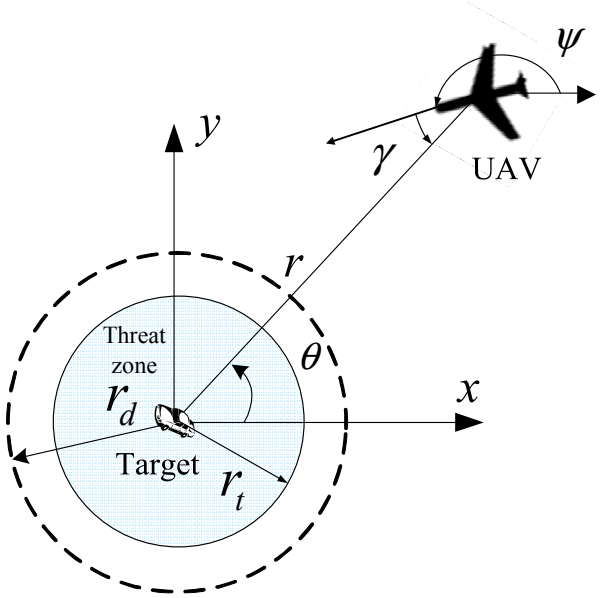

Figure 4.1: Adversarial target tracking geometry and threat zone

***Definition 4.1**:* The disk of radius r_t at whose center the adversarial target locates is the *threat zone* (see Fig. 4.1).

Remark 4.2: If the distance r between the UAV and the target is less than r_t, the UAV is located inside of the threat zone. It is assumed that the initial position of the UAV is located outside of the threat zone. It is obvious that, whether the UAV can avoid the threat zone depends on its initial state.

As depicted in Fig.4.1, γ is the angle between the heading direction and the line connecting the UAV and the target measured from the heading direction in the counterclockwise direction, $\gamma =< \theta + \pi - \psi >\in [-\pi, \pi)$. The distance r and the angle γ can be determined by the UAV state. r_m is the minimum turning radius of the UAV, i.e., $r_m = \frac{v_0}{w_{max}}$. In this chapter, it is assumed that $r_t < r_d$.

Remark 4.3: if $r_t > r_d$, then it is clear that the desired trajectory is within the threat zone, which is undesirable.

Next, the initial state of the UAV will be analyzed. From Fig. 4.2, it can be observed that, there exists a shortest distance r_s between the UAV and the target such that the UAV with an arbitrary heading angle can avoid exposure to the target if the initial distance $r > r_s$. If the initial distance $r \leq r_s$, exposure avoidance of

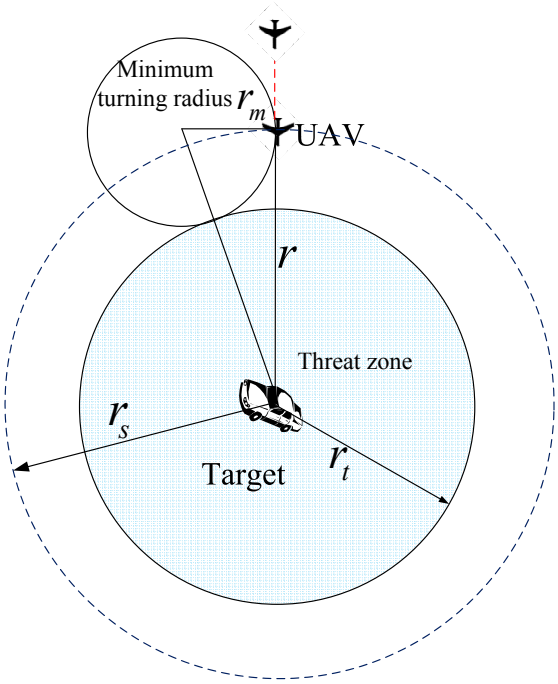

Figure 4.2: The UAV with an arbitrary heading angle can avoid exposure if the initial position is located outside of the circle with radius r_s.

the UAV to the target depends on the initial heading angle. Firstly, the shortest distance r_s should be determined. Given a fixed initial position, it is obvious that if the UAV with the heading which points to the target can avoid exposure, then the UAV with other heading angles is possible to avoid exposure. Therefore, it can be obtained from Fig. 4.2 that,

$$r_s^2 + r_m^2 = (r_m + r_t)^2. \tag{4.3}$$

It can be derived from (4.3) that $r_s = (r_t^2 + 2r_m r_t)^{\frac{1}{2}}$. If $r > (r_t^2 + 2r_m r_t)^{\frac{1}{2}}$, the UAV can avoid the exposure to the target. If the $r \leq (r_t^2 + 2r_m r_t)^{\frac{1}{2}}$, the initial heading angle needs to be taken into account. It is noted from Fig. 4.3 that, for $r_t \leq r \leq (r_t^2 + 2r_m r_t)^{\frac{1}{2}}$, if the UAV flies along the minimum turning orbit which is tangent to the contour of the threat zone, the UAV still can avoid the exposure to the target, which implies that if $|\gamma| \geq \arccos(\frac{r_m^2 + r^2 - (r_m + r_t)^2}{2r_m r}) - \frac{\pi}{2}$ and

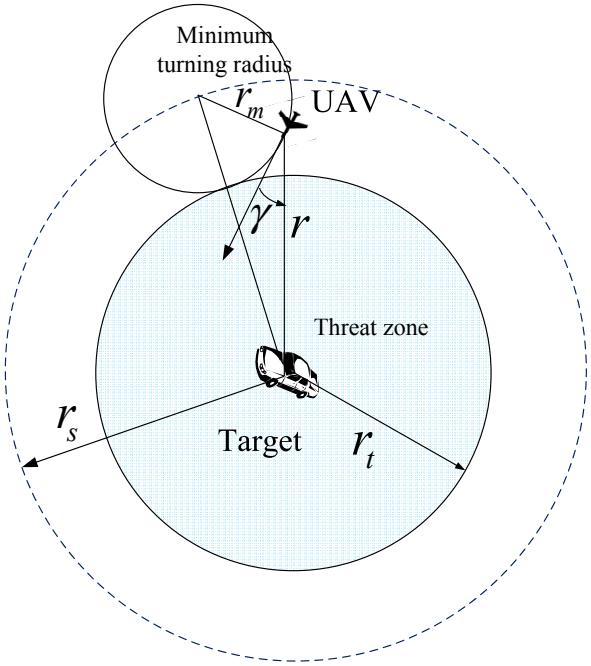

Figure 4.3: Exposure avoidance of the UAV depends on the initial heading angle if the initial distance $r \in [r_t, r_s]$.

$r_t \leq r \leq (r_t^2 + 2r_m r_t)^{\frac{1}{2}}$, the UAV can avoid the exposure to the target. Since the condition of exposure avoidance of the UAV has been analyzed, the following definition can be stated.

Definition 4.2: If $(r, \gamma) \in \{(r, \gamma) | r > (r_t^2 + 2r_m r_t)^{\frac{1}{2}}\} \cup \{(r, \gamma) | r_t \leq r \leq (r_t^2 + 2r_m r_t)^{\frac{1}{2}}$ and $|\gamma| \geq \arccos(\frac{r_m^2 + r^2 - (r_m + r_t)^2}{2r_m r}) - \frac{\pi}{2}\}$, the corresponding UAV state is called *safe state*, otherwise, the UAV state is called *exposure state*. For simplicity, S and E are used to denote the safe state set and the exposure state set respectively.

Now, it is ready to state the problems considered in this chapter.

Problem 4.1: If the initial state of the UAV $(r_0, \gamma_0) \in S$, how to drive the UAV to the desired circular orbit while avoiding exposure of the UAV to the target is discussed, i.e.,

$$u(t) : \psi \to \psi_d \text{ and } r \to r_d, \text{ subject to } (r, \gamma) \in S.$$

Problem 4.2: If the initial state of the UAV (r_0, γ_0) is a exposure state, how to minimize the exposure time and to drive the UAV to the desired circular orbit is discussed, i.e.,

$$\min_{u(t)} J = \int_0^{T_f} 1dt, \text{ subject to } (r, \gamma) \in E$$

$$\text{and } u(t) : \psi \to \psi_d \text{ and } r \to r_d, \text{ subject to } (r, \gamma) \in S.$$

4.3 Controller Design and Performance Analysis

In this section, target tracking control will be discussed. Firstly, a bang-bang heading rate controller is proposed for target tracking. Based on this controller, the performance of the UAV flight in two cases in terms of the initial state of the UAV is analyzed.

4.3.1 Controller Design

The proposed bang-bang heading rate controller is given as follows:

$$u = \begin{cases} w_{max} & \text{if } -\pi \leq \gamma < 0 \\ sgn(\psi_d - \psi) w_{max} & \text{if } 0 \leq \gamma < \pi \text{ and } r \geq r_t \\ -w_{max} & \text{if } 0 \leq \gamma < \pi \text{ and } r < r_t \end{cases} \tag{4.4}$$

Now, it proceeds to analyze the performance of the proposed controller in two cases.

4.3.2 Target Tracking with Exposure Avoidance

When the initial state of the UAV $(r_0, \gamma_0) \in S$, the proposed controller can guarantee the exposure avoidance of the UAV to the target, and the UAV heading can converge to the desired heading angle, so that the UAV will fly along

the desired circular orbit around the target. Next, the above performance will be shown in details. First of all, exposure avoidance of the UAV to the target will be explored. For the sake of simplicity, the following notations are introduced: $C_1 = \{(r,\gamma)|r > (r_t^2 + 2r_m r_t)^{\frac{1}{2}}\}$(see Fig. 4.2), $C_2 = \{(r,\gamma)|r_t \leq r \leq (r_t^2 + 2r_m r_t)^{\frac{1}{2}}$ and $|\gamma| \geq \arccos(\frac{r_m^2+r^2-(r_m+r_t)^2}{2r_m r}) - \frac{\pi}{2}\}$ and $C_3 = \{(r,\gamma)|r_t \leq r \leq (r_t^2 + 2r_m r_t)^{\frac{1}{2}}$ and $|\gamma| < \arccos(\frac{r_m^2+r^2-(r_m+r_t)^2}{2r_m r}) - \frac{\pi}{2}\} \cup \{(r,\gamma)|r < r_t\}$ (see Fig. 4.3). In fact, the safety state set $S = C_1 \cup C_2$, and the exposure state set $E = C_3$.

If $(r_0,\gamma_0) \in C_1$, it implies $r_0 > r_t$. There are two situations that may occur in the future. One is that $(r(t),\gamma(t)) \in C_1, t > t_0$, and the other one is that $(r(t),\gamma(t)) \in C_2, t > t_0$. In both of these two situations, the exposure of the UAV does not happen.

If $(r_0,\gamma_0) \in C_2$, there are three situations that may occur in the future: $(r(t),\gamma(t)) \in C_1$, $(r(t),\gamma(t)) \in C_2$, and $(r(t),\gamma(t)) \in C_3$. In the first two situations, the exposure of the UAV does not happen. Contrarily, in the third situation, the exposure of the UAV to the target can not be avoided. Thus, this work shows that if the initial state $(r_0,\gamma_0) \in C_2$, the state of the UAV will evolve in the sets C_1 and C_2 under the proposed controller (4.4), i.e.,$(r(t),\gamma(t)) \in C_1 \cup C_2, t > t_0$.

Let $\gamma_d = \arccos(\frac{r_m^2+r^2-(r_m+r_t)^2}{2r_m r}) - \frac{\pi}{2}$. It can be observed that $0 \leq \gamma_d \leq \frac{\pi}{2}$ when $r_t \leq r \leq r_s$, and γ_d is continuous with respect to time t. It can also be known that when $|\gamma(t)| \leq \frac{\pi}{2}$, $\gamma(t) =< \theta + \pi - \psi >$ is continuous with respect to time t. The initial state $(r_0,\gamma_0) \in C_2$ leads to that $|\gamma_0| \geq \gamma_d(0)$. If $|\gamma(t)| > \frac{\pi}{2}$, then $|\gamma(t)| > \gamma_d(t)$. If $|\gamma(t)| \leq \frac{\pi}{2}$, consider the case $|\gamma(t)| = \gamma_d(t)$. Differentiating $|\gamma(t)|$ and $\gamma_d(t)$ with respect to time yields

$$\frac{d\sin(|\gamma(t)|)}{dt} = \begin{cases} (u-\dot{\theta})(\cos(\psi-\theta)) & \text{if } \gamma(t) \geq 0 \\ (-u+\dot{\theta})(\cos(\psi-\theta)) & \text{if } \gamma(t) < 0 \end{cases}$$

$$\frac{d\sin(\gamma_d(t))}{dt} = \begin{cases} (-w_{max} - \dot{\theta})(\cos(\psi - \theta)) & \text{if } \gamma(t) \geq 0 \\ (-w_{max} + \dot{\theta})(\cos(\psi - \theta)) & \text{if } \gamma(t) < 0 \end{cases}.$$

Next, it will show that when $0 \leq |\gamma(t)| \leq \frac{\pi}{2}$ and $|\gamma(t)| = \gamma_d(t)$, $\frac{d\sin(|\gamma(t)|)}{dt} = \frac{d\sin(\gamma_d(t))}{dt}$. Firstly, it is noted that if $r_s \leq r_d$, then $r \leq r_d$, which in turn implies that $\pi - \phi \geq \frac{\pi}{2}$. If $0 \leq \gamma(t) \leq \frac{\pi}{2}$, it can be derived that $\psi - \psi_d = \pi - \gamma - \phi > 0$. If $r_s \geq r_d$, the value of $\sin(\pi - \phi) - \sin(\gamma)$ needs to be analyzed in the domain $r \in (r_d, r_s]$.

$$\begin{aligned} \sin(\pi - \phi) - \sin(\gamma) &= \frac{2rr_d}{r^2 + r_d^2} + \frac{r^2 - r_t^2 - 2r_t r_m}{2r_m r} \\ &= \frac{4r^2 r_m r_d + (r^2 + r_d^2)(r^2 - r_t^2 - 2r_t r_m)}{2rr_m(r^2 + r_d^2)} \\ &= \frac{r^4 + r^2(r_d^2 - r_t^2 - 2r_t r_m + 4r_m r_d)}{2rr_m(r^2 + r_d^2)} > 0 \end{aligned} \quad . \tag{4.5}$$

When $r \in (r_d, r_s]$, $\pi - \phi \in (0, \frac{\pi}{2})$ according to the definition of ϕ. If $\gamma \in (0, \frac{\pi}{2})$, it can be obtained from Eq. 4.5 that $\psi - \psi_d = \pi - \gamma - \phi > 0$. When $r \leq r_d$, $\pi - \phi \in [\frac{\pi}{2}, \pi)$ and with $\gamma \in (0, \frac{\pi}{2})$, it is also noted that $\psi - \psi_d = \pi - \gamma - \phi > 0$. Therefore, when $0 \leq \gamma(t) \leq \frac{\pi}{2}$ and $|\gamma(t)| = \gamma_d(t)$, $\psi_d < \psi$, and furthermore according to the proposed heading rate controller (4.4), $u = -w_{max}$.

According to the proposed controller (4.4), When $\gamma(t) < 0$ and $|\gamma(t)| = \gamma_d(t)$, $u = w_{max}$. As a result, when $|\gamma(t)| = \gamma_d(t)$, $\frac{d\sin(|\gamma(t)|)}{dt} = \frac{d\sin(\gamma_d(t))}{dt}$. With the continuity of $\gamma(t)$ and $\gamma_d(t)$, it follows that $|\gamma(t)| \geq \gamma_d(t)$.

Note that from the UAV model (2.7), $r(t)$ is also continuous with respect to time t. Since $|\gamma(t)| \geq \gamma_d(t)$, when $r(t) = r_t$, it can be obtained that $|\gamma| \geq \gamma_d(t) = \frac{\pi}{2}$, which implies that $r(t) \geq r_t$. Combining the above analysis, the following result can be derived. If $(r_0, \gamma_0) \in C_2$, $(r(t), \gamma(t)) \in C_1 \cup C_2$ when $t \geq 0$ under the proposed controller (4.4).

Next, it will be shown that the proposed controller guarantees the convergence of the UAV to the desired circular orbit. In fact, if the heading of the UAV can follow the desired heading, the convergence is guaranteed according to the proposed

guidance law (4.2). Following this idea, the proof for the convergence of the heading to the desired heading is provided in the sequel. According to the proposed controller (4.4), when $-\pi \leq \gamma < 0$, the heading rate input $u = w_{max}$ and furthermore $\dot{\gamma}(t) = \dot{\theta} - \dot{\psi} = \frac{v_0 \sin(\psi-\theta)}{r} - w_{max} < -\delta w < 0$. Therefore, if the initial state $\gamma_0 \in (0, -\pi]$, $\gamma(t) \in [0, \pi)$ when $t > \delta T$, where $\delta T \leq \frac{\pi}{\delta w}$. Thus, it only needs to consider the case that $\gamma_0 \in [0, \pi)$. The heading error can be defined by

$$\psi_e =< \psi - \psi_d > \in [-\pi, \pi). \tag{4.6}$$

In order to make the UAV feasible to track desired heading angle, it is assumed that $w_{max} \geq \frac{4v_0}{r_d}$. According to the result in Chapter 3, the following lemma is obtained.

Lemma 4.1: For the system given by (2.1) and the guidance law given by (4.2), there exists a positive constant $k > 0$ such that,

$$\dot{\psi}_d \geq -w_{max} + k \sin \psi_e, \psi_e \in [0, \pi) \tag{4.7}$$

$$\text{and } \dot{\psi}_d \leq w_{max} + k \sin \psi_e, \psi_e \in [-\pi, 0) \tag{4.8}$$

Proof: see the proof of Lemma 3.2.

For $\gamma_0 \in [0, \pi)$, Lemma 4.1 implies that $\dot{\psi}_e \leq -k \sin \psi_e$ when $\psi_e \in [0, \pi)$, and $\dot{\psi}_e \geq -k \sin \psi_e$ when $\psi_e \in [-\pi, 0)$. Thus, the heading angle of the UAV will converge to the desired heading angle ψ_d. Furthermore, the UAV finally converges to the desired circular orbit.

4.3.3 Target Tracking with Minimum Exposure Time

The previous subsection has discussed the case that the initial state of the UAV belongs to the safe state set. This subsection will study the case that the initial

state of the UAV belongs to the exposure state set. If the UAV starts from this set, its exposure to the target can not be avoided. Thus, how to minimize the exposure time will be the research focus. Here, it is assumed that the UAV initial state $(r_0, \gamma_0) \in \{(r, \gamma) | r_t \leq r \leq (r_t^2 + 2r_m r_t)^{\frac{1}{2}}$ and $0 \leq |\gamma| < \arccos(\frac{r_m^2 + r^2 - (r_m + r_t)^2}{2r_m r}) - \frac{\pi}{2}\}$.

Without loss of generality, it is assumed that the initial position of the UAV is on the boundary of the threat zone. At this position, $|\gamma_0| < \frac{\pi}{2}$, according to the definition of the exposure state set. The time T_f is introduced to denote the time when the UAV exits the threat zone. For simplicity, let the notation $p(t) = (x(t), y(t), \psi(t))^T$. The notations $x(T_f), y(T_f), \psi(T_f)$ and $\gamma(T_f)$ are used to denote the terminal states of the UAV. The terminal states of the UAV satisfy the following equation.

$$Q(T_f) = x(T_f)^2 + y(T_f)^2 - r_t^2 = 0 \tag{4.9}$$

The optimal control problem can be formulated as follows:

$$\min_{u(t)} J = \int_0^{T_f} 1 dt, \tag{4.10}$$

subject to the UAV kinematics (2.1) with input constraint:

$$|u| \leq \omega_{max}$$

and the state constraints:

$$x(0)^2 + y(0)^2 - r_t^2 = 0$$

$$x(t)^2 + y(t)^2 - r_t^2 \leq 0$$

$$Q(T_f) = x(T_f)^2 + y(T_f)^2 - r_t^2 = 0$$

The Hamiltonian for the time optimal control problem is given by

$$\mathcal{H} = 1 + \lambda_1 v_0 \cos\psi(t) + \lambda_2 v_0 \sin\psi(t) + \lambda_3 u$$

where$\lambda = [\lambda_1, \lambda_2, \lambda_3]^T$are the costates. The costate equations are as follows:

$$\begin{aligned}
\dot{\lambda}_1 &= 0 \\
\dot{\lambda}_2 &= 0 \\
\dot{\lambda}_3 &= \lambda_1 v_0 \sin\psi - \lambda_2 v_0 \cos\psi
\end{aligned}$$

which implies that λ_1 and λ_2 are constant. The necessary optimality condition for the minimum principle states that along the extremal trajectory,

$$\mathcal{H}(p^*, u^*, \lambda^*, t) \leq \mathcal{H}(p^*, u, \lambda^*, t)$$

for $0 \leq t \leq T_f$, and where p^*, u^*, λ^* are the optimal state, optimal input and optimal costates. According to the result in [99], when $\lambda_3 = 0$, the optimal heading must be constant, i.e., the optimal heading rate input is 0. According to the result in [45], line segments can not be part of the optimal path. When $\lambda_3 \neq 0$, the optimal control is $u = -sgn(\lambda_3) w_{max}$. In terms of the Pontryagin's minimum principle [97], the terminal constates can be given by

$$\begin{aligned}
\lambda_1(T_f) &= \frac{\partial Q}{\partial x} = 2x(T_f)k \\
\lambda_2(T_f) &= \frac{\partial Q}{\partial y} = 2y(T_f)k \\
\lambda_3(T_f) &= 0
\end{aligned} \tag{4.11}$$

where, k is a constant Lagrange multiplier. In addition, the following equation also

needs to be satisfied

$$\frac{\partial Q}{\partial T_f} + \mathcal{H}(T_f) = 0. \tag{4.12}$$

Then, combining (4.11) and (4.12) leads to that

$$k = \frac{-1}{2x(T_f)v_0\cos\psi(T_f) + 2y(T_f)v_0\sin\psi(T_f)}$$

Then, λ_1 and λ_2 can be obtained as follows:

$$\lambda_1(t) = \frac{-x(T_f)}{x(T_f)v_0\cos\psi(T_f) + y(T_f)v_0\sin\psi(T_f)}$$
$$\lambda_2(t) = \frac{-y(T_f)}{x(T_f)v_0\cos\psi(T_f) + y(T_f)v_0\sin\psi(T_f)}$$

$\dot{\lambda}_3(t)$ can also be derived as

$$\begin{aligned}\dot{\lambda}_3(t) &= \frac{-x(T_f)\sin\psi(t) + y(T_f)\cos\psi(t)}{x(T_f)\cos\psi(T_f) + y(T_f)\sin\psi(T_f)} \\ &= \frac{\sin(\theta(t) - \psi(T_f))}{\cos(\theta(T_f) - \psi(T_f))}.\end{aligned}$$

Following the approach proposed in [45] leads to the following result in the interval (s, T_f).

$$\lambda_3(t) = \begin{cases} \frac{1}{w_{max}}\left(\frac{\cos(\theta(T_f)-\psi(t))}{\cos(\theta(T_f)-\psi(T_f))} - 1\right), & u = w_{max} \\ \frac{-1}{w_{max}}\left(\frac{\cos(\theta(T_f)-\psi(t))}{\cos(\theta(T_f)-\psi(T_f))} - 1\right), & u = -w_{max} \end{cases} \tag{4.13}$$

Next, it will show that the heading rate for the optimal path does not change the sign in the threat zone. Without loss of generality, it is assumed that the terminal state $0 \leq \theta(T_f) - \psi(T_f) < \frac{\pi}{2}$. First, the state $0 < \theta(T_f) - \psi(T_f) < \frac{\pi}{2}$ is considered. If the heading rate is $-w_{max}$ in a small interval (s, T_f), $0 < \theta(T_f) - \psi(t) < \theta(T_f) - \psi(T_f)$, which implies that $\lambda_3 < 0$ according to (4.13). In terms of the optimal control, $u = -w_{max}$ implies that $\lambda_3 > 0$. Thus, the above two results contradict, and therefore, if the terminal state $0 < \theta(T_f) - \psi(T_f) < \frac{\pi}{2}$, the heading rate must

be $u = w_{max}$. Then, $\frac{\theta(T_f)-\psi(t)}{\cos(\theta(T_f)-\psi(T_f))} < 1$ until $\theta(T_f) - \psi(t) = -(\theta(T_f) - \psi(T_f))$. Since $0 < \theta(T_f) - \psi(T_f) < \frac{\pi}{2}$, $|\psi(t) - \psi(T_f)| > \pi$. For any initial heading angle $\psi(0)$, one can always find a path that $|\psi(T_f) - \psi(0)| < \pi$ with minimum turning radius. Therefore, for the optimal path, $|\psi(t)-\psi(T_f)| > \pi$ will never happen. Thus, for $0 < \theta(T_f) - \psi(T_f) < \frac{\pi}{2}$, the heading rate must always be $u = w_{max}$. For the case $\theta(T_f) - \psi(T_f) = 0$, $\lambda_3(t)$ does not change the sign. Therefore, the minimum exposure path is a single arc with minimum turning radius.

For each entrance point, there are two candidate optimal trajectories. It is clear that when $-\frac{\pi}{2} < \gamma_0 < 0$, left turn arc is the optimal path, and similarly, when $0 < \gamma_0 < \frac{\pi}{2}$, right turn arc is the optimal path. When $\gamma_0 = 0$, both of right turn arc and left turn arc are optimal paths. However, in order to achieve circular target tracking, right turn is the better choice. From the above analysis, it can be concluded that the proposed controller can guarantee the minimum exposure time. Meanwhile, the exposure time depends on the angle γ at the entrance point. The lager $|\gamma|$ is, the shorter the exposure time is.

When the UAV exits the threat zone, $|\gamma| > \frac{\pi}{2}$, which implies that the state of the UAV $(r(t), \gamma(t)) \in C_2$. Then, the UAV will converge to the desired circular orbit with exposure avoidance.

4.4 Simulation Results

In this section, simulation results are presented to demonstrate the effectiveness of the proposed approach. The simulation includes two scenarios: in scenario one, the initial UAV state $(r_0, \gamma_0) \in C_2$; in scenario two, the initial UAV state $(r_0, \gamma_0) \in \{(r, \gamma) | r_t \leq r \leq (r_t^2 + 2r_m r_t)^{\frac{1}{2}}$ and $0 \leq |\gamma| < \arccos(\frac{r_m^2+r^2-(r_m+r_t)^2}{2r_m r}) - \frac{\pi}{2}\}$. In the previous section, the bang-bang controller is used to provide the rigorous proof. It is well known that, chattering phenomenon which is undesirable in practice is the

major drawback of the bang-bang controller. In order to minimize or eliminate the chattering effect, many approaches have been proposed by researchers worldwide. In the simulation, the following function is used to approximate the bang-bang controller.

$$u = \begin{cases} w_{max} & \text{if } -\pi \leq \gamma < 0 \\ w_{max} sat(g(\psi, r)) & \text{if } 0 \leq \gamma < \pi \text{ and } r \geq r_t \\ -w_{max} & \text{if } 0 \leq \gamma < \pi \text{ and } r < r_t \end{cases} \tag{4.14}$$

where

$$g(\psi, r) = sat(\frac{\psi_d - \psi}{\epsilon})(1 + \frac{4v_0 r_d^3}{(r_d^2 + r^2)^2 w_{max}}) + \frac{4v_0 r_d^3}{(r_d^2 + r^2)^2 w_{max}}$$

$$sat(x) = \begin{cases} x & \text{if } |x| < 1 \\ 1 & \text{if } x \geq 1 \\ -1 & \text{if } x \leq -1 \end{cases}$$

It can be observed that from Eq. 4.14, when the UAV is inside of the threat zone, maximum heading rate control input is applied to minimize the exposure time. When the UAV is located outside the threat zone and the heading is aligned with the desired one, the heading rate $u = \frac{4v_0 r_d^3}{(r_d^2 + r^2)^2}$, which is the desired heading rate for target tracking so that chattering may be avoided. Table 4.1 shows the specifications of the UAV and control law parameters.

Table 4.1: Specifications for adversarial target tracking

Parameter	Value
Nominal airspeed v_0	20 m/s
Maximum heading rate w_{max}	0.2 rad/s
Desired distance r_d	400 m
Threat zone radius r_t	300 m
Boundary layer thickness ϵ	0.1

4.4.1 Scenario One

In this scenario, the UAV starts the mission of target tracking at the position $(x_r, y_r) = (300, 20)$ m with initial heading angle $\psi_0 = \frac{3\pi}{2}$. It can be calculated that the angle $\gamma_0 = 1.504\ rad$, $(r_t^2 + 2r_m r_t)^{\frac{1}{2}} = 387$m, and $\arccos(\frac{r_m^2+r^2-(r_m+r_t)^2}{2r_m r}) - \frac{\pi}{2} = 1.44\ rad$. Therefore, the initial state $(r_0, \gamma_0) \in C_2$. Fig. 4.4 shows the trajectory of the UAV. In order to avoid exposure to the target, at the beginning, the UAV turns left with minimum turning radius. Eventually, the UAV converges to the desired circular orbit. Fig. 4.5 shows the distance between the UAV and target. As shown in Fig. 4.5, although the UAV firstly is very close to the threat zone, it does not enter the threat zone, i.e., the exposure is avoided. The heading rate control input is shown in Fig. 4.6. It can be observed that from Fig. 4.6 and Fig. 4.7 , due to the large heading error, the heading rate control input reaches saturation at the beginning of the mission; as heading error is small enough, heading rate converges to the desired one for target tracking.

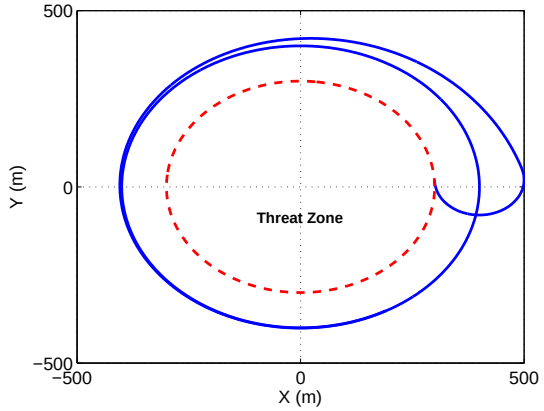

Figure 4.4: Trajectories of the UAV

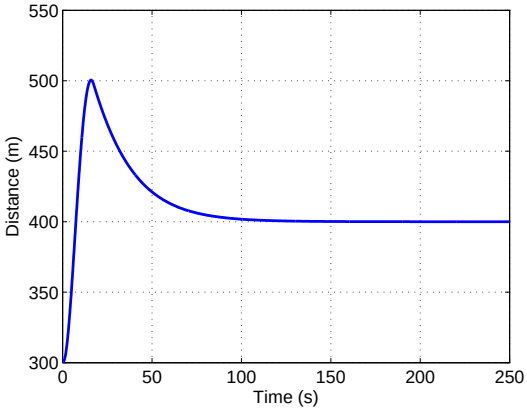

Figure 4.5: The distance between the target and the UAV

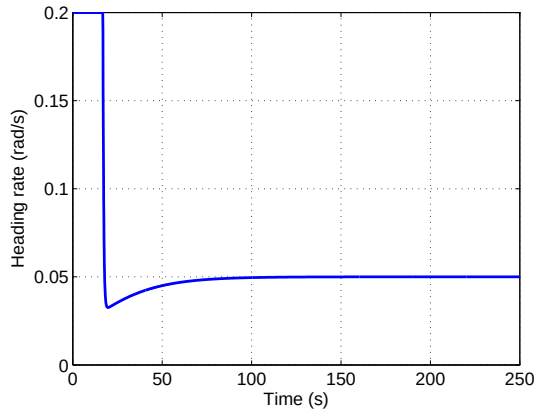

Figure 4.6: Heading rate

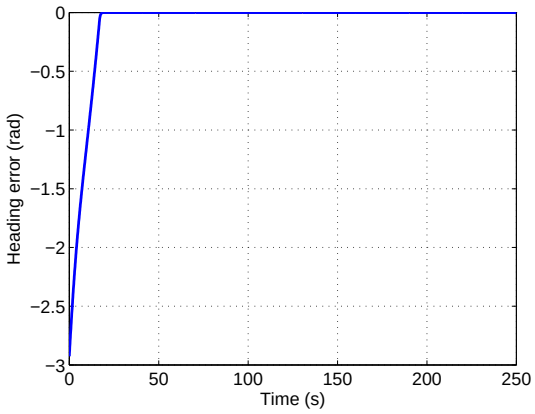

Figure 4.7: Heading error

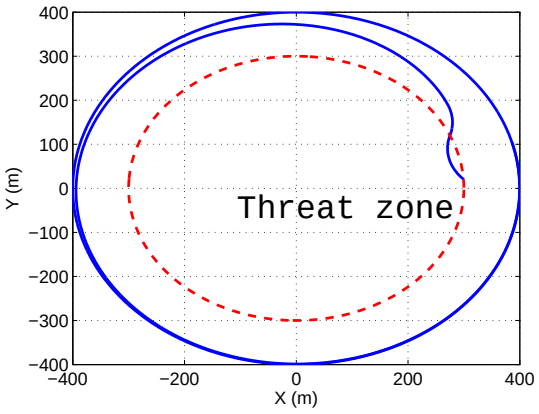

Figure 4.8: Trajectories of the UAV

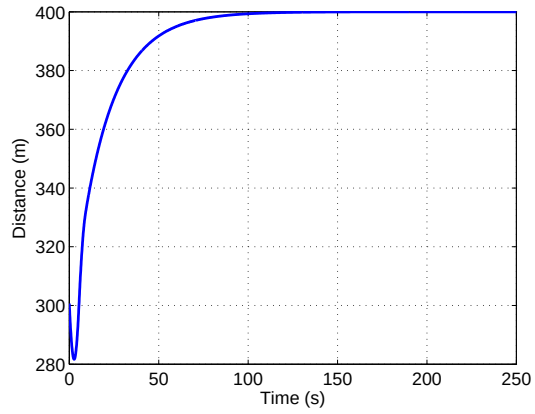

Figure 4.9: The distance between the target and the UAV

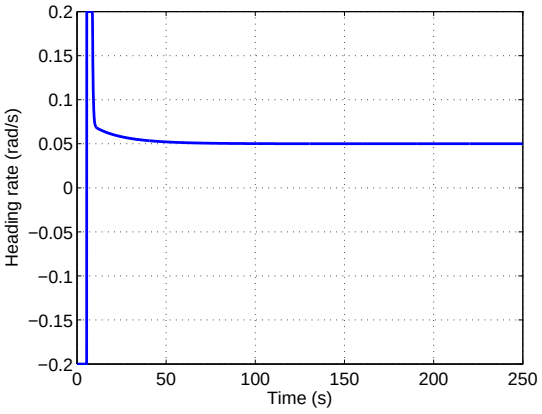

Figure 4.10: Heading rate

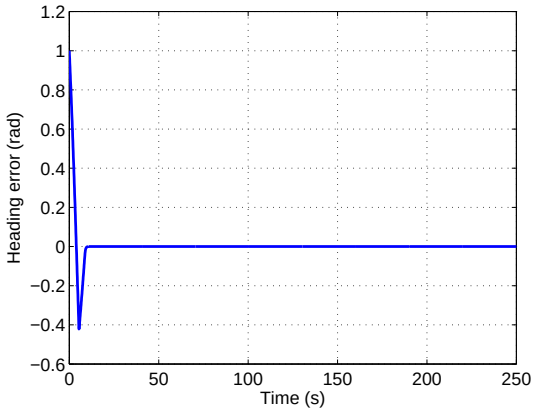

Figure 4.11: Heading error

4.4.2 Scenario Two

In this scenario, the UAV starts the mission of target tracking at the position $(x_r, y_r) = (300, 20)$m with initial heading angle $\psi_0 = \frac{3\pi}{4}$. It can be calculated that the angle $\gamma_0 = 0.8522\ rad$, $(r_t^2 + 2r_m r_t)^{\frac{1}{2}} = 387$ m, and $\arccos(\frac{r_m^2 + r^2 - (r_m + r_t)^2}{2r_m r}) - \frac{\pi}{2} = 1.44\ rad$. Therefore, the initial state $(r_0, \gamma_0) \in C_3$. Fig. 4.8 shows the trajectory of the UAV. In order to minimize the exposure time, at the beginning, the UAV turns right with minimum turning radius. Eventually, the UAV converges to the desired circular orbit. Fig. 4.9 shows the distance between the UAV and the target. As shown in Fig. 4.9, the distance becomes smaller than r_t at the beginning. After the UAV exits the threat zone, it will never enter the threat zone. Fig. 4.10 and Fig. 4.11 show the UAV heading rate and heading error, respectively. It can be observed that from Figs. 4.10-4.11, when the UAV exits the threat zone, heading error is still very large, and therefore maximum heading rate is used to drive the UAV to the desired heading.

4.5 Conclusions

The problem of adversarial ground target tracking using UAVs subject to input constraints has been studied in this chapter. In order to achieve target tracking and exposure avoidance, a bang-bang heading rate controller is proposed. The proposed controller can guarantee the exposure avoidance while the initial state of the UAV belongs to the safe state set, as well as guarantee minimizing the exposure time of the UAV while the initial state belongs to the exposure state set. In both cases, the convergence of the UAV to the desired circular orbit is ensured under the proposed controller. Future works may include the extension of this proposed approach to the moving target case.

Chapter 5

Cooperative Ground Target Tracking

Technical advances in sensing, communication and control systems have spurred the development of multi-agent cooperation. As compared to single UAV target tracking discussed in Chapter 3 and Chapter 4, cooperation of multiple UAVs can provide better performance with higher precision, improved sensitivity, and enhanced robustness. This chapter focuses on the problem of cooperative target tracking in which multiple UAVs are used to track a moving target in constant wind.

5.1 Problem Statement

Many control strategies have been proposed for multi-agent cooperation. However, most of cooperative control strategies use first order integrator or second order integrator as the agent model. These cooperative control strategies may not be suitable for the cooperation of multiple fixed-wing UAVs, due to the UAV properties such as nonholonomic property and input constraints. Recently, Lyapunov vector field approaches [19,23,31] were proposed to achieve multi-UAV cooperation. Collective

motion of the multiple Newtonian particles was studied in [90–92].

Circular formation of UAVs is commonly used for target tracking, and equal space separation along the circular orbit has been proved to be an effective formation structure [100]. However, equal space separation might not be achieved in the presence of strong wind or fast target motion due to physical constraints of the UAV. Therefore, instead of the equal space separation, equal temporal separation could be one choice for multi-UAV cooperation. In [29], the notion of splay state is introduced to represent the equal temporal separation configuration, where the agent velocity is constant.

This chapter aims to control multiple UAVs to fly along a circular orbit around the moving target in the presence of wind. To avoid occluding the line of sight to the target, the cooperative control strategy is developed to distribute the UAVs around the target with equal temporal separation. A new notion called temporal phase is proposed to represent the temporal separation. Background wind, target motion and UAV input constraints are taken into account during controller design. In addition, the stability proof of target tracking with multiple UAVs is provided as well.

5.2 Circular Formation for Target Tracking

5.2.1 Heading Controller

In this section, the cooperative control strategy of multiple UAVs is studied. The relative motion models (2.6) and (2.7) are used in this section, and Assumption 3.1 holds. As discussed in the Chapter 3, if the UAV follows the guidance law (3.1), i.e. the relative course is aligned with the desired relative course, the UAV will converge to the desired circular orbit with the desired distance r_d in a finite time. Then, the cooperative control strategy is just to design the airspeed controller for

each UAV to achieve temporal separation. In order to decouple the relative course rate control of a single UAV from the cooperative control of multiple UAVs, the following assumptions are made.

Assumption 5.1: The initial relative course of the UAV is aligned with the desired one generated by (3.1), and the relative course rate controller is designed as follows:

$$\dot{\chi} = \dot{\chi}_d = \dot{\theta} + \dot{\phi} = \frac{4v_r r_d^3}{(r^2 + r_d^2)^2}, \tag{5.1}$$

where, the definitions of all notations are the same as that in chapter 3.

Remark 5.1: In fact, the relative course rate is achieved through the heading rate which is the actual control input. If the initial relative course is not aligned with the desired relative course, then the heading rate controller should be appropriately designed to regulate the relative course to the desired one.

By the assumption 5.1, the relative motion model (2.7) of the ith UAV can be represented as the following equations:

$$\begin{bmatrix} \dot{r}_i \\ r_i\dot{\theta}_i \end{bmatrix} = \begin{bmatrix} v_{ri}\cos(\phi_i) \\ v_{ri}\sin(\phi_i) \end{bmatrix} = \begin{bmatrix} -\frac{v_{ri}(r_i^2 - r_d^2)}{r_i^2 + r_d^2} \\ \frac{2v_{ri}r_i r_d}{r_i^2 + r_d^2} \end{bmatrix} \tag{5.2}$$

where $v_{ri} = (v_i^2 + T_x^2 + T_y^2 - 2v_i(T_x\cos\psi_{di} + T_y\sin\psi_{di}))^{\frac{1}{2}}$.

Assumption 5.2: there exists a nominal airspeed v_0 and a constant $\Delta v > 0$, such that the following inequalities are satisfied: $v_0 - \Delta v > (T_x^2 + T_y^2)^{\frac{1}{2}}$ and $v_{min} + \Delta v \leq v_0 \leq v_{max} - \Delta v$.

Remark 5.2: This assumption is used to guarantee that the airspeed of the UAV is always faster than moving target velocity and satisfies the control constraints.

Lemma 5.1: [99] Given the UAV relative motion model defined by (2.6), the heading $\psi \in [-\pi, \pi)$ and the relative course $\chi \in [-\pi, \pi)$ are in one-to-one correspondence if and only if $v > (T_x^2 + T_y^2)^{\frac{1}{2}}$.

Remark 5.3: Combining Lemma 5.1 and Assumption 5.2, it can be concluded that, if $v \in (v_0 - \Delta v, v_0 + \Delta v)$ and the desired relative course χ_d is given by (3.1), the desired heading is unique in the domain $[-\pi, \pi)$ and can be calculated by the following equation:

$$\psi_d = \arcsin\left(\frac{T_y \cos\chi_d - T_x \sin\chi_d}{v}\right) + \chi_d. \tag{5.3}$$

Lemma 5.2: If the airspeed control input $v \in (v_0 - \Delta v, v_0 + \Delta v)$, then the relative speed v_r strictly increases monotonically with respect to v .

Proof: Suppose that $v_1, v_2 \in (v_0 - \Delta v, v_0 + \Delta v)$ are two different airspeeds, and $v_1 > v_2$. The two corresponding relative speeds can be denoted by v_{r1}, v_{r2}.

$$\begin{aligned} v_{r1} - v_{r2} &= \frac{v_{r1}^2 - v_{r2}^2}{v_{r1} + v_{r2}} \\ &= \frac{v_1^2 - v_2^2 - 2(v_1 - v_2)(T_x \cos\psi + T_y \sin\psi)}{v_{r1} + v_{r2}} \\ &= \frac{(v_1 - v_2)(v_1 + v_2 - 2(T_x \cos\psi + T_y \sin\psi))}{v_{r1} + v_{r2}} \\ &> 0 \end{aligned}$$

The proof for Lemma 5.2 is completed.

Remark 5.4: Lemma 5.2 implies that if the airspeed of the UAV increases, then the corresponding relative speed will increase as well. This lemma will be used in the proof of stability of the temporal separation. Since the airspeed and the corresponding relative speed have the same performance, the airspeed controller will be developed instead of the relative speed controller. Thus, the airspeed input constraint can be directly taken into account in the procedure of airspeed controller design.

Remark 5.5: It is worth noting that each UAV complies with the above two lemmas, so the subscript i is omitted.

5.2.2 Temporal Separation Controller

Based on the analysis of single UAV control, it is ready to study the problem of cooperative target tracking. For space separation, the clock angle θ is used to represent the space phase of the UAV. Similar to the space phase, a new notation τ is introduced to denote the temporal phase which is expressed as follows:

$$\tau_i(\theta_i) = \begin{cases} \frac{2\pi}{T_\tau}\int_0^{\theta_i+2\pi}\frac{r_d d\theta}{v_{r_d}} - \pi, & \theta_i \in [-\pi, 0) \\ \frac{2\pi}{T_\tau}\int_0^{\theta_i}\frac{r_d d\theta}{v_{r_d}} - \pi, & \theta_i \in [0, \pi) \end{cases} \tag{5.4}$$

where θ_i is the clock angle of the ith UAV with respect to the target, $\tau_i(\theta_i)$ is the temporal phase of the ith UAV, and

$$\begin{aligned} T_\tau &= \int_0^{2\pi}\frac{r_d d\theta}{v_{r_d}}, \\ v_{r_d} &= (v_0^2 + T_x^2 + T_y^2 - 2v_0(T_x\cos\psi_{r_d} + T_y\sin\psi_{r_d}))^{\frac{1}{2}}, \\ \psi_{r_d} &= \arcsin\left(\frac{T_y\cos\chi_d - T_x\sin\chi_d}{v_0}\right) + \chi_d. \end{aligned}$$

Remark 5.6: v_{r_d} represents the relative speed while the UAV flies with a constant nominal airspeed v_0 in the presence of moving target velocity. ψ_{r_d} denotes the desired heading when the UAV is located at the desired circular orbit. Therefore, T_τ is the time that the UAV with a constant nominal airspeed spends completing a circle of flight along the desired circle. T_τ is then used to normalize the flight time of the UAV. Thus, the temporal phase represents the normalized time that the UAV needs to fly from clock angle 0 to the current clock angle along the desired circle.

From the definition of temporal phase (5.4), it can also be observed that the temporal phase is related to the space phase. When the moving target velocity is zero, the temporal phase is equivalent to the space phase. In addition, according to the definition of temporal phase, $\tau_i(\theta_i) \in [-\pi, \pi)$. The detailed temporal separation

of multiple UAVs is illustrated in Fig. 5.1.

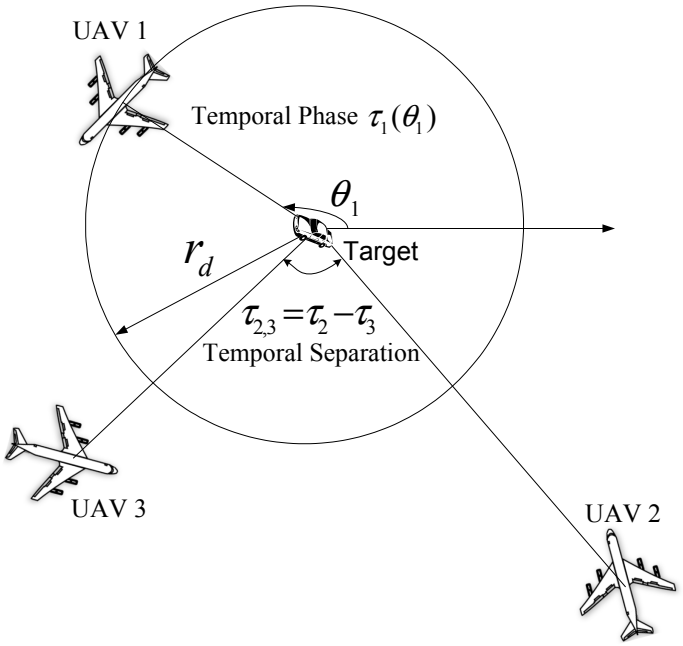

Figure 5.1: Temporal separation of multiple UAVs.

The temporal separation between two neighbor UAVs can be defined as

$$\tau_{i,i+1} = \tau_i - \tau_{i+1}. \tag{5.5}$$

In order to achieve equal temporal separation, cooperative control strategy needs to be designed. In this chapter, leader follower control strategy is used to regulate the temporal separation. Suppose that there are $n(n > 2)$ UAVs. By the assumption 5.1, all the UAVs follow the guidance law (3.1) by varying their heading angles so that they will eventually converge to the desired circular orbit around the target. Meanwhile, as depicted in Fig. 5.1, the UAV 1 is designated as the leader, and the airspeed of UAV 1 is the nominal airspeed v_0 and is held constant. Then, the second UAV follows the first UAV, and varies its airspeed to achieve the desired temporal separation with the first UAV. By analogy, the $(i + 1)$th UAV follows the ith UAV and varies its airspeed to achieve the desired temporal separation with the ith UAV.

If all the UAVs fly along the desired orbit with desired temporal separations, the cooperative target tracking is achieved.

Here, the separation error between the actual separation and the desired separation is defined by the following equation:

$$\Delta\tau_{i+1} = \tau_i - \tau_{i+1} - \tau_d, \tag{5.6}$$

where τ_d is the desired temporal separation between UAVs, which is a prespecified constant according to the number of UAVs.

The separation error (5.6) represents the difference between the actual temporal separation and the desired separation. Differentiating this separation error yields the following dynamics:

$$\begin{aligned}\Delta\dot{\tau}_{i+1} = \dot{\tau}_i - \dot{\tau}_{i+1} &= \frac{2r_d\pi}{T_\tau}\left(\frac{\dot{\theta}_i}{v_{r_di}} - \frac{\dot{\theta}_{i+1}}{v_{r_d(i+1)}}\right) \\ &= \frac{4r_d^2\pi}{T_\tau}\left(\frac{v_{ri}}{(r_i^2 + r_d^2)v_{r_di}} - \frac{v_{r(i+1)}}{(r_{(i+1)}^2 + r_d^2)v_{r_d(i+1)}}\right).\end{aligned} \tag{5.7}$$

Now, the airspeed feedback controllers can be designed as follows:

$$v_1 = v_0, \tag{5.8}$$

$$v_i = v_0 + \frac{\Delta v\Delta\tau_i}{\pi}\frac{r_{i-1}^2 + r_d^2}{r_{i-1}^2 + r_i^2}, i = 2, 3, \cdots, n. \tag{5.9}$$

Remark 5.7: Note from the controller (5.9) that, if the temporal separation is smaller than the desired one, i.e. $\Delta\tau_i < 0$, the ith UAV will reduce its airspeed so that the temporal separation between the $(i-1)$th and ith UAVs will increase. It is also assumed that the initial distances between UAVs and the target are larger than the desired one, i.e. $r_i > r_d$. Then, it can be known that the proposed airspeed controller (5.9) is bounded and satisfies the input constraints (2.2) according to

Assumption 5.2. It is worth noting that when r_i is very large, the second term of the controller (5.9) is small, which implies that target tracking is dominant. When the UAV approaches the desired distance to the target, $\frac{r_{i-1}^2+r_d^2}{r_{i-1}^2+r_i^2} \to 1$, which means that the temporal separation is carried out by the UAV. Next, the system stability will be analyzed.

5.2.3 Stability Analysis

With Assumption 5.1, it can be shown that the distance $r_i (i = 1, 2, \cdots, n)$ will exponentially converge to r_d. Suppose that after the time $t > T_f$, the distance error can be ignored. Then, the dynamics of temporal separation error in (5.7) can be expressed in the following form:

$$\begin{aligned} \Delta\dot{\tau}_i &= -\frac{2\pi}{T_\tau}\left(\frac{v_{ri}}{v_{r_di}} - \frac{v_{r(i-1)}}{v_{r_d(i-1)}}\right) \\ &= -\frac{2\pi}{T_\tau}\left(\frac{v_{ri}-v_{r_di}}{v_{r_di}} - \frac{v_{r(i-1)}-v_{r_d(i-1)}}{v_{r_d(i-1)}}\right) \end{aligned} \tag{5.10}$$

With the variable airspeed controllers (5.8) and (5.9), the following equations can be obtained:

$$\begin{aligned} &\frac{v_{r1}-v_{r_d1}}{v_{r_d1}} = 0, \\ &\frac{v_{ri}-v_{r_di}}{v_{r_di}} = \frac{\Delta v \Delta\tau_i (v_i + v_0 - 2(T_x\cos\psi_{di} + T_y\sin\psi_{di}))}{\pi(v_{ri}+v_{r_di})}, i = 2, 3, \cdots, n. \end{aligned}$$

Then, combining the error dynamics (5.10) and Lemma 5.2 leads to the following system:

$$(\Delta\dot{\tau}_2, \Delta\dot{\tau}_3, \cdots, \Delta\dot{\tau}_n)^T = -A(\Delta\tau_2, \Delta\tau_3, \cdots, \Delta\tau_n)^T \tag{5.11}$$

where

$$A = \begin{bmatrix} K_2 & 0 & \cdots & \cdots \\ -K_2 & K_3 & 0 & \cdots \\ \vdots & -K_3 & \ddots & 0 \\ \vdots & \vdots & -K_{n-1} & K_n \end{bmatrix}$$

$$K_i = \frac{2\Delta v(v_i + v_0 - 2(T_x \cos\psi_{di} + T_y \sin\psi_{di}))}{T_\tau(v_{ri} + v_{r_d i})} > 0.$$

The error dynamics system (5.11) is a cascade-connected system. It can be observed that the state $\Delta\tau_i$ of the upper subsystem $\Delta\dot{\tau}_i = -K_i\Delta\tau_i + K_{i-1}\Delta\tau_{i-1}$ acts as an input to the lower subsystem $\Delta\dot{\tau}_{i+1} = -K_{i+1}\Delta\tau_{i+1} + K_i\Delta\tau_i$. In addition, it can be observed from (5.11) that $|\Delta\tau_2(t)| \leq |\Delta\tau_2(0)|, t \geq 0$, which implies that $\Delta\tau_2(t)$ is bounded, and in turn, $\Delta\tau_i, i = 3, 4, \cdots, n$ is bounded. Then, according to the stability theorem of cascade-connected system [98], the overall error dynamics system is asymptotically stable. It also implies that $(\Delta\tau_2, \Delta\tau_3, \cdots, \Delta\tau_n)^T \to (0, 0, \cdots, 0)^T$.

Based on the above analysis, the major contribution of this chapter can be summarized by the following theorem:

Theorem 5.1: Under the assumptions 5.1 and 5.2, given a group of UAVs with the relative motion model (5.2) and the cooperative airspeed controllers (5.8) and (5.9), the group of UAVs can achieve the desired temporal separation along the circular orbit, i.e., $\Delta\tau_i \to 0, i = 2, 3, \cdots, n$, where, the temporal separation is defined as (5.4).

5.3 Simulation Results

In this section, three simulation scenarios using the proposed approach will be presented. In all the three scenarios, three UAVs are used to execute cooperative target tracking mission. The proposed cooperative control strategy is to distribute the three UAVs with equal temporal separation, i.e. $\Delta\tau_{1,2} = \Delta\tau_{2,3} = 2\pi/3$ along

the desired circular orbit. In the first scenario, three UAVs start the mission with desired initial heading angle without moving target velocity. In the second scenario, the three UAVs perform the same mission with desired initial heading angle in the presence of wind and target motion. In the third scenario, the three UAVs perform the mission with arbitrary initial heading angle in the presence of wind and target motion. Table 5.1 shows the specifications of the UAV and control law parameters. Here, for the sake of simplicity, the direction of the moving target velocity is assumed to be along the x axis.

Table 5.1: Specifications for cooperative target tracking

Parameter	Value
Nominal airspeed v_0	20 m/s
Δv	5 m/s
Maximum heading rate w_{max}	0.2 rad/s
Desired distance r_d	400 m
Moving Target velocity	$(6, 0)$ m/s

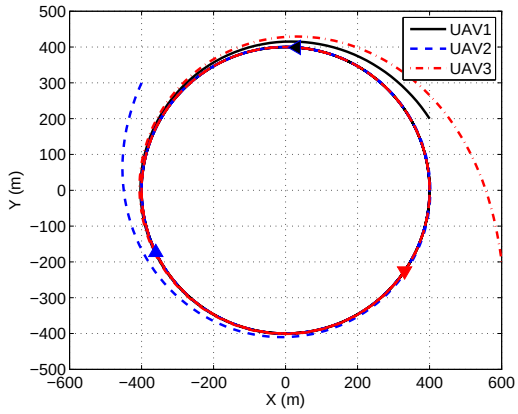

Figure 5.2: UAV Trajectories (Scenario one)

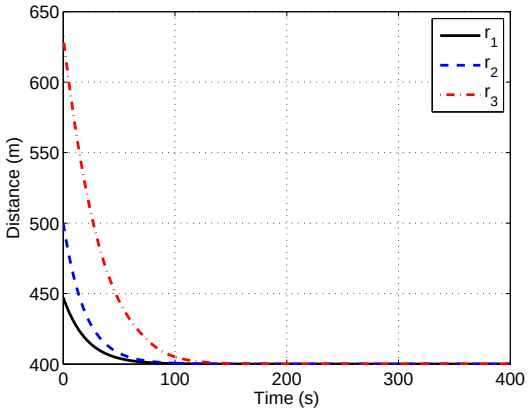

Figure 5.3: Distances between UAVs and target (Scenario one)

In the first scenario, the initial positions of three UAVs are as follows: (400, 200)m, (-400, 300)m, (600, -200)m. The initial heading angles are aligned with the desired ones. Figs. 5.2-5.5 describe the simulation results for the first scenario. Fig. 5.2 and

Fig. 5.3 show that the three UAVs can converge to the desired circular orbit in a finite time. Fig. 5.4 and Fig. 5.5 show space separation error ($\Delta\theta_i = \Delta\theta_{i-1,i} - \theta_d, i = 2, 3$) and temporal separation error $\Delta\tau_i, i = 2, 3$, respectively. As seen from Fig. 5.4 and Fig. 5.5 that the space separation errors and the temporal separation errors have the same dynamics. It implies that the temporal phase and the space phase are equivalent in the absence of moving target velocity.

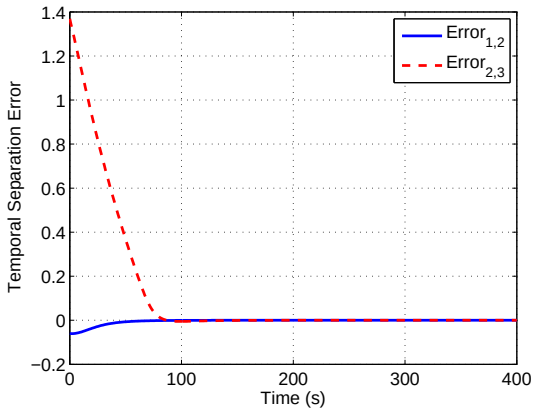

Figure 5.4: Temporal separation error (Scenario one)

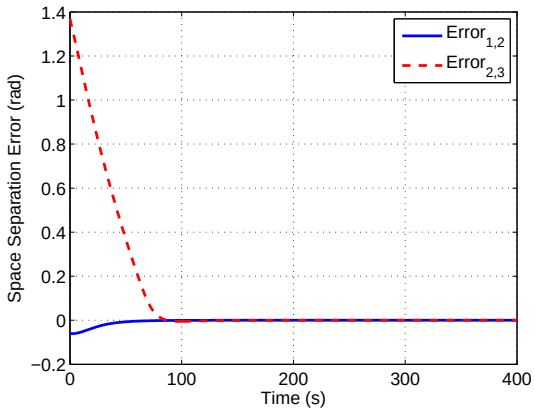

Figure 5.5: Space separation error (Scenario one)

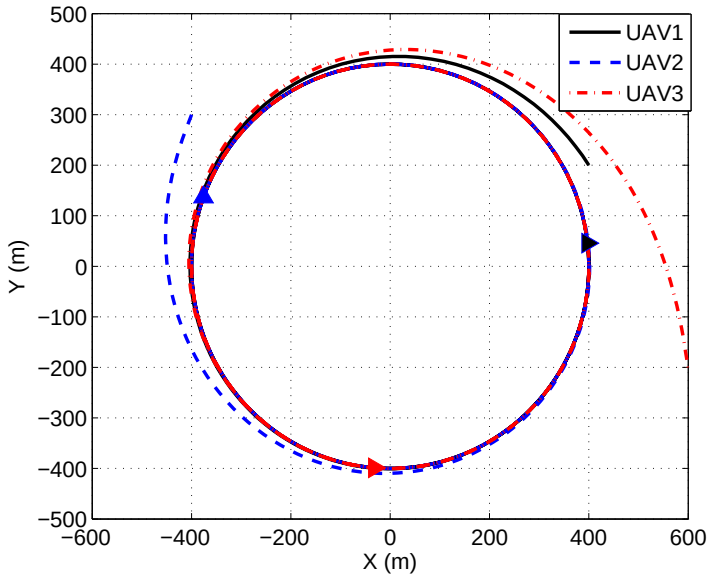

Figure 5.6: UAV Trajectories (Scenario two)

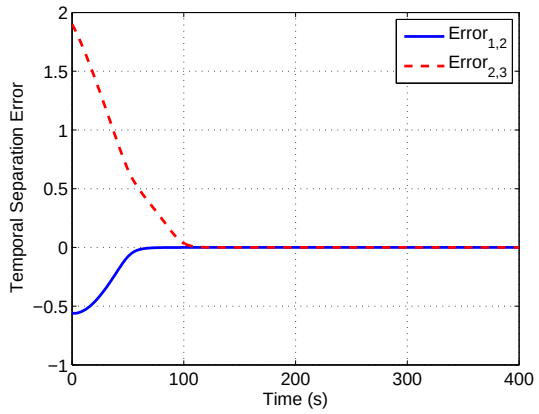

Figure 5.7: Temporal separation error (Scenario two)

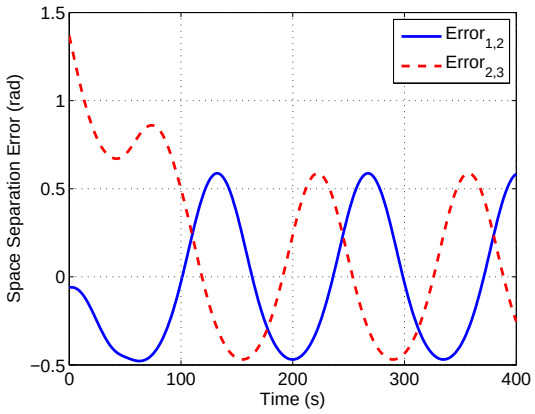

Figure 5.8: Space separation error (Scenario two)

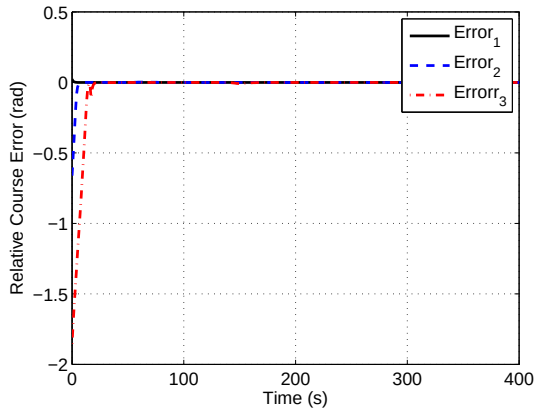

Figure 5.9: Relative course error (Scenario three)

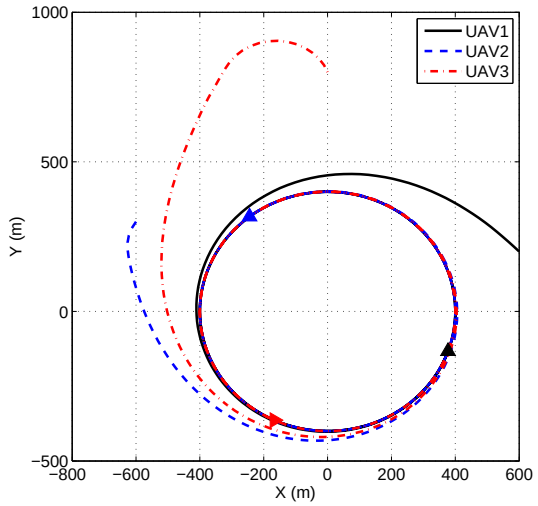

Figure 5.10: UAV Trajectories (Scenario three)

In the second scenario, the initial positions of three UAVs are as follows: (400, 200)m, (-400, 300)m, (600, -200)m. The initial heading angles are also aligned with the desired ones. Moving target velocity is taken into account during simulation, and moving target velocity is (6,0)m/s. Fig. 5.6 shows the trajectories of the three UAVs. It can be observed that the final positions of these three UAVs are not equally spaced. It can be seen from Fig. 5.7 that the temporal separation errors finally converge to zero, which is the same as the first scenario. However, the space

separation errors illustrated in Fig. 5.8 can not converge to zero.

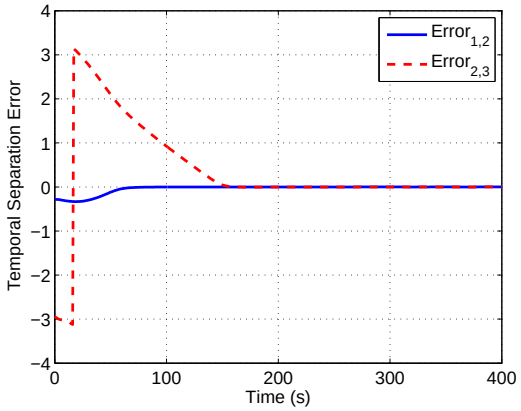

Figure 5.11: Temporal separation error (Scenario three)

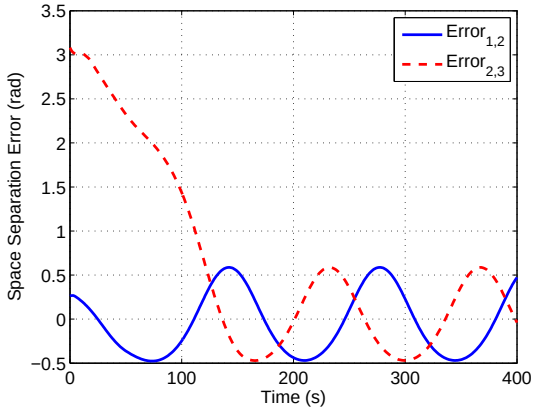

Figure 5.12: Space separation error (Scenario three)

In the third scenario, the initial positions of three UAVs are as follows: (600, 200)m, (-600, 300)m, (0, 800)m. The initial relative course angle of the UAV is not aligned with the desired one. By designing an appropriate heading rate controller, the relative course errors will converge to zero as shown in Fig. 5.9 and furthermore the UAVs can converge to the desired orbit as depicted in Fig. 5.10. The temporal separation errors and space separation errors are shown in Fig. 5.11 and Fig. 5.12, respectively.

5.4 Conclusions

Cooperative target tracking using multiple UAVs is discussed in this chapter. The variable airspeed controller for each UAV is designed to achieve temporal separation under the assumption that the UAV relative course angle is well aligned with the desired angle provided by the guidance law. The proposed approach can provide global stability for equal temporal separation. Simulation results demonstrate the effectiveness of the proposed approach. In addition, simulation results also show that although the initial relative course of the UAV is not well aligned with desired one,

the temporal separation error between UAVs still can converge to zero by designing the heading rate controller appropriately.

Chapter 6

Cooperative Source Seeking

Target tracking is discussed in the previous chapters. The position of the target is assumed to be known in target tracking while the position of the source is unknown in the problem of source seeking. Advances in multi-agent technologies and UAV technologies make it possible to take advantage of cooperation of multiple UAVs for source seeking. This chapter focuses on moving source seeking using multiple UAVs with input constraints. Firstly, a least-squares method is introduced to estimate the gradient of the scalar field at the leader UAV location based on the measurements of all UAVs. Since the moving source velocity is unknown, an adaptive estimator is designed to obtain the velocity. Based on the estimated gradient and velocity, a guidance law for the leader UAV is proposed. In order for the leader to follow the desired heading angle, a sliding mode based heading rate controller is designed. Heading rate controller for each follower UAV is also developed to achieve circular formation around the leader UAV. Furthermore, the gradient estimation error is analyzed and its influence on moving source velocity estimation and level tracking accuracy is explored as well.

6.1 Problem Statement

In the real world, there are various sources which can generate vector fields or scalar fields. This chapter considers the scalar field source, where only a scalar value can be obtained at one point. Scalar fields may represent the temperature distribution throughout space, the strength of an acoustic signal, the concentration of a chemical agent, etc. In each scalar field, there may exist one or more sources which could be pointwise, area, or volume sources. Scalar field source seeking is to find the source using one or more agents based on the measured data. Many different approaches have been proposed to solve the problem in the literature. These works can mainly be classified into two categories: single-agent source seeking, and multi-agent source seeking. For single-agent source seeking, only one agent is used to carry out the mission, where the dithering movement is commonly used to estimate the scalar field gradient [46,47,49]. For multi-agent source seeking, cooperation of multiple robots is carried out for source seeking, which has many advantages over single-agent source seeking as discussed in Chapter 1 [52,53,62].

This chapter studies the problem of cooperative source seeking using multiple UAVs. In order to illustrate the problem formulation clearly, firstly the scalar field source properties need to be defined and described. It is assumed that there is a unique source in the scalar field and the location of the source is $\vec{r}_s = col(x_s, y_s)$. We also need to make the following assumptions for the source.

***Assumption 6.1*:** The scalar field $f(\vec{r}) = f(||\vec{r} - \vec{r}_s||) : \mathbf{R}^2 \to \mathbf{R}$ is a function with respect to $\vec{r}$ and reaches its maximum at $\vec{r} = \vec{r}_s$ [60], where $\vec{r} = col(x, y)$ is the two-dimensional position of the UAV.

***Assumption 6.2*:** The source is moving with a constant velocity $\dot{\vec{r}}_s = \vec{v}_s = col(v_{sx}, v_{sy})$ and $||\vec{v}_s|| < v_l$. The position and velocity of the source are unknown. UAVs can only measure the magnitude of the scalar field.

***Assumption 6.3*:** The hessian matrix H of the scalar field satisfies the following

condition: $-\delta_1 \leq \Lambda(H) \leq -\delta_2$, where $\Lambda(\cdot)$ represents the eigen value of the matrix and δ_1 and δ_2 are positive constants.

Remark 6.1: It is noted from Assumption 6.1 that, the scalar field value $f(\vec{r})$ only depends on the distance from the UAV current location to the source. For instance, $f(\vec{r}) = f_{max}[1 - \tanh(\alpha||\vec{r} - \vec{r}_s||^{\beta})], \alpha > 0, \beta > 0$. Since sources may be far away from the seeking agents like UAVs, it is reasonable to assume that the position and velocity of the source are unknown. In Assumption 6.2, v_l is a constant related to the UAV airspeed which will be determined in the sequel. The introduction of this constant makes it possible for UAVs to achieve source seeking. Assumption 6.3 implies that curvature of the scalar field is bounded.

Based on the above source definition and assumptions, now it is necessary to analyze the source seeking problem. First of all, a cooperative strategy needs to be determined for multiple-UAV control mission. As discussed in Chapter 1, there are mainly three formation strategies: leader-follower, behavior-based, and virtual-structure. Since the source position is unknown, other information is required to achieve source seeking and gradient estimation is considered instead of the position. The gradient of the scalar field needs to be estimated based on the measurement data from multiple UAVs, so leader-follower formation could be adopted where the leader UAV is used to process the gradient estimation. It is assumed that each follower UAV can get the position and velocity information of the leader UAV, and the leader UAV can get the positions and the scalar field values from all follower UAVs. With the assumption 6.2, the constant source velocity is unknown, thus, source velocity estimation is needed in order to achieve accurate source seeking. After the gradient and source velocity are obtained, how to approach the source with a group of UAVs is a problem. As it is well known, the fixed-wing UAV can not stop on top of the source due to its physical constraints if the source velocity is lower. In addition, if the source is a hazardous source which means the UAV must

avoid to be too close to the source. Therefore, level tracking is carried out in this chapter for source seeking. Level tracking implies that the UAV will fly along a trajectory around the source on which the scalar field has the same value. Based on the level tracking, the formation of UAVs can remain in the vicinity of the source. Now, it is ready to state the proposed problem.

Problem: The objective of this chapter is to design algorithms to estimate the gradient and source velocity under the Assumptions 6.1, 6.2 and 6.3, and based on these estimates, to develop controllers for UAVs so that level tracking around the source can be achieved. Furthermore, gradient estimation error and its influence on source velocity estimation error and level tracking accuracy also need to be studied.

6.2 Gradient and Moving Source Velocity Estimation

In this section, the scalar field gradient and moving source velocity are estimated. Firstly, a least-squares method is introduced to estimate the scalar field gradient. Secondly, the estimation error of the gradient is analyzed. Thirdly, moving source velocity is estimated by using an adaptive observer. Lastly, the velocity estimation error is investigated in terms of the gradient estimation error.

6.2.1 Gradient Estimation

As discussed in the previous section, the position of the source is unknown and only the scalar field value can be measured by each UAV. Unlike the approach for gradient estimate in [55], the proposed approach in this section requires the cooperation of all UAVs, including the leader and all followers.

Here, $\vec{r}_1 = col(x_1, y_1)$ denotes the leader position, $\vec{r}_i = col(x_i, y_i)$, $i = 2, 3, \cdots, n,\ n \geq 3$, denotes the ith follower position, and $f_i, i = 1, 2, 3, \cdots, n$, denotes the scalar field

value measured by the ith UAV. If there are n UAVs ($n \geq 3$), it is easy to ensure that the locations of UAVs are non-collinear. Based on the measured scalar field values $f_i, i = 1, 2, 3, \cdots, n$, the leader UAV needs to estimate the scalar field gradient, which is the first order derivative of the scalar field. The scalar field values and all UAV positions are known by the leader UAV. If the scalar field is continuous and smooth, and the distances between the leader UAV and all follower UAVs are short enough, the scalar field value at the follower position can be approximated by using Taylor series expansion at the leader position. The first order approximation of the scalar field at the ith follower location is as follows:

$$f_i \approx f_1 + \frac{\partial f}{\partial x}|_{x=x_1}(x_i - x_1) + \frac{\partial f}{\partial y}|_{y=y_1}(y_i - y_1), \tag{6.1}$$

where $\nabla f = col(\frac{\partial f}{\partial x}|_{x=x_1}, \frac{\partial f}{\partial y}|_{y=y_1})$ is the scalar field gradient at the leader location. For simplicity, $(\frac{\partial f}{\partial x_1}, \frac{\partial f}{\partial y_1})$ will be used instead of $(\frac{\partial f}{\partial x}|_{x=x_1}, \frac{\partial f}{\partial y}|_{y=y_1})$, and $\vec{r}_{ij} = \vec{r}_i - \vec{r}_j, i = 1, 2, 3, \cdots, j = 1, 2, 3, \cdots$.

Remark 6.2: It should be noted that $f_i, i = 1, 2, 3, \cdots, n$ is known by the leader UAV. In order to obtain accurate gradient estimate, the distances between follower UAVs and leader UAV should be as short as possible so that the first order term of the Taylor series expansion dominates. However, if the distances are too short, the existence of the measurement noise may lead to large errors in the differences between the measured scalar field values.

Then, stacking the approximations of the scalar field at all follower locations leads to the following equations:

$$\begin{bmatrix} f_2 - f_1 \\ f_3 - f_1 \\ \vdots \\ f_n - f_1 \end{bmatrix} \approx \begin{bmatrix} x_2 - x_1 & y_2 - y_1 \\ x_3 - x_1 & y_3 - y_1 \\ \vdots & \vdots \\ x_n - x_1 & y_n - y_1 \end{bmatrix} \bullet \begin{bmatrix} \frac{\partial f}{\partial x_1} \\ \frac{\partial f}{\partial y_1} \end{bmatrix}. \tag{6.2}$$

For the purpose of simplicity, the notation P is introduced to denote the following matrix:

$$P = \begin{bmatrix} x_2 - x_1 & y_2 - y_1 \\ x_3 - x_1 & y_3 - y_1 \\ \vdots & \vdots \\ x_n - x_1 & y_n - y_1 \end{bmatrix}. \tag{6.3}$$

In order to estimate the gradient $(\frac{\partial f}{\partial x_1}, \frac{\partial f}{\partial y_1})$, a least-squares formula is used such that

$$\begin{bmatrix} G_x \\ G_y \end{bmatrix} = (P^T P)^{-1} P^T \begin{bmatrix} f_2 - f_1 \\ f_3 - f_1 \\ \vdots \\ f_n - f_1 \end{bmatrix}, \tag{6.4}$$

where $\vec{G} = col(G_x, G_y)$ is the estimated gradient at the leader location.

Since there exist noises in the measurement data and the first order approximation of the scalar field ignores the second and higher order terms, there may exist errors in the gradient estimation. In this section, the influence of the second order term of the Taylor series expansion on the gradient estimation error is analyzed. The following second order approximation of the scalar field is taken into account [52]:

$$f_i \approx f_1 + \nabla f \cdot \vec{r}_{i1} + \frac{1}{2} \vec{r}_{i1}^T H_1 \vec{r}_{i1}, \tag{6.5}$$

where, H_1 is the hessian matrix at the leader location. Then, it can be obtained that:

$$\nabla f = (P^T P)^{-1} P^T \begin{bmatrix} f_2 - f_1 \\ f_3 - f_1 \\ \vdots \\ f_n - f_1 \end{bmatrix} - \frac{1}{2} (P^T P)^{-1} P^T \begin{bmatrix} \vec{r}_{21}^T H_1 \vec{r}_{21} \\ \vdots \\ \vec{r}_{i1}^T H_1 \vec{r}_{i1} \\ \vdots \\ \vec{r}_{n1}^T H_1 \vec{r}_{n1} \end{bmatrix}. \tag{6.6}$$

Subtracting (6.6) from (6.4) leads to the following result:

$$\Delta\vec{G} = \vec{G} - \nabla f = \frac{1}{2}(P^T P)^{-1} P^T \begin{bmatrix} \vec{r}_{21}^T H_1 \vec{r}_{21} \\ \vdots \\ \vec{r}_{i1}^T H_1 \vec{r}_{i1} \\ \vdots \\ \vec{r}_{n1}^T H_1 \vec{r}_{n1} \end{bmatrix}, \tag{6.7}$$

where $\Delta\vec{G} = col(\Delta G_x, \Delta G_y)$ is the gradient estimation error.

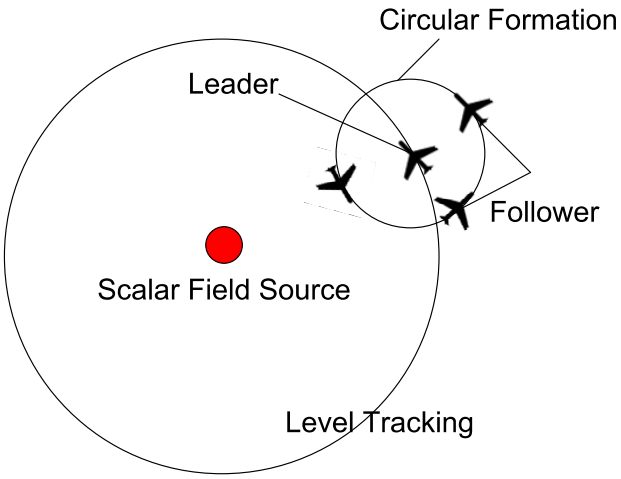

Figure 6.1: Level tracking and circular formation

It can be observed from (6.7) that the gradient estimation error depends on the relative positions between UAVs and the hessian matrix of the scalar field at the leader location. Thus, if the UAV formation is well designed, the gradient estimation error can be reduced. In this chapter, circular formation is used where the leader UAV is located at the center of the formation and all follower UAVs fly along the circle around the leader as depicted in Fig. 6.1. In this circular formation, the distances between the leader UAV and follower UAVs are constant and could be short enough for communication. If the circular formation is assumed to be well

maintained, it can be obtained that

$$\vec{r_i} = \vec{r_1} + r_c(\cos\theta_i, \sin\theta_i)^T, i = 2, 3, \cdots, n, \tag{6.8}$$

where, r_c is the radius of the circular formation, θ_i is the clock angle of the ith follower UAV with respect to the leader. Substituting (6.8) into $(P^TP)^{-1}$ leads to

$$\begin{aligned}(P^TP)^{-1} &= \frac{1}{r_c^2}\begin{bmatrix} \sum_{i=2}^n \cos^2\theta_i & \sum_{i=2}^n \sin\theta_i\cos\theta_i \\ \sum_{i=2}^n \sin\theta_i\cos\theta_i & \sum_{i=2}^n \sin^2\theta_i \end{bmatrix}^{-1} \\ &= \frac{1}{r_c^2\sum_{i<j,i=2,j=3}^{i=n-1,j=n}\sin^2(\theta_i-\theta_j)}\begin{bmatrix} \sum_{i=2}^n \sin^2\theta_i & -\sum_{i=2}^n \sin\theta_i\cos\theta_i \\ -\sum_{i=2}^n \sin\theta_i\cos\theta_i & \sum_{i=2}^n \cos^2\theta_i \end{bmatrix}\end{aligned} \tag{6.9}$$

With Assumption 6.3, Substituting (6.8) and (6.9)into (6.7) results in that

$$||\Delta\vec{G}|| \leq \frac{r_c\delta_1}{\sum_{i<j,i=2,j=3}^{i=n-1,j=n}\sin^2(\theta_i-\theta_j)}||g(\theta_2,\theta_3,\cdots)|| \tag{6.10}$$

where, $g(\cdot)$ is a bounded function of clock angles.

Remark 6.2: It is observed from (6.10) that the gradient estimation error bound depends on the radius r_c of the circular formation. Smaller radius may result in a more accurate estimation. However, the formation radius is constrained by two factors. One is the UAV physical constraints such as the bounded UAV heading rate. The other factor is that if the radius is too small, then the measured field differences between UAVs are very tiny so that measurement noise may lead to large estimation error.

Remark 6.3: It also can be noted from (6.10) that the gradient estimation error bound depends on the space separation of the follower UAVs. Here, two cases are analyzed, where three and four UAVs are used for source seeking.

Case 1: Three UAVs including one leader and two followers

In this case, n=3 and the gradient estimation error bound is as follows:

$$||\Delta\vec{G}|| \leq \frac{r_c\delta_1}{\sin^2(\theta_2-\theta_3)}||g(\theta_2,\theta_3)||. \tag{6.11}$$

$\theta_2-\theta_3=0$ implies that the two followers are located at the same point and $|\theta_2-\theta_3|=\pi$ implies that the three UAVs are collinear. Since $\sin(\theta_2-\theta_3)=0$, (P^TP) is singular, which implies that there is a large estimation error. When $|\theta_2-\theta_3|=\frac{\pi}{2}$, $\sin(|\theta_2-\theta_3|)=1$ and in turn it implies that the estimation error bound attains the minimum.

Case 2: Four UAVs including one leader and three followers

In this case, n=4 and the gradient estimation error bound is as follows:

$$||\Delta\vec{G}|| \leq \frac{r_c\delta_1}{\sum_{i<j,i=2,j=3}^{i=3,j=4}\sin^2(\theta_i-\theta_j)}||g(\theta_2,\theta_3,\theta_4)||. \tag{6.12}$$

In order to analyze the error bound, let $F(\theta_2,\theta_3,\theta_4)=\sum_{i<j,i=2,j=3}^{i=3,j=4}\sin^2(\theta_i-\theta_j)$ and $\theta_{ij}=\theta_i-\theta_j$. It is known that $\sin^2(\theta_{24})=\sin^2(\theta_{23}+\theta_{34})$. By using $\theta_{23}+\theta_{34}$ to replace θ_{24}, differentiating F with respect to θ_{23} and θ_{34} yields that

$$\frac{\partial F}{\partial\theta_{23}}=2\sin(\theta_{23})\cos(\theta_{23})+2\sin(\theta_{23}+\theta_{34})\cos(\theta_{23}+\theta_{34}) \tag{6.13}$$

$$\frac{\partial F}{\partial\theta_{34}}=2\sin(\theta_{34})\cos(\theta_{34})+2\sin(\theta_{23}+\theta_{34})\cos(\theta_{23}+\theta_{34}) \tag{6.14}$$

Let $\frac{\partial F}{\partial\theta_{23}}=0$ and $\frac{\partial F}{\partial\theta_{34}}=0$, and according the corresponding hessian matrix, one can obtain the following solutions: when $\theta_{23}=\theta_{34}=\frac{\pi}{3},\theta_{24}=\frac{2\pi}{3}$ and $\theta_{23}=\theta_{34}=\theta_{42}=\frac{2\pi}{3}$, F attains the maximum which implies that the estimation error bound reaches the minimum; when $\theta_{23}=\theta_{34}=\theta_{24}=0$, F attains the minimum point which implies that the estimation error bound approaches infinity.

6.2.2 Moving Source Velocity Estimation

Based on the estimated gradient, one can proceed to estimate the moving source velocity. According to the definition of the scalar field, differentiating the scalar field at the leader location with respect to time yields that

$$\dot{f}_1 = \frac{\partial f}{\partial x_1}(\dot{x}_1 - v_{sx}) + \frac{\partial f}{\partial y_1}(\dot{y}_1 - v_{sy}). \tag{6.15}$$

The following adaptive observer is proposed to estimate the velocity:

$$\dot{\hat{f}}_1 = G_x(\dot{x}_1 - \hat{v}_{sx}) + G_y(\dot{y}_1 - \hat{v}_{sy}) + L\Delta f_1 + ksgn(\Delta f_1). \tag{6.16}$$

where, L and k are the design gains, $\hat{f}_1$ is the estimated scalar field value at the leader location, $\hat{v}_s = (\hat{v}_{sx}, \hat{v}_{sy})^T$ is the moving source velocity estimate and $\Delta f_1 = f_1 - \hat{f}_1$ is the field estimation error. Here, $\Delta v_{sx} = v_{sx} - \hat{v}_{sx}$, and $\Delta v_{sy} = v_{sy} - \hat{v}_{sy}$. As there exists error in the gradient estimate, the sign function is introduced to reject this error. Differentiating the scalar field estimation error Δf_1 with respect to time leads to

$$\begin{aligned}\Delta\dot{f}_1 &= \dot{f}_1 - \dot{\hat{f}}_1 \\ &= -[G_x(\Delta v_{sx}) + G_y(\Delta v_{sy}) + \Delta G_x(\dot{x}_1 - v_{sx})) \\ &\quad + \Delta G_y(\dot{y}_1 - v_{sy})) + L\Delta f_1 + ksgn(\Delta f_1)].\end{aligned} \tag{6.17}$$

As discussed in the previous section, the gradient estimation error is affected by the circular formation. Here, it is assumed that the gradient estimation error is bounded and small enough. Consider the following Lyapunov function candidate:

$$V_1 = \frac{1}{2}(\Delta f_1^2 + \Delta v_{sx}^2 + \Delta v_{sy}^2). \tag{6.18}$$

Differentiating this Lyapunov function leads to

$$\dot{V}_1 = \Delta f_1 \Delta \dot{f}_1 + \Delta v_{sx} \Delta \dot{v}_{sx} + \Delta v_{sy} \Delta \dot{v}_{sy}. \tag{6.19}$$

Substituting $\nabla f = \vec{G} - \Delta \vec{G}$ into Eq. (6.19) yields

$$\begin{aligned} \dot{V}_1 &= -\Delta f_1 [G_x(\Delta v_{sx}) + G_y(\Delta v_{sy}) + \Delta G_x(\dot{x}_1 - v_{sx})) \\ &\quad + \Delta G_y(\dot{y}_1 - v_{sy})) + L\Delta f_1 + ksgn(\Delta f_1)] \\ &\quad + \Delta v_{sx} \Delta \dot{v}_{sx} + \Delta v_{sy} \Delta \dot{v}_{sy}. \end{aligned} \tag{6.20}$$

The adaptive update laws for $\hat{v}_{sx}$ and $\hat{v}_{sy}$ are as follows:

$$\dot{\hat{v}}_{sx} = -\Delta f_1 G_x; \dot{\hat{v}}_{sy} = -\Delta f_1 G_y. \tag{6.21}$$

The gain k is designed as follows:

$$k = ||\Delta G_x(\dot{x}_1 - v_{sx}) + \Delta G_y(\dot{y}_1 - v_{sy})||_\infty \leq ||\Delta \vec{G}||_\infty (v_1 + ||\vec{v}_s||), \tag{6.22}$$

where, v_1 is the airspeed of the leader UAV and $||\vec{v}_s||$ is the speed of the moving source.

Substituting Eqs.(6.21) and (6.22) into Eq.(6.20) results in that

$$\begin{aligned} \dot{V}_1 &= -L\Delta f_1^2 - k|\Delta f_1| - \Delta f_1(\Delta G_x(\dot{x}_1 - v_{sx}) + \Delta G_y(\dot{y}_1 - v_{sy})) \\ &\leq -L\Delta f_1^2. \end{aligned} \tag{6.23}$$

It is noted from Eq.(6.23) that, $\Delta f_1, \Delta v_{sx}$ and Δv_{sy} are bounded. In addition, according to Assumption 6.3, $\Delta \dot{\vec{G}} = \dot{\vec{G}} - \nabla \dot{f}$ and $\Delta \dot{f}_1$ are also bounded, which implies that $\ddot{V}_1$ is bounded. Therefore, according to Barbalat's lemma, $\dot{V}_1 = 0$ as

$t \to \infty$, which in turn implies that $\Delta f_1 = 0$ and $\Delta \dot{f}_1 = 0$ as $t \to \infty$. Hence, one can obtain the following equation from Eq. (6.17):

$$-G_x(\Delta v_{sx}) - G_y(\Delta v_{sy}) = (\dot{x}_1 - v_{sx}, \dot{y}_1 - v_{sy})\Delta\vec{G} + ksgn(\Delta f_1) \tag{6.24}$$

$$||G_x(\Delta v_{sx}) + G_y(\Delta v_{sy})|| \leq 2||\Delta\vec{G}||_\infty(v_1 + ||\vec{v}_s||) \tag{6.25}$$

$$||\vec{G}||||(\Delta v_{sx}, \Delta v_{sy})|| \cos\Phi \leq 2||\Delta\vec{G}||_\infty(v_1 + ||\vec{v}_s||) \tag{6.26}$$

It can be known from Eqs.(6.21) that when $\Delta f_1 \to 0$, $(\Delta v_{sx}, \Delta v_{sy})$ will be constant. Then, Φ is dependent on $\vec{G}$. For any $\Phi \in [-\pi, \pi)$, the equation (6.26) holds. Thus, it can be derived that

$$||\Delta\vec{v}_s|| = ||(\Delta v_{sx}, \Delta v_{sy})|| \leq \frac{2||\Delta\vec{G}||_\infty(v_1 + ||\vec{v}_s||)}{\min_{(x,y)\in S}||\vec{G}||}, \tag{6.27}$$

where, S denotes the area in which the leader UAV locates. It can be observed from Eq. (6.27) that, the source velocity estimation error depends on the minimum gradient. When the UAV flies close to the source, the gradient will increase so that the velocity estimation error will be reduced. It can also be concluded that the moving source velocity estimation error is determined by the gradient error. Therefore, if the gradient error is small enough, then one can obtain an accurate estimate for the source velocity.

6.3 Level Tracking of Multiple UAVs

In the previous section, scalar field gradient and moving source velocity are estimated and the estimation errors are also analyzed. Now it is ready to design controllers for UAVs so that level tracking around the source is achieved. In this

section, a guidance law based on the estimated gradient and moving source velocity is proposed for the leader UAV. Heading rate controller for the leader UAV is designed such that the desired heading generated by the guidance law is always followed. The overall control structure is described in Fig. 6.2. Then, level tracking error is explored in terms of the gradient estimation error. Lastly, in order for follower UAVs to achieve circular formation, heading rate controllers are designed.

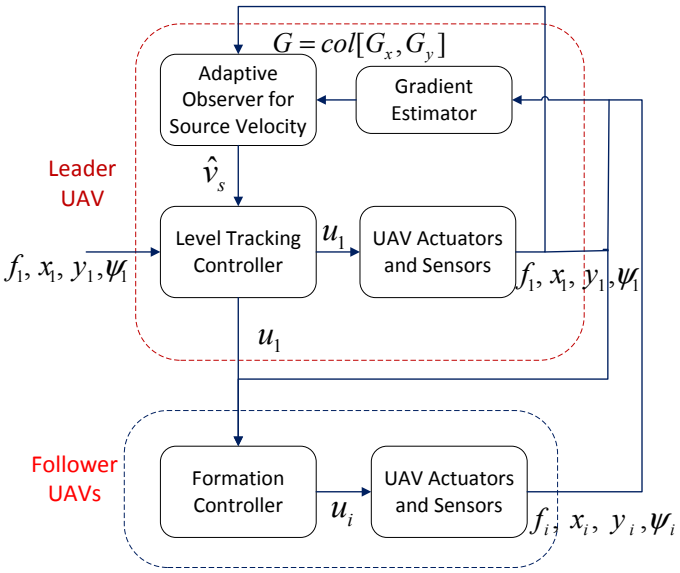

Figure 6.2: Control structure for source seeking

6.3.1 Guidance Law and Controller Design for Leader UAV

Level tracking of the scalar field by the leader UAV will be discussed in the sequel. Different from the previous work [102], moving source is considered in this chapter. Thus, the guidance law proposed in [102] needs to be modified. Firstly, consider the

leader UAV kinematics:

$$\begin{aligned} \dot{x}_1 &= v_1 \cos\psi_1 &&= v_{1r}\cos\chi_1 + \hat{v}_{sx} \\ \dot{y}_1 &= v_1 \sin\psi_1 &&= v_{1r}\cos\chi_1 + \hat{v}_{sy} \ , \\ \dot{\psi}_1 &= u_1 &&= \tfrac{\dot{\chi}_1}{\lambda_u(\psi)} \end{aligned} \tag{6.28}$$

where, χ_1 denotes the relative course angle, v_{1r} denotes the relative speed, and

$$v_{1r} = (v_1^2 + \hat{v}_{sx}^2 + \hat{v}_{sy}^2 - 2v_1(\hat{v}_{sx}\cos\psi_1 + \hat{v}_{sy}\sin\psi_1))^{\frac{1}{2}}, \tag{6.29}$$

$$\chi_1 = \arctan 2(v_1\sin\psi_1 - \hat{v}_{sy}, v_1\cos\psi_1 - \hat{v}_{sx}), \tag{6.30}$$

$$\lambda_u(\psi_1) = \frac{v_1^2 - v_1(\hat{v}_{sx}\cos\psi_1 + \hat{v}_{sy}\sin\psi_1)}{v_{1r}^2}. \tag{6.31}$$

Remark 6.4: In Assumption 6.2, the source velocity $v_s < v_l$. In order for the leader UAV to achieve level tracking, the leader velocity should satisfy the following condition: $v_1 \geq v_l$. It is also assumed that the prespecified field level value is f_d, and the following guidance law for the relative course angle is proposed.

$$\chi_1^d = \arctan 2(G_y, G_x) - \pi + 2\arctan(\frac{f_d}{f_1}) \in [-\pi, \pi) \tag{6.32}$$

Based on this desired relative course angle, one also can compute the desired heading angle by using Eq.(6.30). According to the results in [102], if there exist no errors in gradient estimate and moving source estimate, the proposed guidance law can drive the leader UAV to the desired level set. However, estimation errors are usually inevitable in practice. Therefore, next, it proceeds to analyze the stability and level tracking error bound. Here, it is assumed that the UAV heading angle is always equal to the desired one. Consider the following Lyapunov function candidate:

$$V_2 = \frac{1}{2}(f_1 - f_d)^2. \tag{6.33}$$

Differentiating this function (6.33) with respect to time leads to that

$$\begin{aligned}
\dot{V}_2 &= (f_1 - f_d)\dot{f}_1 \\
&= (f_1 - f_d)[\frac{\partial f}{\partial x_1}, \frac{\partial f}{\partial y_1}][\dot{x}_1 - v_{sx}, \dot{y}_1 - v_{sy}]^T \\
&= -(f_1 - f_d)[\frac{\partial f}{\partial x_1}, \frac{\partial f}{\partial y_1}][v_{1r}\cos(\chi_1^d) + \hat{v}_{sx} - v_{sx}, v_{1r}\sin(\chi_1^d) + \hat{v}_{sy} - v_{sy}]^T \\
&= -(f_1 - f_d)[\frac{\partial f}{\partial x_1}, \frac{\partial f}{\partial y_1}]v_{1r}\frac{G_x(f_1^2 - f_d^2) - 2G_y f_1 f_d}{\sqrt{G_x^2 + G_y^2}(f_1^2 + f_d^2)} \\
&\quad -\Delta v_{sx}, v_{1r}\frac{G_y(f_1^2 - f_d^2) + 2G_x f_1 f_d}{\sqrt{G_x^2 + G_y^2}(f_1^2 + f_d^2)} - \Delta v_{sy}]^T
\end{aligned}$$

$$\begin{aligned}
\dot{V}_2 &= -(f_1 - f_d)[v_{1r}\frac{(\frac{\partial f}{\partial x_1}^2 + \frac{\partial f}{\partial y_1}^2 + \frac{\partial f}{\partial x_1}\Delta G_x + \frac{\partial f}{\partial y_1}\Delta G_y)(f_1^2 - f_d^2)}{\sqrt{G_x^2 + G_y^2}(f_1^2 + f_d^2)} \\
&\quad -\frac{2(\frac{\partial f}{\partial x_1}\Delta G_y - \frac{\partial f}{\partial y_1}\Delta G_x)f_1 f_d}{\sqrt{G_x^2 + G_y^2}(f_1^2 + f_d^2)} - \frac{\partial f}{\partial x_1}\Delta v_{sx} - \frac{\partial f}{\partial y_1}\Delta v_{sy}] \\
&\leq -v_{1r}(f_1 + f_d)\frac{||\nabla f||^2(f_1 - f_d)^2}{\sqrt{G_x^2 + G_y^2}(f_1^2 + f_d^2)} \\
&\quad +v_{1r}\frac{(|f_1^2 - f_d^2||f_1 - f_d| + 2|f_1 - f_d|f_1 f_d)||\Delta G||||\nabla f||}{\sqrt{G_x^2 + G_y^2}(f_1^2 + f_d^2)} \\
&\quad +||\nabla f||||\Delta v_s|||f_1 - f_d|
\end{aligned} \tag{6.34}$$

It can be observed from (6.34) that if

$$\begin{aligned}
|f_1 - f_d| &> \frac{(|f_1^2 - f_d^2| + 2f_1 f_d)||\Delta G||}{||\nabla f||(f_1 + f_d)} \\
&\quad +\frac{||\Delta v_s||\sqrt{G_x^2 + G_y^2}(f_1^2 + f_d^2)}{v_{1r}||\nabla f||(f_1 + f_d)},
\end{aligned}$$

then, it can be obtained that

$$\dot{V}_2 < 0 \tag{6.35}$$

It can be concluded that the level tracking error $|f_1 - f_d|$ is bounded and eventually

converges to the following region: $[0, \frac{v_{1r}(|f_1^2-f_d^2|+2f_1f_d)||\Delta G||+||\Delta v_s||\sqrt{G_x^2+G_y^2}(f_1^2+f_d^2)}{v_{1r}||\nabla f||(f_1+f_d)}]$.

Next, the heading rate controller is designed so that the UAV always follows the desired heading angle. Here, firstly a sliding mode based relative course rate controller is designed as follows:

$$\dot{\chi}_1 = -w_1^0 sgn(\chi_1 - \chi_1^d), \tag{6.36}$$

where w_1^0 is a positive constant.

To guarantee that the UAV can follow the desired relative course, it is assumed that $|\dot{\chi}_1^d| < w_1^0$. Let $V_3 = (\chi_1 - \chi_1^d)^2$, and then the time derivative

$$\begin{aligned} \dot{V}_3 &= 2(\chi_1 - \chi_1^d)(-w_1^0 sgn(\chi_1 - \chi_1^d) - \dot{\chi}_1^d) \\ &= -2k(\chi_1 - \chi_1^d)^2 \leq 0, \end{aligned} \tag{6.37}$$

where $k > 0$ and $-w_1^0 sgn(\chi_1 - \chi_1^d) = -k(\chi_1 - \chi_1^d) + \dot{\chi}_1^d$.

Based on this relative course rate, the heading rate controller can also be obtained by using Eq.(6.31). By using the proposed course rate controller (6.36), the actual course of the leader UAV will eventually converge to the desired one. Hence, the leader UAV will finally fly along the desired level curve around the source, if the estimated gradient and moving source velocity is accurate enough. It is worth noting that, the course rate control parameter w_1^0 and the constant airspeed v_1 of the leader must be carefully selected so that the follower UAVs have a high enough level of maneuverability to follow the leader. Since the sliding mode controller may lead to undesirable chattering, in order to overcome this problem, the following continuous function is used to replace the sliding mode controller (6.36):

$$\dot{\chi}_1 = -w_1^0 sat(\mu(\chi_1 - \chi^d)), \tag{6.38}$$

where $\mu > 0$ and $sat(x) = \begin{cases} 1, & \text{if } x > 1 \\ x, & \text{if } |x| \leq 1 \\ -1, & \text{if } x < -1 \end{cases}$.

6.3.2 Controller Design for Follower UAVs

The proposed relative course rate controller for the leader can also be transformed to the heading rate controller. In this section, follower heading rate controller is designed so that the circular formation can be achieved and well maintained. It is ready to proceed to design the heading rate controller for the follower UAVs.

The relative position of the follower UAV with respect to the leader can be represented as

$$x_{i1} = x_i - x_1, y_{i1} = y_i - y_1, i = 2, 3, \cdots n. \tag{6.39}$$

χ_i is introduced to denote the relative course angle of the follower UAV with respect to the leader. Then, relative kinematics can be represented as

$$\begin{cases} \dot{x}_{i1} = v_{i1} \cos \chi_i \\ \dot{y}_{i1} = v_{i1} \sin \chi_i \end{cases} i = 2, 3, \cdots n. \tag{6.40}$$

where, $v_{i1} = ((\dot{x}_i - \dot{x}_1)^2 + (\dot{y}_i - \dot{y}_1)^2)^{\frac{1}{2}}$ and $\chi_i = \arctan 2(\dot{y}_i - \dot{y}_1, \dot{x}_i - \dot{x}_1)$. Here, it can be observed that if $v_i > v_1$, then $v_{i1} \geq \Delta > 0$, where Δ is a positive constant. In this chapter, it is assumed that $v_i > v_1$ and the airspeeds of all followers are the same.

The relationship between the actual heading rate and the relative course rate can be represented by the following formula

$$\dot{\psi}_i = \frac{[v_{i1}\dot{\chi}_i + v_1 u_1 \cos(\chi_i - \psi_1)]}{v_i \cos(\chi_i - \psi_i)}. \tag{6.41}$$

It can be observed from Fig.6.3 that, if $v_i > v_1$, $\cos(\chi_i - \psi_i) > 0$. Furthermore, if

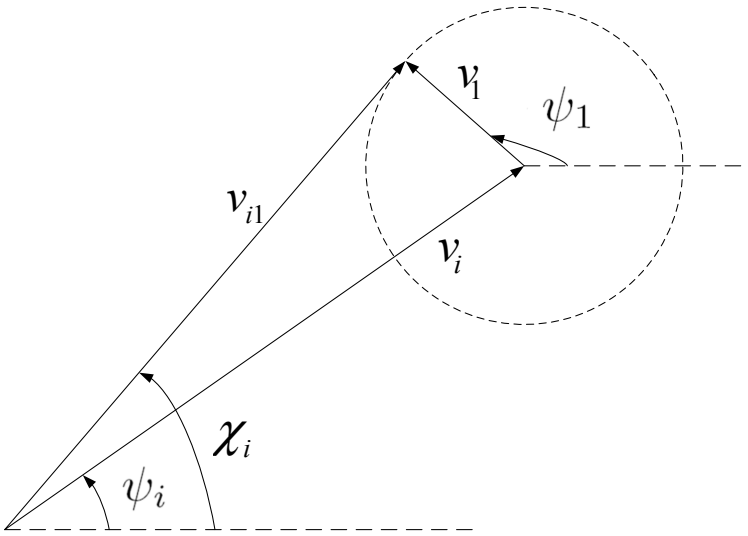

Figure 6.3: Relative course and actual heading

$\dot{\chi}_i$ is bounded, $\dot{\psi}_i$ can also be bounded according to the equation (6.41).

Next, it proceeds to design the heading rate controller for each follower UAV to achieve a circular formation subject to the physical constraints of the fixed-wing UAV. In this circular formation, the leader UAV is located at the center of the formation and executes the mission of level tracking while the follower UAVs are located along the circle around the leader and keep a desired distance r_c to the leader (see Fig. 6.1).

The relative course rate is designed as follows

$$\dot{\chi}_i = \frac{1}{r_c}[v_{i1}+\delta w \tanh(k_1(x_{i1}\cos\chi_i + y_{i1}\sin\chi_i))], \tag{6.42}$$

where $\delta w > 0$ and $k_1 > 0$.

The point $c_i = (x_{ic}, y_{ic})$ that the follower UAV flies around can be expressed as

$$x_{ic} = x_i - r_c\sin\chi_i, y_{ic} = y_i + r_c\cos\chi_i. \tag{6.43}$$

The relative position of the point c_i with respect to the leader can be represented

as

$$x_{ic1} = x_i - r_c \sin\chi_i - x_1, y_{ic1} = y_i + r_c \cos\chi_i - y_1. \tag{6.44}$$

Differentiating this relative position with respect to time yields that

$$\dot{x}_{ic1} = v_{i1}\cos\chi_i - r_c\dot{\chi}_i\cos\chi_i, \dot{y}_{ic1} = v_{i1}\sin\chi_i - r_c\dot{\chi}_i\sin\chi_i. \tag{6.45}$$

Consider the following Lyapunov function candidate

$$V = (x_i - x_1 - r_c\sin\chi_i)^2 + (y_i - y_1 + r_c\cos\chi_i)^2. \tag{6.46}$$

Differentiating this Lyapunov function candidate with respect to time t yields that

$$\begin{aligned}\dot{V} =& 2(x_i - r_c\sin\chi_i - x_1)(v_{i1}\cos\chi_i - r_c\dot{\chi}_i\cos\chi_i)\\ &+ 2(y_i + r_c\cos\chi_i - y_1)(v_{i1}\sin\chi_i - r_c\dot{\chi}_i\sin\chi_i).\end{aligned}$$

Substituting the formula (6.42) into the derivative of the Lyapunov function candidate results in

$$\begin{aligned}\dot{V} =& -2\delta w((x_{i1} - r_c\sin\chi_i)\cos\chi_i + (y_{i1} + r_c\cos\chi_i)\\ &\cdot\sin\chi_i)\tanh(k_1(x_{i1}\cos\chi_i + y_{i1}\sin\chi_i))\\ =& -2\delta w(x_{i1}\cos\chi_i + y_{i1}\sin\chi_i)\tanh(k_1(x_{i1}\cos\chi_i + y_{i1}\sin\chi_i))\\ \leq& 0\end{aligned}$$

Here, it can be observed that if $x_{i1} - r_c\sin\chi_i \neq 0$, $y_{i1} + r_c\cos\chi_i \neq 0$ and $(x_{i1} - r_c\sin\chi_i)\cos\chi_i = -(y_{i1} + r_c\cos\chi_i)\sin\chi_i$, then $\dot{V} = 0$. However, this is an unstable equilibrium point. When $x_{i1} - r_c\sin\chi_i = 0$ and $y_{i1} + r_c\cos\chi_i = 0\}$ with the proposed controller (6.42), it can be calculated that $\dot{x}_{ic1} = 0, \dot{y}_{ic1} = 0$. Therefore, it can be known that $\{(x_{i1}, y_{i1})|x_{i1} - r_c\sin\chi_i = 0, y_{i1} + r_c\cos\chi_i = 0\}$ is the invariant set.

According to LaSalle's Invariance Principle, the system asymptotically converges to the invariant set. Thus, the center (x_{ic}, y_{ic}) coincides with the leader, which in turn implies that the follower finally converges to the desired circular orbit around the leader. Based on the designed relative course rate (6.42), the heading rate control input can be obtained by equation (6.41).

6.4 Simulation Results

Table 6.1: Specifications for source seeking

Parameter	Value
Leader airspeed v_1	8 m/s
Follower airspeed v_i	20 m/s
w_1^0	0.1 rad/s
w_{max}	0.5 rad/s
f_{max}	800
f_d	600
α	1/1600
β	1
μ	50
$\delta\omega$	5
k_1	5
v_{sx}	2 m/s
v_{sy}	4 m/s
k	0.4

In this section, three simulation scenarios using the proposed approach will be presented. In the first scenario, five UAVs including one leader and four followers are controlled to execute the mission of source seeking while the moving source velocity is not estimated, where the radius of the circular formation is $r_c = 100$ meters. In the second scenario, as compared to the first scenario, the moving source

velocity is estimated and the proposed controllers are applied. In the third scenario, the radius of the circular formation are smaller than those in the first two scenarios. Here, the scalar field $f(\vec{r}) = f_{max}[1 - \tanh(\alpha||\vec{r} - \vec{r}_s||^{\beta})], \alpha > 0, \beta > 0$ is used and the initial source position is $\vec{r}_s = (0, 0)$. Table 6.1 shows the specifications of the UAV, the scalar field parameters and the control law parameters.

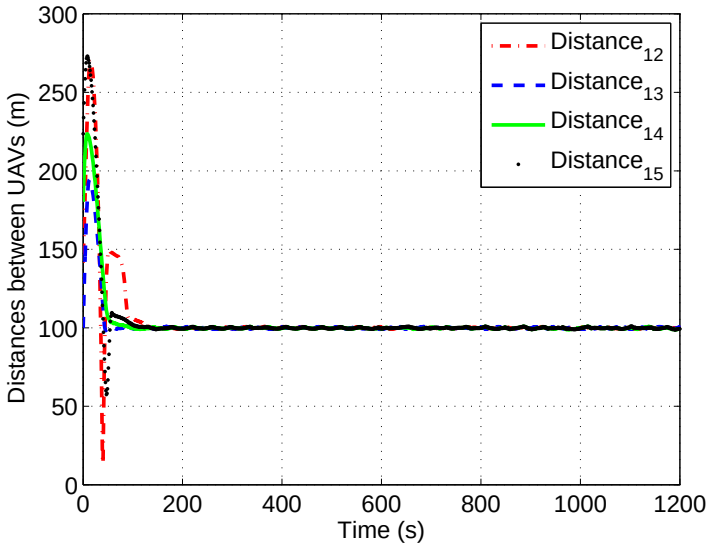

Figure 6.4: Distances between leader UAV and four follower UAVs (Scenario one)

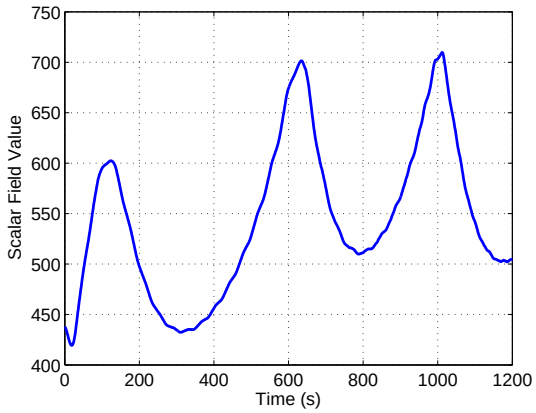

Figure 6.5: Scalar field level tracking (Scenario one)

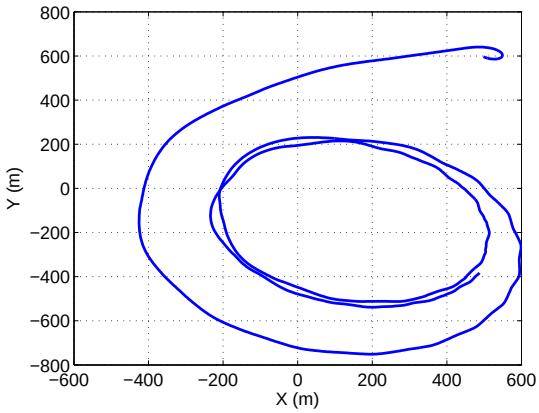

Figure 6.6: Trajectory of the leader UAV (Scenario one)

In scenario one, the initial positions of the five UAVs are as follows:(500,600), (600,700), (600,600), (650,500) and (700,500). Fig. 6.4 shows the distances between

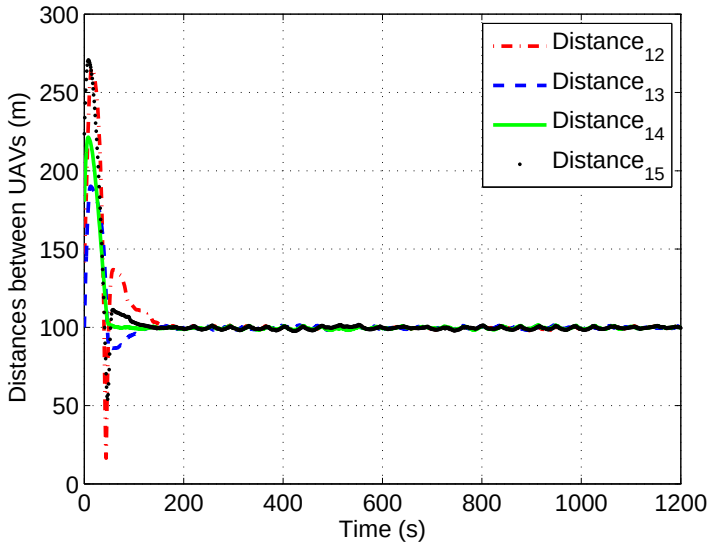

Figure 6.7: Distances between UAVs (Scenario two)

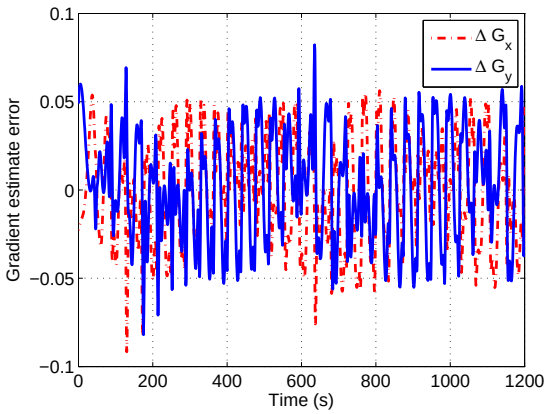

Figure 6.8: Gradient estimation error (Scenario two)

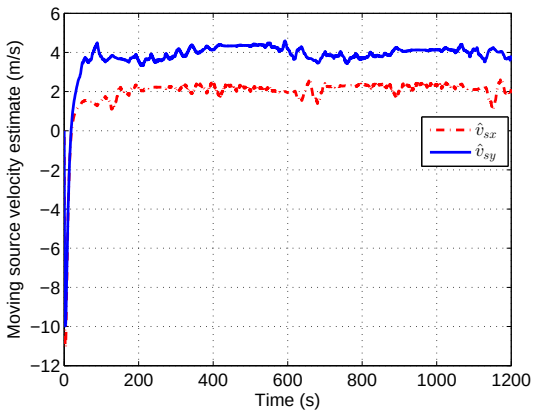

Figure 6.9: Moving source velocity estimation (Scenario two)

the leader UAV and the four follower UAVs. As claimed in the section 6.3.2, the follower UAVs converge to the circular orbit with a desired distance to the leader UAV. It can be observed from Fig. 6.5 that, the level tracking error is very large due to the source movement. Fig. 6.6 shows the trajectory of the leader UAV, where it can be seen that the distance between the leader UAV and the source significantly changes, which may result in the loss of source.

In scenario two, the initial positions of the five UAVs are the same as those in

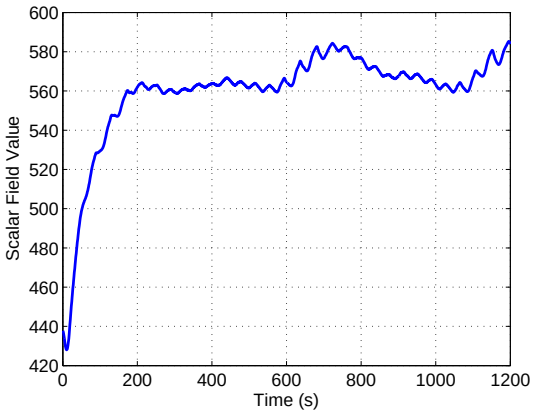

Figure 6.10: Scalar field level tracking (Scenario two)

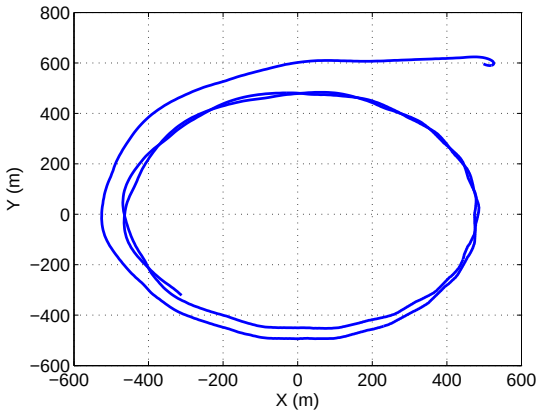

Figure 6.11: Leader UAV trajectory w.r.t. source (Scenario two)

scenario one. Compared with scenario one, scenario two takes the moving source velocity into account. An adaptive observer is utilized to estimate the velocity which is used to generate the guidance law for the leader UAV. Fig. 6.7 describes the distances between leader and follower UAVs. Fig. 6.8 shows the gradient estimate error. Since UAVs are not evenly distributed along the circular orbit, there always exists gradient estimate error. Fig. 6.9 shows the moving source velocity estimation, where the estimate converges to the vicinity of the actual value. Due to the existence of gradient estimation error, the velocity estimation error can not converge to zero. Figs. 6.10 and 6.11 depict the measured scalar field at the leader location and the leader UAV trajectory with respect to the moving source, respectively. Compared with the scenario one, it is observed from Fig. 6.10 that the level tracking error is much smaller in scenario two, which verifies the effectiveness of the proposed adaptive observer and controllers.

In the last scenario, the desired formation radius is smaller than those in the previous two scenarios, where the radius is $r_c = 50$ m. Fig. 6.12 describes the distances between leader and follower UAVs. It is seen from Fig. 6.13 that, the gradient estimation error is smaller than that in scenario two, which implies that the gradient estimation accuracy depends on the formation radius. Figs. 6.14-6.16

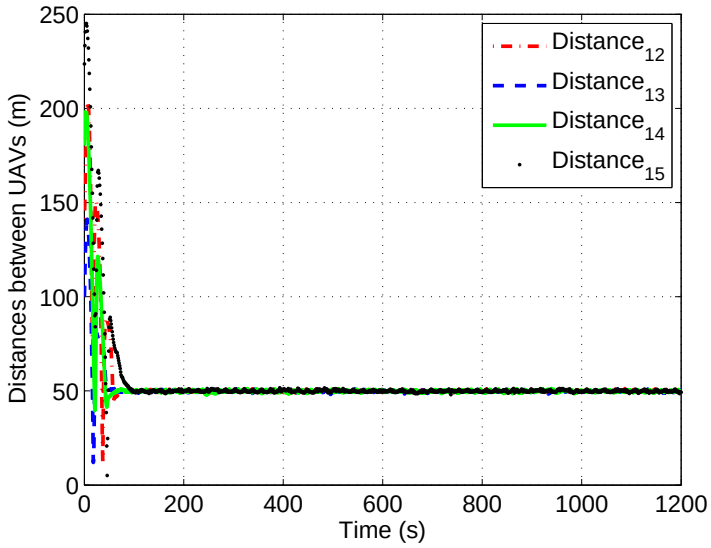

Figure 6.12: Distances between UAVs (Scenario three)

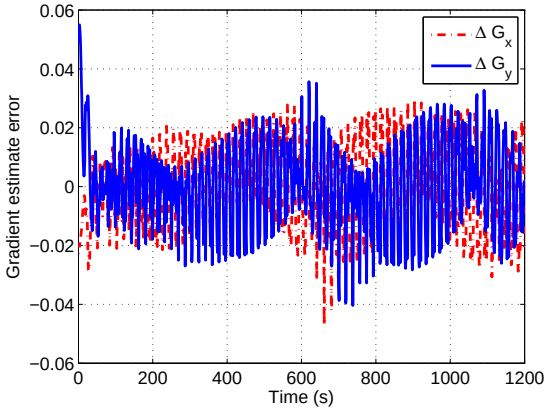

Figure 6.13: Gradient estimation error (Scenario three)

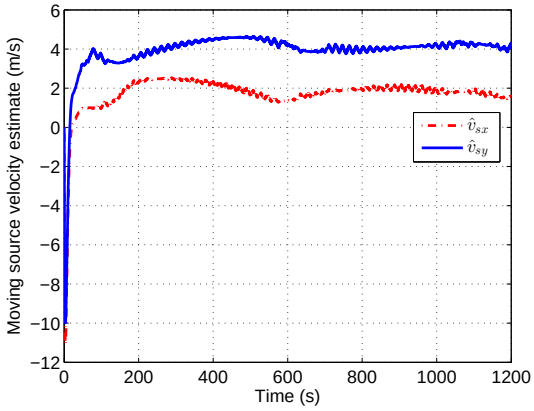

Figure 6.14: Moving source velocity estimation (Scenario three)

show the moving source velocity estimate, scalar field measurement, and leader UAV trajectory, respectively. It can be concluded that the smaller gradient estimation error results in better level tracking performance.

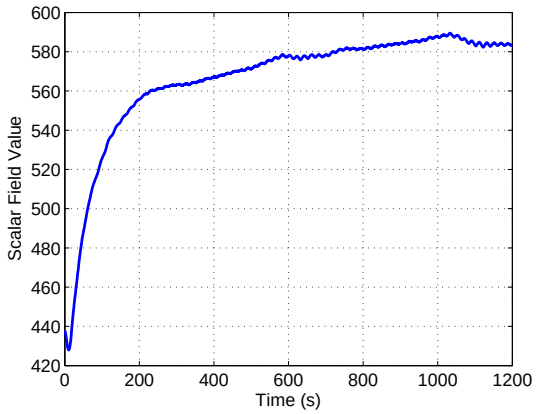

Figure 6.15: Scalar field level tracking (Scenario three)

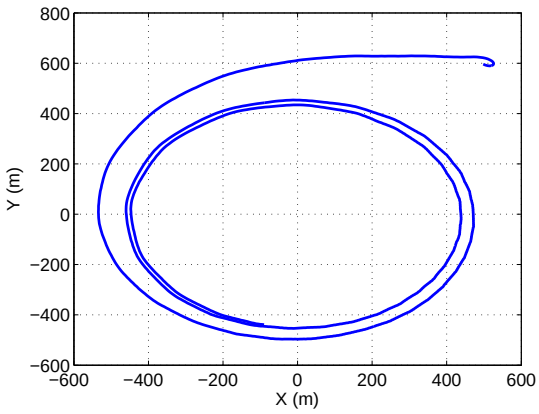

Figure 6.16: Leader UAV trajectory w.r.t. source (Scenario three)

6.5 Conclusions

Cooperation of multiple UAVs for moving source seeking is discussed in this chapter. Scalar field gradient is estimated by using a least-squares method. Based on the gradient estimate, an adaptive observer is proposed to estimate the moving source velocity. Then, both gradient and moving source velocity estimates are used to generate a guidance law for the leader UAV to achieve level tracking. Heading rate controllers are designed for UAVs so that level tracking and circular formation are executed. Furthermore, gradient estimate error and its influence on moving source velocity estimation and level tracking accuracy are also analyzed.

Chapter 7

Conclusions and Recommendations

7.1 Conclusions

Target tracking as a fundamental mission for UAVs has been studied in this thesis, where flight control for single UAV and cooperation strategy for multiple UAVs are explored. As a potential application, cooperative source seeking is also discussed in this thesis. The main results of this thesis are as follows:

The first part of the thesis studies the problem of ground target tracking using a single UAV with control input constraints. The proposed guidance law can be used to generate the feasible command for the fixed-wing UAV. The saturated heading rate controller makes the UAV with physical constraints capable of achieving target tracking. The rigorous proof for global stability provides the application scope of the proposed approach. An bounded adaptive observer is designed to estimate the unknown constant background wind and target motion. The boundedness of the estimate guarantees that the estimate can be incorporated to the saturated target tracking controller. However, fast time-varying moving target velocity estimation

has not been addressed in this thesis.

The second achievement is to solve the problem of adversarial ground target tracking using a single UAV with input constraints. The conditions that whether the UAV can avoid exposure to the adversarial target are provided. The proposed bang-bang controller can achieve two objectives: circular tracking around the target; avoiding exposure to the target or minimizing the exposure time.

The third part is devoted to designing a cooperative control strategy for multiple UAVs to achieve target tracking. Heading rate controller and airspeed controller are separately designed to achieve target tracking and muti-UAV cooperation. A new notion called temporal phase is proposed to represent the temporal separation. Based on this notion, an cooperative airspeed controller is designed to achieve temporal separation of UAVs while tracking a moving target. Background wind, target motion and UAV input constraints are taken into account during controller design. In addition, the stability proof of target tracking with multiple UAVs is also provided.

The last one but not least achievement is to solve cooperative source seeking using multiple UAVs with input constraints. Source seeking is a potential application of UAVs thanks to technological advances in sensing, communication, and control system. This thesis designs a least-squares method to estimate the gradient of the scalar field at the leader UAV location based on the measurements of all UAVs. Using the estimated gradient, an adaptive estimator is designed to obtain the unknown source velocity. Based on the gradient and source velocity estimates, UAV flight controllers are developed to achieve level tracking around the source. The level tracking strategy has two advantages: this strategy takes the fixed-wing constraints into account so that feasible UAV commands can be obtained; UAVs can avoid to be too close to the hazard source. Furthermore, the gradient estimation error is analyzed and its influence on moving source velocity estimation and level tracking

accuracy is explored as well.

7.2 Recommendations

Based on the work conducted in this thesis, some future works and possible extensions are identified as follows:

For the adversarial target tracking, in this thesis, the target is assumed to be stationary. However, in practice, many adversarial targets are moving targets such as tanks and armored vehicles. Therefore, moving adversarial target tracking could be one research topic of interest. In this topic, several issues need to be addressed, such as target velocity estimation and exposure avoidance strategy.

In this thesis, leader-follower formation strategy is used for UAV cooperation. Although this strategy is easy to implement, the failure of the leader resulting in the whole mission failure is a significant drawback. In addition, this centralized structure may lead to a heavy communication and computing burden on the leader UAV. In order to overcome the above critical issues, a decentralized cooperative strategy for target tracking may be pursued in the future study. Consensus-based formation could be one possible solution. However, the inherent properties of the fixed-wing UAV will make controller design very challenging. For example, the nonholonomic property hinders the UAV movement such that the UAV can not move to some directions quickly.

Single-target tracking or single-source seeking is studied in this thesis. In many real missions, there may exist more than one target or source of interest. If multiple UAVs are used to track these targets, the control strategy is still an open question. In this scenario, target classification such as tracking priority of the target needs to be determined. The allocation algorithms of UAVs to each target are also a possible research direction. For multiple sources, gradient estimation based source seeking

may lead the UAVs to a local minimum, since the scalar field generated by multiple sources may be significantly different from single source scalar field. Therefore, how to achieve multi-source seeking is worth of future exploration.

Although 2-D UAV model can be used in many applications, in some cases, 3-D model and 3-D movement may be required. For example, 3-D source seeking may require the UAV to take up 3-D flight. Since the pitch angle is coupled with the horizontal movement, 3-D motion control may be much more complicated than 2-D motion control. In addition, real application is the final objective of the research. Before the real application, experimental verification for the proposed approaches is necessary. Therefore, the implement of algorithms on real UAVs would be an interesting and challenging research direction. Due to the environment requirement and high cost for the fixed-wing UAV, currently it is difficult to carry out the fixed-wing UAV experiment. Instead of the fixed-wing UAV, there are two potential alternatives: mobile robot and quadrotor UAV. For the mobile robot, the forward speed is required to be constant or positive. Sensors such as laser, IMU, GPS, cameras, etc. are required to detect and localize the target. Communication between mobile robots can be realized by using wifi or other methods. For quadrotor UAV, the control can be classified into two hierarchies: low level control and high level control. The low level control is used to convert the quadrotor UAV motion to the fixed-wing UAV motion. The high level is to verify the proposed approaches in this thesis.

AUTHOR'S PUBLICATIONS

Journal Papers

1. S. Zhu and D. Wang. Adversarial ground target tracking using UAVs with input constraints. *Journal of Intelligent and Robotic Systems*, vol. 65, no. 1-4, pp. 521-532,2012.

2. S. Zhu, D. Wang, and C. B. Low. Ground target tracking using UAV with input constraints. *Journal of Intelligent and Robotic Systems*, vol. 69, no.1-4, pp. 417-429, 2013.

3. S. Zhu, D. Wang, and C. B. Low. Cooperative control of multiple UAVs for source seeking. *Journal of Intelligent and Robotic Systems*, vol. 70, no. 1-4, pp. 293-301, 2013.

4. S. Zhu, D. Wang, and C. B. Low. Cooperative control of multiple UAVs for moving source seeking. *Journal of Intelligent and Robotic Systems*, vol. 74, no. 1-2, pp. 333-346, 2014.

5. X. Wang, D. Wang, S. Zhu, and E. K. Poh. Fractional describing function analysis of PWPF modulator. *Mathematical Problems in Engineering*, vol. 2013, pp. 1-5, 2013.

Conference Papers

1. S. Zhu, D. Wang, and Q. Chen. Standoff tracking control of moving target in unknown wind. in *Proceedings of the IEEE Conference on Decision and Control*, pp. 776-781, Shanghai, China, December 2009.

2. S. Zhu and D. Wang. Cooperative ground target tracking with input constraints. in *11th International Conference on Control Automation Robotics and Vision (ICARCV)*, pp. 1051-1056, Singapore, December 2010.

3. S. Zhu, D. Wang, and C. B. Low. Cooperative control of multiple UAVs for moving source seeking. in *International Conference on Unmanned Aircraft System*, pp. 193-202, Atlanta, USA, May 2013.

Bibliography

[1] B. Grocholsky, J. Keller, V. Kumar, and G. Pappas. Cooperative air and ground surveillance. *IEEE Robotics and Automation Magazine*, vol. 13, no. 3, pp. 16-25, 2006.

[2] D. W. Casbeer, D. B. Kingston, and R. W. Beard. Cooperative forest fire surveillance using a team of small unmanned air vehicles. *International Journal of Systems Sciences*, vol. 37, no. 6, pp. 351-360, 2006.

[3] R. W. Beard, T. W. McLain, D. B. Nelson, D. Kingston, and D. Johanson. Decentralized cooperative aerial surveillance using fixed-wing miniature UAVs. *Proceedings of the IEEE*, vol. 94, no. 7, pp. 1306-1324, 2006.

[4] A. R. Girard, A. S. Howell, and J. K. Hedrick. Border patrol and surveillance missions using multiple unmanned air vehicles. in *Proceedings of the IEEE Conference on Decision and Control*, pp. 620-625, Nassau, December 2004.

[5] P. Doherty and P. Rudol. A UAV search and rescue scenario with human body detection and geolocalization. in *Proceedings of the 20th Australian Joint Conference on Artificial Intelligence*, pp. 1-13, Gold Coast, Australia, December 2007.

[6] J. Elston and E. Frew. Net-centric cooperative tracking of moving targets. in *AIAA Infotech@Aerospace Conference and Exhibit*, Rohnert Park, CA, May 2007.

[7] P. Singer. Military robots and the laws of war. *The New Atlantis: A Journal of Technology and Society*, no. 23, pp. 25-45, 2009.

[8] P. Singer. Wired for war: The robotics revolution and conflict in the 21st century. New York: Penguin Group, 2009.

[9] D. Lawrence, E. Frew, and W. Pisano. Lyapunov vector fields for autonomous unmanned aircraft flight control. *AIAA Journal of Guidance, Control, and Dynamics*, vol. 31, no. 5, pp. 1220-1129, 2008.

[10] W. Ren. Trajectory tracking control for a miniature fixed-wing unmanned air vehicle. *International Journal of Systems Science*, vol. 38, no. 4, pp. 361-368, 2007.

[11] W. Ren and R. W. Beard. Trajectory tracking for unmanned air vehicles with velocity and heading rate constraints. *IEEE Transactions on Control Systems Technology*, vol. 12, no. 5, pp. 706-716, 2004.

[12] W. Ren. Consensus seeking, formation keeping, and trajectory tracking in multiple vehicle cooperative control. *PhD thesis*, Brigham Young University, 2004.

[13] G. Walsh, D. Tilbury, S. Sastry, R. Murray, and J. Laumond. Stabilization of trajectories for systems with nonholonomic constraints. *IEEE Transactions on Automatic Control*, vol. 39, no. 1, pp. 216-222, 1994.

[14] I. Kaminer, A. Pascoal, E. Hallberg, and C. Silvestre. Trajectory tracking controllers for autonomous vehicles: An integrated approach to guidance and control. *AIAA Journal of Guidance, Control, and Dynamics*, vol. 21, no. 1, pp. 29-38, 1998.

[15] J. R. T. Lawton, R. W. Beard, and B. J. Young. A decentralized approach to formation maneuvers. *IEEE Transactions on Robotics and Automation*, vol. 19, no. 6, pp. 933-941, 2003.

[16] Z. P. Jiang and H. Nijmeijer. Tracking control of mobile robots: A case study in backstepping. *Automatica*, vol. 33, no. 7, pp. 1393-1399, 1997.

[17] T. C. Lee, K. T. Song, C. H. Lee, and C. C. Teng. Tracking control of unicyclemodeled mobile robots using a saturation feedback controller. *IEEE Transactions on Control Systems Technology*, vol. 9, no. 2, pp. 305-318, 2001.

[18] Z. P. Jiang, E. Lefeber, and H. Nijmeijer. Saturated stabilization and track control of a nonholonomic mobile robot. *Systems and Control Letters*, vol. 42, pp. 327-332, 2001.

[19] D. R. Nelson, D. B. Barber, T. W. McLain, and R. W. Beard. Vector field path following for miniature air vehicles. *IEEE Transactions on Robotics*, vol. 23, no. 3, pp. 519-529, 2007.

[20] R. Rysdyk. Unmanned aerial vehicle path following for target observation in wind. *AIAA Journal of Guidance, Control, and Dynamics*, vol. 29, no. 5, pp. 1092-1100, 2006.

[21] G. P. Carole, T. Olivier, D. Andre, and P. Eric. Receding horizon model-based predictive control for dynamic target tracking: a comparative study. in *AIAA Guidance, Navigation, and Control Conference and Exhibit*, Chicago, August 2009.

[22] S. Kim, H. Oh, and A. Tsourdos. Nonlinear model predictive coordinated standoff tracking of a moving ground vehicle. *AIAA Journal of Guidance, Control, and Dynamics*, vol. 36, no. 2, pp. 557-566, 2013.

[23] E. Frew and D. Lawrence. Cooperative standoff tracking of moving targets using Lyapunov guidance vector fields. *AIAA Journal of Guidance, Control, and Dynamics*, vol. 31, no. 2, pp. 290-306, 2008.

[24] E. Frew, S. Spry, and T. McGee. Flight demonstrations of self-directed collaborative navigation of small unmanned aircraft. in *AIAA 3rd "Unmanned Unlimited" Technical Conference, Workshop and Exhibit*, Reston, September 2004.

[25] S. O. Lee, Y. J. Cho, B. M. Hwang, B. J. You, and S. R. Oh. A stable target-tracking control for unicycle mobile robots. in *Proceedings of the IEEE/RSJ International Conference on Intelligent Robots and Systems*, pp. 1822-1827, Takamatsu, October 2000.

[26] S. Park, J. Deyst, and J. P. How. A new nonlinear guidance logic for trajectory tracking. in *AIAA Guidance, Navigation, and Control Conference*, Rhode Island, August 2004.

[27] S. Park, J. Deyst, and J. P. How. Performance and Lyapunov stability of a nonlinear path-following guidance method. *AIAA Journal of Guidance, Control, and Dynamics*, vol. 30, no. 6, pp. 1718-1728, 2007.

[28] F. Rafi, S. Khan, K. Shafiq, and M. Shah. Autonomous target following by unmanned aerial vehicles. in *Proceedings of SPIE*, Orlando, Florida, May 2006.

[29] D. Kingston and R. Beard. UAV splay state configuration for moving targets in wind. *Advances in Cooperative Control and Optimization*, pp. 109-128, 2007.

[30] S. R. Griffiths. Vector field approach for curved path following for miniature aerial vehicles. in *Proceedings of AIAA Guidance, Navigation, and Control Conference*, August 2006.

[31] T. H. Summers, M. R. Akella, and M. J. Mears. Coordinated standoff tracking of moving targets: control laws and information architectures. *AIAA Journal of Guidance, Control, and Dynamics*, vol. 32, no. 1, pp. 56-69, 2009.

[32] S. Lim, Y. Kim, D. Lee, and H. Bang. Standoff target tracking using a vector field for multiple unmanned aircrafts. *Journal of Intelligent and Robotic Systems*, vol. 69, no. 1-4, pp. 347-360, 2013.

[33] H. Chen, K. C. Chang, and C. S. Agate. A dynamic path planning algorithm for UAV tracking. in *Proceedings of SPIE*, 2009.

[34] H. Chen, K. C. Chang, and C. S. Agate. Tracking with UAV using tangent-plus-Lyapunov vector field guidance. in *12th International Conference on Information Fusion*, Seattle, USA, July 2009.

[35] H. Chen, K. C. Chang, and C. S. Agate. UAV path planning with tangent-plus-Lyapunov vector field guidance and obstacle avoidance. *IEEE Transactions on Aerospace and Electronic Systems*, vol. 49, no. 2, pp. 840-856, 2013

[36] S. Zhu, D. Wang, and Q. Chen. Standoff tracking control of moving target in unknown wind. in *Proceedings of the IEEE Conference on Decision and Control*, pp. 776-781, Shanghai, China, December 2009.

[37] N. E. Leonard and E. Fiorelli. Virtual leaders, artificial potentials and coordinated control of groups. in *Proceedings of the IEEE Conference on Decision and Control*, pp. 2968-2973, Orlando, Florida, December 2001.

[38] J. Yan, X. P. Guan, and F. X. Tan. Target tracking and obstacle avoidance for multi-agent systems. *International Journal of Automation and Computing*, vol. 7, no. 4, pp. 550-556, 2010.

[39] K. P. Tee, S. S. Ge, and E. H. Tay. Barrier Lyapunov functions for the control of output-constrained nonlinear systems. *Automatica*, vol. 45, no. 4, pp. 918-927, 2009.

[40] J. Ruz, O. Arevalo, J. M. de la Cruz, and G. Pajares. Using MILP for UAVs Trajectory Optimization under radar detection risk. in *Proceedings of the IEEE Conference on Emerging Technologies and Factory Automation*, pp. 957-960, Prague, September 2006.

[41] B. Pfeiffer, R. Batta, K. Klamroth, and R. Nagi. Path planning for UAVs in the presence of threat zones using probabilistic modeling. in *Handbook of Military Industrial Engineering*, Taylor and Francis, USA, 2008.

[42] L. E. Dubins. On curves of minimal length with a constraints on average curvature, and with prescribed initial and terminal positions and tangents. *American Journal of Mathematics*, vol. 79, no. 3, pp. 497-516, 1957.

[43] J. Boissonnat, A. Crzo, and J. Leblond. Shortest paths of bounded curvature in the plane. *Journal of Intelligent and Robotic Systems*, vol. 11, no. 1-2, pp. 5-20, 1994.

[44] X. N. Bui, J. Boissonnat, P. Soueres, and J. Laumond. Shortest path synthesis for Dubins non-holonomic robot. in *Proceedings of the IEEE International Conference on Robotics and Automation*, pp. 2-7, San Diego, May 1994.

[45] X. C. Ding, A. R. Rahmani, and M. Egerstedt. Multi-UAV convoy protection: an optimal approach to path planning and coordination. *IEEE Transactions on Robotics*, vol. 26, no. 2, pp. 256-268, 2010.

[46] J. Cochran and M. Krstic. Nonholonomic source seeking with tuning of angular velocity. *IEEE Transactions on Automatic Control*, vol. 54, no. 4, pp. 717-731, 2009.

[47] C. Zhang, D. Arnold, N. Ghods, A. Siranosian, and M. Krstic. Source seeking with nonholonomic unicycle without position measurement and with tuning of forward velocity. *Systems and Control Letters*, vol. 56, pp. 245-252, 2007.

[48] J. Cochran, A. A. Siranosian, N. Ghods, and M. Krstic. 3-D source seeking for underactuated vehicles without position measurement. *IEEE Transactions on Robotics*, vol. 25, no. 1, pp. 117-129, 2009.

[49] A. S. Matveev, H. Teimoori, and A. V. Savkin. Navigation of a unicycle-like mobile robot for environmental extremum seeking. *Automatica*, vol. 47, no. 1, pp. 85-91, 2011.

[50] A. S. Matveev, H. Teimoori, and A. V. Savkin. Range-only measurements based target following for wheeled mobile robots. *Automatica*, vol. 47, no. 1, pp. 177-184, 2011.

[51] S. Azuma, M. S. Sakar, and G. J. Pappas. Stochastic source seeking by mobile robots. *IEEE Transactions on Automatic Control*, vol. 57, no. 9, pp. 2308-2321, 2012.

[52] P. Ogren, E. Fiorelli, and N. E. Leonard. Cooperative control of mobile sensor networks: adaptive gradient climbing in a distributed environment. *IEEE Transactions on Automatic Control*, vol. 49, no. 8, pp. 1292-1302, 2004.

[53] F. Zhang and N. E. Leonard. Cooperative filters and control for cooperative exploration. *IEEE Transactions on Automatic Control*, vol. 55, no. 3, pp. 650-663, 2010.

[54] J. Hu and X. Hu. Nonlinear filtering in target tracking using cooperative mobile sensors. *Automatica*, vol. 46, no. 12, pp. 2041-2046, 2010.

[55] E. Biyik and M. Arcak. Gradient climbing in formation via extremum seeking and passivity-based coordination rules. in *Proceedings of the IEEE Conference on Decision and Control*, pp. 3133-3138, New Orleans, LA, December 2007.

[56] N. Ghods and M. Krstic. Multiagent deployment over a source. *IEEE Transactions on Control System Technology*, vol. 20, no. 1, pp. 277-285, 2012.

[57] M. E. Campbell and W. Whitacre. Cooperative tracking using vision measurments on seaScan UAVs. *IEEE Transactions on Control Systems Technology*, vol. 15, no. 4, pp. 613-626, 2007.

[58] M. E. Campbell and W. Whitacre. Vision based geolocation tracking system for UAVs. *AIAA Journal of Guidance, Control, and Dynamics*, vol. 33, no. 2, pp. 521-532, 2010.

[59] W. Whitacre and M. E. Campbell. Decentralized geolocation and bias estimation for uninhabited aerial vehicles with articulating cameras. *AIAA Journal of Guidance, Control, and Dynamics*, vol. 34, no. 2, pp. 564-573, 2011.

[60] S. Li and Y. Guo. Distributed source seeking by cooperative robots: all-to-all and limited communications. in *IEEE International Conference on Robotics and Automation*, pp. 1107-1112, USA, May 2012.

[61] L. Brinon-Arranz, A. Seuret and C. Canudas-de-Wit. Collaborative estimation of gradient direction by a formation of AUVs under communication constraints. in *50th IEEE Conference on Decision and Control and European Control Conference (CDC-ECC)*, pp. 5583-5588, Orlando, December 2011.

[62] B. J. Moore and C. Canudas-de-Wit. Source seeking via collaborative measurements by a circular formation of agents. in *Proceedings of the American Control Conference*, pp. 6417-6422, Baltimore, June 2010.

[63] D. Swaroop and J. K. Hedrick. String stability of interconnected systems. *IEEE Transactions on Automatic Control*, vol. 41, no. 3, pp. 349-357, 1996.

[64] A. Pant, P. Seiler, and K. Hedrick. Mesh stability of look-ahead interconnected systems. *IEEE Transactions on Automatic Control*, vol. 47, no. 2, pp. 403-407, 2002.

[65] H. G. Tanner, G. J. Pappas, and V. Kumar. Leader-to-formation stability. *IEEE Transactions on Robotics and Automation*, vol. 20, no. 3, pp. 443-455, 2004.

[66] J. A. Fax and R. M. Murray. Information flow and cooperative control of vehicle formations. *IEEE Transactions on Automatic Control*, vol. 49, no. 9, pp. 1465-1476, 2004.

[67] R. Olfati-Saber and R. Murray. Consensus problems in networks of agents with switching topology and time-delays. *IEEE Transactions on Automatic Control*, vol. 49, no. 9, pp. 1520-1533, 2004.

[68] L. Moreau. Stability of multiagent systems with time-dependent communication links. *IEEE Transactions on Automatic Control*, vol. 50, no. 2, pp. 169-182, 2005.

[69] W. Ren and R. W. Beard. Consensus seeking in multiagent systems under dynamically changing interaction topologies. *IEEE Transactions on Automatic Control*, vol. 50, no. 5, pp. 655-661, 2005.

[70] P. Ogren, M. Egerstedt, and X. Hu. A control Lyapunov function approach to multiagent coordination. *IEEE Transactions on Robotics and Automation*, vol. 18, no. 5, pp. 847-851, 2002.

[71] X. H. Liu, A. Goldsmith, S. S. Mahal, and J. K. Hedrick. Effects of communication delay on string stability in vehicle platoons. in *Proceedings of the IEEE International Conference on Intelligent Transportation Systems*, pp. 625-630, Oakland, CA, August 2001.

[72] Y. Chen, and Z. Wang. Formation control: a review and a new consideration. in *IEEE/RSJ International Conference on Intelligent Robots and Systems*, pp. 3181-3186, August 2005.

[73] P. K. C. Wang. Navigation strategies for multiple autonomous mobile robots moving in formation. *Journal of Robotic Systems*, vol. 8, no. 2, pp. 177-195, 1991.

[74] J. P. Desai, J. Ostrowski, and V. Kumar. Controlling formations of multiple mobile robots. in *Proceedings of the IEEE International Conference on Robotics and Automation*, pp. 2864-2869, Leuven, May 1998.

[75] L. Consolini, F. Morbidi, D. Prattichizzo, and M. Tosques. Leader-follower formation control of nonholonomic mobile robots with input constraints. *Automatica*, vol. 44, no. 5, pp. 1343-1349, 2008.

[76] T. Balch and R. C. Arkin. Behavior-based formation control for multirobot teams. *IEEE Transactions on Robotics and Automation*, vol. 14, no. 6, pp. 926-939, 1998.

[77] M. A. Lewis and K. H. Tan. High precision formation control of mobile robots using virtual structures. *Autonomous Robots*, vol. 4, no. 4, pp. 387-403, 1997.

[78] R. W. Beard, J. R. Lawton, and F. Y. Hadaegh. A coordination architecture for formation control. *IEEE Transactions on Control Systems Technology*, vol. 9, no. 6, pp. 777-790, 2001.

[79] W. Ren and R. W. Beard. Decentralized scheme for spacecraft formation flying via the virtual structure approach. *AIAA Journal of Guidance, Control and Dynamics*, vol. 27, no. 1, pp. 73-82, 2004.

[80] W. Ren, R. W. Beard, and J. W. Curtis. Satisficing control for multi-agent formation maneuvers. in *Proceedings of the IEEE Conference on Decision and Control*, pp. 2433-2438, Las Vegas, December 2002.

[81] Q. Li and Z. P. Jiang. Formation Tracking Control of Unicycle Teams with Collision Avoidance. in *Proceedings of the IEEE Conference on Decision and Control*, pp. 496-501, Cancun, December 2008.

[82] E. Lalish, K. A. Morgansen, and T. Tsukamaki. Formation tracking control using virtual structures and deconfliction. in *Proceedings of the IEEE Conference on Decision and Control*, pp. 5699-5705, San Diego, December 2006.

[83] K. D. Do. Output-feedback formation tracking control of unicycle-type mobile robots with limited sensing ranges. *Robotics and Autonomous Systems*, vol. 57, no. 1, pp. 34-47, 2009.

[84] B. D. O. Anderson, C. Yu, B. Fidan, and J. M. Hendrickx. Rigid graph control architectures for autonomous formations. *IEEE Control Systems Magazine*, vol. 28, no. 6, pp. 48-63, 2008.

[85] D. Van Der Walle, B. Fidan, A. Sutton, C. Yu, and B. D. O. Anderson. Non-hierarchical UAV formation control for surveillance tasks. in *Proceedings of the American Control Conference*, pp. 777-782, Seattle, June 2008.

[86] C. Yu, J. M. Hendrickx, B. Fidan, B. D. O. Anderson, and V. D. Blondel. Three and higher dimensional autonomous formations: Rigidity, persistence and structural persistence. *Automatica*, vol. 43, no. 3, pp. 387-402, 2007.

[87] Y. Chen, and Y. Tian. A backstepping design for directed formation control of three-coleader agents in the plane. *International Journal of Robust and Nonlinear Control,* vol. 19, no. 7, pp. 729-745, 2009.

[88] M. Arcak. Passivity as a design tool for group coordination. *IEEE Transactions on Automatic Control*, vol. 52, no. 8, pp. 1380-1390, 2007.

[89] W. Zhao, T. H. Go, and E. Low. Formation flight control using model predictive approach. in *47th AIAA Aerospace Sciences Meeting Including The New Horizons Forum and Aerospace Exposition*, Orlando, January 2009.

[90] D. A. Paley and C. Peterson. Stabilization of collective motion in a time-invariant flowfield. *AIAA Journal of Guidance, Control, and Dynamics*, vol. 32, no. 3, pp. 771-779, 2009.

[91] C. Peterson and D. A. Paley. Cooperative control of unmanned vehicle in a time-varying flowfield. in *Proceedings of AIAA Guidance, Navigation, and Control Conference*, Chicago, August 2009.

[92] C. Peterson and D. A. Paley. Multiple coordination in an estimated time-varying flowfield. *AIAA Journal of Guidance, Control, and Dynamics*, vol. 34, no. 1, pp. 177-191, 2011.

[93] A. W. Proud, M. Pachter, and J. J. D'Azzo. Close formation flight control. in *Proceedings of AIAA Guidance, Navigation, and Control Conference*, Portland, August 1999.

[94] R. W. Beard, T. W. McLain, M. Goodrich, and E. P. Anderson. Coordinated target assignment and intercept for unmanned air vehicles. *IEEE Transactions on Robotics and Automation*, vol. 18, no. 6, pp. 911-922, 2002.

[95] H. K. Khalil. Nonlinear Systems, Prentice Hall, Englewood Cliffs, New Jersy, 1996.

[96] J. J. E. Slotine and W. Li. Applied nonlinear control, Prentice Hall, Englewood Cliffs, New Jersy, 1991.

[97] D. E. Kirk. Optimal control theory, an introduction, Dover Publications, 2004.

[98] A. Isidori. Nonlinear control systems II, Springer, 1999.

[99] L. Techy and C. A. Woolsey. Minimum-time path planning for unmanned aerial vehicles in steady uniform winds. *AIAA Journal of Guidance, Control, and Dynamics*, vol. 32, no. 6, pp. 1736-1746, 2009.

[100] E. Frew. Sensitivity of cooperative target geolocalization to orbit coordination, *AIAA Journal of Guidance, Control, and Dynamics*, vol. 31, no. 4, pp. 1028-1040, 2008.

[101] J. Han, Y. Xu, L. Di, and Y. Chen. Low-cost multi-UAV technologies for contour mapping of nuclear radiation field. *Journal of Intelligent and Robotic Systems*, vol. 70, no. 1-4, pp. 401-410, 2013.

[102] S. Zhu, D. Wang, and C. B. Low. Cooperative control of multiple UAVs for source seeking. *Journal of Intelligent and Robotic Systems*, vol. 70, no. 1-4, pp. 293-301, 2013.